Archvied in Dspace@nitr

http://dspace.nitrkl.ac.in/dspace

A new approach to Power System Protection using Time-frequency analysis and Pattern Recognition

Thesis submitted in partial fulfillment of the requirements for the award of the Doctor of Philosophy

By

Subhransu Ranjan Samantaray

July-2007

Under the guidance of

Prof.(Dr.) G. Panda
Prof.(Dr.) P. K. Dash

Electronics and Communication Engineering
National Institute of Technology
Rourkela-769008

To my family

Certificate

This is to certify that the thesis entitled "**A new approach to Power System Protection using Time-frequency analysis and Pattern Recognition**" by Mr. Subhransu Ranjan Samantaray, submitted to the National Institute of Technology, Rourkela for the degree of Doctor of Philosophy, is a record of bona fide research work, carried out by him in the department of Electronics and Communication Engineering under our supervision. We believe that the thesis fulfills part of the requirements for the award of degree of Doctor of Philosophy. The results embodied in the thesis have not been submitted for award of any other degree.

Prof.(Dr.) G. Panda
Professor and Head
Dept. of ECE
NIT, Rourkela

Prof.(Dr.) P. K. Dash
Director
College of Engineering
Bhubaneswar

Acknowledgement

I am indebted to many people who contributed through their support, knowledge and friendship, to this work and the years at NIT Rourkela.

I am grateful to my advisor, Prof. P. K Dash and Prof. G. Panda, who gave me the opportunity to realize this work in the laboratory. They encouraged, supported and motivated me with much kindness throughout the work. In particular, they showed me the interesting side of the power system engineering and those of the highly interdisciplinary project work. I always had the freedom to follow my own ideas, which I am very grateful for. I really admire them for patience and staying power to carefully read the whole manuscript.

I am also grateful to NIT Rourkela for providing me adequate infrastructure, experimental facilities to carry out the present investigations.

I am thankful to Prof. K. K. Mohapatra, Prof S. K. Patra, Dr. A. K. Panda for extending their valuable suggestions whenever I approached.

My special thanks to Dr B. K. Panigrahi, Dr. A. Routray, Dr. S. Mishra, Dr. A. K. Pradhan and Dr. Ranjan Jena for their constant inspiration and encouragement during my research.

My hearty thanks to Mr. Pravat Kumar Rout, Mr. Birendra Biswal, Mr. Sangram Routray and Mr. Niranjan Nayak for their help, co-operation and encouragement.

I acknowledge all staffs, research scholars, friends and juniors of Center for research in Electrical, Electronics and Computer Engineering, Bhubaneswar and Electronics and Communication Engineering department, NIT, Rourkela for helping me during my research work.

I render my respect to all my family members for giving me mental support and inspiration for carrying out my research work.

Subhransu Ranjan Samantaray

Contents

VII

List of Tables

List of Figures

Chapter 3

Chapter 4

Chapter 5

Chapter 6

Abstract

The fault diagnosis of Electric Power System is a process of discriminating the faulted system elements by protective relays and subsequent tripping by circuit breakers. Specially, as soon as some serious faults occur on a power system, a lot of alarm information is transmitted to the control center. Under such situation, the operators are required to judge the cause, location, and the system elements with faults rapidly and accurately. Thus, good fault diagnosis methods can provide accurate and effective diagnostic information to dispatch operators and help them take necessary measures in fault situation so as to guarantee the secure and stable operation of the Electric power system.

This thesis reports various techniques used for detection, classification and localization of faults on the high voltage transmission line. The distance protection scheme for transmission line is employed for various power networks such as single-circuit line, double-circuit line, and lines having FACTS devices. The faulted voltage and current signal samples are retrieved at the relaying point for all 11 types of shunt faults at various operating conditions like variation in source impedance, fault resistance, inception angle, and fault locations. These sampled voltage and current signals are used for detection, classification, and location of different types of faults.

Unlike the conventional relaying schemes, using fuzzy systems and neural networks, the proposed research work presents a novel technique for distance and differential protection, using time-frequency analysis and pattern recognition approach. The time-frequency transform such as S-Transform and its variations are used for fault detection, classification and location determination for transmission lines. The S-Transform is an extension of Wavelet Transform which possesses superior property over the latter as the moving functions are fixed with respect to time axis while the localizing scalable Gaussian window dilates and translates. The S-Transform uses an analysis window whose width is decreasing with frequency providing a frequency dependent resolution. Phase spectrum obtained in this transform is always with respect to fixed reference point and the real and imaginary spectrum can be localized independently.

Such a transform with moving and scalable localizing Gaussian window, therefore, provides excellent time localization property for different signals.

The proposed research work includes pre-processing the fault current and voltage signal samples through S-Transform and finding out the phasor information such as amplitude and phase, which are used for impedance calculation to the fault point. Also energy and standard deviation of the S-matrix are computed to detect and classify the fault patterns. Another variation of the S-Transform such as Hyperbolic S-Transform is also used to detect and localize the fault with various operating conditions of the power network. Wavelet Transform is also applied to the faulted voltage and current signals and multi-resolution analysis is done to detect and classify the faulty section and section identification of the transmission line including FACTS.

Intelligent techniques such as Radial Basis Function Neural network (RBFNN) and Support Vector Machine (SVM) are embedded to the proposed protection schemes for automatic recognition of the fault patterns for transmission line including FACTS. The RBFNN and SVMs are trained and tested to design a robust fault classifier which provides accurate results for different types of faults with wide variations in operating conditions.

In another approach, a differential equation based fault locator is designed for transmission line including Unified Power Flow Controller (UPFC). The faulted power network is drawn and differential equations are developed for voltage and current at the fault point. Using the faulted voltage and current information at both sending and receiving end, the line inductance to the fault point is calculated which directly reflects the location of the fault point from the relaying location.

Another variation of S-Transform known as complex windowed S-Transform is used to extract the time-frequency contours of the inrush current and fault current signals, to distinguish the inrush current and fault current, used for power transformer protection. The time-frequency contours at different frequencies are extracted and an energy index is devised to distinguish both signals. The proposed method provides better results compared to existing 2nd harmonic restraint protection for power transformer.

Chapter-1

Introduction

An electrical power network, as a whole, consists of generation, transmission and distribution. The performance of a power network is frequently affected by the transmission line faults, which give rise to disruption in power flow. Therefore, transmission of electric power and necessary protective measures are the vital issues need to be addressed properly. Distance protection is used to protect the transmission line against faults by measuring the line voltages and currents at remote end buses using digital fault recorders.

Faults on transmission lines need to be detected, classified, located accurately, and cleared as fast as possible. In power transmission line protection, faulty phase identification and location of fault are the two most important items which need to be addressed in a reliable and accurate manner. Distance relaying techniques based on the measurement of the impedance at the fundamental frequency between the fault location and the relaying point have attracted wide spread attention. The sampled voltage and current data at the relying point are used to locate and classify the fault involving the line with or without fault resistance present in the fault path. The accuracy of the fault classification and location also depends on the amplitude of the DC offset and harmonics in comparison to the fundamental component.

1.1 Background

In recent years, different protection algorithms are proposed for transmission line using Fourier Transforms, Differential equations, Waveform modeling, Kalman filters, Fuzzy Logic, Neural Networks, and Wavelet Transforms [1-24] for fault detection and location calculation. Also some proposed methods used only the sampled current values at the relying point during faults for classification of fault types and distance calculations.

Filtering requirements for digital relaying are very much essential which removes the non-fundamental frequencies and provides required phasor. One such filter which is widely used in digital distance relays is the Discrete Fourier Transform (DFT). DFT based distance protection algorithms [1, 2] are most popular and become standard in the industry.

A steady state voltage signal in the time domain can be represented by

$$V(t) = V_m \cos(\omega t + \theta) \tag{1.1}$$

In a digital relay, the signal contains 'N' samples per cycle and thus the input signal can be represented by $V(k)$, where $k = 0$ to $N - 1$. The Discrete Fourier Transform calculation of the fundamental components can be defined by the following equations.

$$V_{real} = \frac{2}{N} \sum_{k=0}^{N-1} V(k) \cos(\frac{2\pi k}{N}) \tag{1.2}$$

$$V_{imag} = \frac{2}{N} \sum_{k=0}^{N-1} -V(k) \sin(\frac{2\pi k}{N}) \tag{1.3}$$

The magnitude and phase can be calculated as

$$V_{mag} = \sqrt{V_{real}^2 + V_{imag}^2} \tag{1.4}$$

$$\theta_v = tan^{-1} \frac{V_{imag}}{V_{real}} \tag{1.5}$$

Representations of a signal by DFT are best observed for periodic signals. But the performance is adversely affected for non-periodic signal such as electromagnetic transients. To reduce the effect of non-periodic signals on the DFT, the Short Time Fourier Transform (STFT) is used which assumes local periodicity within a continuously translated time window. This, however, locates the start time of the transient only to the specific window.

Kalman filter is another widely used technique for numerical protection of transmission line. The faulted voltage and current signals are modeled in state space, and phasor estimation is done using the Extended Kalman Filter (EKF). The estimated phasors are used for fault detection and location determination in distance relaying.

The fault signal contains fundamental and harmonics along with a decaying DC component and is represented by

$$Z_k = A_1 \, sin(kwT_s + \varphi) + A_2 \, sin(3kwT_s + \varphi) + ...$$
$$+ A_6 \, sin(13kwT_s + \varphi_{13}) + A_0 e^{-\alpha kT_S} \tag{1.6}$$

The discrete signal can be represented in state space as

$$x_{k+1} = F_k x_k \tag{1.7}$$

Where

$$x_k(1) = A_1 \cos\phi, \quad x_k(2) = A_1 \sin\phi, \quad x_k(3) = A_2 \cos\phi,$$
$$x_k(4) = A_2 \sin\phi ....,$$
$$x_k(11) = A_6 \cos\phi, x_k(12) = A_6 \sin\phi$$
$$x_k(13) = e^{-T_S}, \quad x_k(14) = A_0 e^{-kT_S} \tag{1.8}$$

The state transition matrix given by

$$F_k = \begin{bmatrix}
1 & 0 & 0 & 0 & 0 & 0 & 0 & 0 & 0 & 0 & 0 & 0 \\
0 & 1 & 0 & 0 & 0 & 0 & 0 & 0 & 0 & 0 & 0 & 0 \\
0 & 0 & 1 & 0 & 0 & 0 & 0 & 0 & 0 & 0 & 0 & 0 \\
0 & 0 & 0 & 1 & 0 & 0 & 0 & 0 & 0 & 0 & 0 & 0 \\
0 & 0 & 0 & 0 & 1 & 0 & 0 & 0 & 0 & 0 & 0 & 0 \\
0 & 0 & 0 & 0 & 0 & 1 & 0 & 0 & 0 & 0 & 0 & 0 \\
0 & 0 & 0 & 0 & 0 & 0 & 1 & 0 & 0 & 0 & 0 & 0 \\
0 & 0 & 0 & 0 & 0 & 0 & 0 & 1 & 0 & 0 & 0 & 0 \\
0 & 0 & 0 & 0 & 0 & 0 & 0 & 0 & 1 & 0 & 0 & 0 \\
0 & 0 & 0 & 0 & 0 & 0 & 0 & 0 & 0 & 1 & 0 & 0 \\
0 & 0 & 0 & 0 & 0 & 0 & 0 & 0 & 0 & 0 & 1 & 0 \\
0 & 0 & 0 & 0 & 0 & 0 & 0 & 0 & 0 & 0 & 0 & 1 \\
0 & 0 & 0 & 0 & 0 & 0 & 0 & 0 & 0 & 0 & 1 & 0 \\
0 & 0 & 0 & 0 & 0 & 0 & 0 & 0 & 0 & 0 & 0 & e^{-kT_s}
\end{bmatrix}$$

$$\tag{1.9}$$

The observation matrix is given by

$$G_k = [\sin(kwT_s) \quad \cos(kwT),$$
$$\sin(3kwT_s) \quad \cos(3kwT),$$
$$\sin(5kwT_s) \quad \cos(5kwT),$$
$$........\sin(13kwT_s) \quad \cos(13kwT),0,1]$$

$$(1.10)$$

Then the Kalman Filter algorithm is obtained as follows:

$$\widehat{x}_{k/k} = \widehat{x}_{k/k} + K_k(Z_k - H_k x_{k/k-1})$$

$$Z_k = H_k x_k \qquad (1.11)$$

where

$$H_k = \frac{\partial G}{dx}\bigg|_{k,k-1} = \begin{bmatrix} x(1)kT_s \cos(wkT_s) - x(2)kT_s \sin(wkT_s) \\ x(3)kT_s \cos(3wkT_s) - x(4)kT_s \sin(3wkT_s).... \\ x(11)kT_s \sin(13wkT_s) - x(12)kT_s \cos(13wkT_s) \\ 0 \\ 1 \end{bmatrix}. \qquad (1.12)$$

The Kalman filter gain K_k is obtained as

$$K_k = \widehat{P}_{K/K-1}H_k^T(H_k\widehat{P}_{k/k-1}H^T + R)^{-1} \qquad (1.13)$$

$$\widehat{P}_{k/k} = P_{k/k-1} - K_k H_k \widehat{P}_{k/k-1} \qquad (1.14)$$

$$\widehat{P}_{k+1/k} = P_{k/k} + Q \qquad (1.15)$$

where Q is the covariance matrix and R is the measurement noise covariance.

A. A. Girgis *et al.* [3] presented Kalman filter and adaptive Kalman filter based digital protection schemes for advanced series compensated line. The proposed technique uses the line current noise signals for fault location determination for line including Advanced Series Compensated (ASC) line. For fault not including the ASC, the fault current consists of are decaying DC, fundamental of steady state fault current and high frequency components. But for faults encountering ASC, the fault current constitutes non-fundamental decaying DC, odd harmonic due to Metal Oxide Varistor (MOV)

conduction, high frequency due to resonance between line capacitance and inductance, and fundamental component of steady state fault current. Thus after fault detection, the adaptive Kalman filter begins to operate on all the three phase fault currents. From the weight factors, the fault classification and location with respect to ASC are achieved. After the fault classification, the impedance to the fault point is determined. If the impedance is less than the relay setting for three consecutive samples, then the relay should send the tripping signal to the circuit breaker.

The research work presented using wavelet–transform [15] describes the multi-resolution property of the Wavelet Transform in time and frequency domain and effect of different parameters on its performance. The technique includes decomposition and reconstruction of the faulted signal to extract the low-frequency components of the signal. This provides a new technique to isolate the impulse and high frequency component and extract fundamental frequency component using a small data window. In another approach, Omar A. S. Youssef [16] proposed a combined fuzzy-logic wavelet based technique for identifying faulty phase in faulted power system network. The technique uses only fault currents, which are processed through Wavelet Transform to remove the high frequency harmonics and non-harmonic components. The ratios of amplitude and phase angle of the line currents are fuzzified and the corresponding rule is fired from the designed rule base to classify the type of fault. The proposed classifier was tested for the fault type under variation in fault resistance, location, source impedance etc.

A.H.Osman *et al.* [17] presented another wavelet based protection scheme for digital relaying. The technique includes preprocessing the fault voltage and current signal samples through Wavelet Transform and corresponding coefficients are extracted around fundamental frequency band. The technique used the detailed coefficients at level-1 for fault detection in the faulted power network. The phasor estimation (amplitude and phase) is done using the approximate coefficients at level-2 decomposition which are used to compute the impedance to the fault point from the relaying location.

The magnitude of the measured signal is found out as

$$Y = \frac{|1||A_{2S}|}{|A_{2R2}|} \tag{1.16}$$

where A_{2R2} and A_{2S} are the approximate coefficients of the constructed signal and measured signal respectively. Similarly the phase can be found out by

$$\theta = \cos^{-1} \frac{(A_{2R1}.A_{2S})}{|A_{2R1}||A_{2S}|}$$

(1.17)

where A_{2R1} and A_{2S} are the approximate coefficients of the reference signal and measured signal, respectively.

Another wavelet based multi-resolution analysis was presented by D.Chnada *et al.* [18], for fault location determination. The three phase fault currents are processed through Wavelet Transform and Cubic interpolation technique is used for fault location determination. The effects of fault inception angle and resistance are examined with wide variations. W. Chen *et al.* [19] proposed an ultra high speed directional transmission line protection scheme which using Wavelet Transform. The traveling wave and its sign are identified using the theory of singularity of the Wavelet Transform.

The neural network based protection scheme proposed by Whei-Min Lin *et al.* [20] includes fault classification based on Radial Basis Function Neural Network with orthogonal least square (OLS) methods. The OLS learning procedure generates the RBF network whose hidden layer is smaller than that of the RBF network with randomly selected centers. It uses fault voltage and current signal samples as input to the network and provides information regarding the faulty phase involved in the fault process.
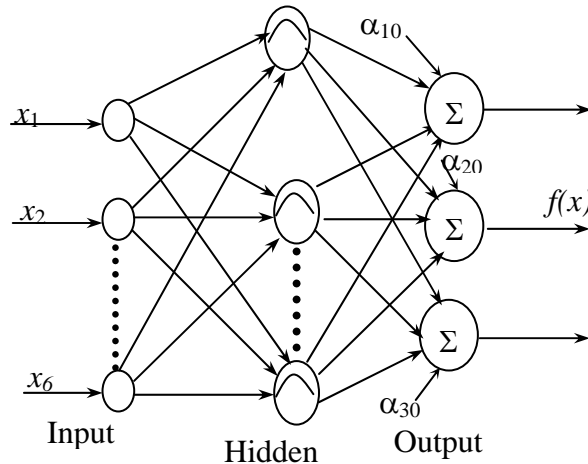
Fig. 1.1 Neural Network

P K. Dash *et al.* [21] proposed a novel Fuzzy Neural Network (FNN) for fault classification and location determination. In the proposed approach, a simple neural network is used to implement a fuzzy rule based classifier of a power system. The FNN model is seen in neural viewpoint for training and fuzzy viewpoint is utilized to gain into the system and to simplify the model. The rules required are determined by the data itself. Pruning strategy is incorporated to eliminate the redundant rules and justification neurons. The peaks and the DC component are estimated by the Extended Kalman Filter form the sampled data. The FNNS are trained and tested for fault classification and location separately and provides accurate results for wide variations in operating conditions.

The Kalman filtering approach finds its limitation, as fault resistance can not be modeled and further it requires a number of different filters to accomplish the task. Also, in the fault classification and location tasks, the neural networks cannot produce accurate results due to the inaccuracies in the input phasor data. Also the above approaches are sensitive to system frequency-changes, and require large training sets and training time and a large number of neurons. The phasor estimation proposed using Wavelet Transform gets affected in presence of noise. Thus the impedance to the relaying point is not so accurate leading to overreach or underreach phenomena.

Another new technique proposed by C.E de M Pereira *et al.* [22], calculates the fault location based on steady state measured phasors in local terminal. The remote end pre-fault voltage and currents are calculated using local terminal pre-fault voltage and currents. Thus the fault voltage can be calculated from the fault current and admittance matrix. The fault type classification information is extracted form the admittance matrix. Then the fault distance is calculated which is the function of the measured and extracted voltage phasors. The main advantage is that it uses pre-fault current avoiding the CT saturation effect due to fault condition.

Fault location algorithm for multi-terminal transmission line is proposed by S. Brahma [23], uses the synchronized voltage and current measurements form all terminals. Using the positive sequence components, it estimates the positive sequence impedance. From the impedance matrix, the fault section and fault location are determined. Parallel transmission line fault location algorithm is proposed by G. Song *et al* [24] using

differential component net. The proposed method based on the fact that the difference between voltage distributions, calculated from two terminal currents is the smallest at the fault point.

Differential protection for power transformer proposed by Omar A.S. Youssef [25] uses Wavelet Transform for discriminating inrush current form internal fault. The proposed technique detects the inrush current by extracting the wavelet componets contained in the three line currents using data window less than half power frequency cycle. P L.Mao *et al.* [26] used combined Wavelet Transform and neural network for differential protection. Wavelet Transform is used to decompose the differential signal of the power transformer and spectral energies of the wavelet detailed coefficients are calculated at required decomposition level. These extracted features are used to train and test the neural network to distinguish inrush current form internal fault current.

The existing differential protection using 2nd harmonic restraint works successfully when the 2nd harmonic component differs widely in inrush current compared to internal fault. But the same algorithm fails when the 2nd harmonic component is same in inrush current as well as in internal faults.

After reviewing the above techniques and their limitations, new distance and differential protection schemes are proposed using time-frequency analysis and pattern recognition approach. The proposed approach effectively exploits the time-frequency information of the faulted signals to provide improved solution to power system protection. The following sections deal with the objectives and outline of the proposed thesis.

1.2 Objectives of the Thesis

The proposed approach presents a novel technique for distance and differential protection, using time-frequency analysis and pattern recognition approach. The time-frequency transform such as S-Transform [27-29] and its variants are used for fault detection, classification and location determination for transmission lines. The S-Transform is an extension of Wavelet Transform which possesses superior property over the latter as the moving functions are fixed with respect to time axis while the localizing scalable Gaussian window dilates and translates. The window function is inversely

proportional to the frequency content of the signal. Phase spectrum obtained in this transform is always with respect to fixed reference point and the real and imaginary spectrum can be localized independently. Such a transform with moving and scalable localizing Gaussian window, therefore, provides excellent time localization property for different signals.

Another variant of the S-Transform known as Hyperbolic S-Transform (HS-Transform) [30] is also used for fault detection, classification and location determination of the transmission line, where a pseudo-gaussian hyperbolic window is used to provide better time and frequency resolutions at low and high frequencies unlike the S-Transform using the Gaussian window. Here the hyperbolic window has frequency dependence in its shape in addition to its width and height. The increased asymmetry of the window at low frequencies leads to an increase in the width in the frequency domain, with consequent interference between major noise frequencies.

In another study, a complex windowed S-Transform [31] is used to distinguish between inrush and fault currents in power transformer. The phase function modulates the frequency of the Fourier sinusoid to give better time-frequency localization of the time series. That means if the time series contains a specific asinusoidal waveform that is expected at all scales, then the complex gaussian window can give better time-frequency resolution of event signatures than the un-modulated, real valued gaussian window of the original signal.

Attempt is made to develop a differential equation based fault locator to find out fault location for transmission line including FACTS. The line inductance to the fault point is found out from the sending and receiving end faulted current and voltage information which directly reflects the fault location. A thorough investigation is made to test the proposed method with wide variations in operating conditions of the power system network including FACTS.

Machine intelligence technique such as Support vector machine (SVM) [32-34] is trained and tested with faulted current and voltage signal samples to design accurate and fast fault classifier for protective relaying. The SVM is a relatively new computational learning method based on the statistical learning theory. In SVM, original input space is mapped into a high-dimensional dot product space called a feature space, and in the

feature space the optimal hyperplane is determined to maximize the generalization ability of the classifier. The optimal hyperplane is found by exploiting the optimization theory, and respecting insights provided by the statistical learning theory. SVMs have the potential to handle very large feature spaces, because training of SVM is carried out so that the dimension of classified vectors does not have as distinct influence on the performance of SVM as it has on the performance of conventional classifiers. That is why it is noticed to be especially efficient in large classification problems.

The main objectives of the thesis are to:

1. Design robust and fast acting protection schemes to detect, classify and locate the fault in single circuit and double circuit line using S-Transform and its variations.

2. Design SVM based fault classifier for fault classification, ground detection and section identification for transmission line including FACTS.

3. Investigate the performance of the differential equation based fault locator for transmission line including FACTS.

4. Develop a pattern recognition approach for faulty phase and faulty line selection for line including FACTS using S-Transform and Wavelet multi-resolution analysis.

5. Develop a new pattern recognition technique to distinguish inrush current and fault in case of power transformer using time-frequency analysis.

1.3 Thesis Organization

The thesis is organized as follows

Chapter-1

Chapter-1 gives a brief introduction of the problem associated with the power system, both in transmission line and power transformer. The present status of available techniques and the limitations are discussed. The objectives and contributions of the thesis are highlighted.

Chapter-2

Chapter-2 focuses on the distance protection of transmission line using time-frequency analysis and pattern recognition approach. The proposed research uses S-Transform and its variants for protection of single circuit and double-circuit transmission lines. The techniques include fault detection, classification and impedance calculation from the estimated phasors.

Chapter-3

Chapter-3 describes the machine intelligence technique such as Support Vector Machine (SVM) for distance relaying. The protection scheme is designed for distance relaying of transmission line including thyristors controlled series capacitor (TCSC). Also single circuit transmission line is tested using the same technique with wide variations in operating conditions and improved results are found out.

Chapter-4

Chapter-4 investigates the performance of differential equation approach for protection of transmission line including unified power flow controller (UPFC). The proposed method includes designing a differential equation based fault locator to calculate the location of the fault from relaying point. The fault location is calculated for faults before and after UPFC in the transmission line.

Chapter-5

Chapter-5 presents the protection of compensated line using time-frequency analysis. The proposed method uses S-Transform and Wavelet multi resolution analysis for faulty phase selection and fault section identification in transmission line including TCSC. Different computed spectrums resulted from S-Transform clearly demonstrates the potential of the proposed approach.

Chapter-6

Power transformer protection using complex windowed S-Transform is discussed in Chapter-6. S-Transform with complex window is used discriminate inrush current and fault. An *energy index* is found out to distinguish the two events which provide better protection measures compared to existing differential protection based on 2nd harmonic restraint.

Chapter-7

This chapter provides comprehensive summary and conclusions of all different approaches for transmission line and power transformer protection.

1.4 Summary

In this thesis, some important issues of power system faults and respective protection measures are addressed. Novel techniques of distance and differential protection schemes using time-frequency analysis and pattern recognition approach are presented. S-Transform and its variants are applied to find effective solution to distance protection problems over conventional relaying techniques. Also machine intelligence technique such as Support Vector Machine is used to develop fault classifier and ground detector for distance relaying of transmission line including TCSC. A differential equation based fault locator is presented for transmission line including UPFC. Both general transmission line and line including FACTS (TCSC, UPFC) are extensively studied and improved results are derived. Also a new technique for power transformer protection is designed using time-frequency analysis and pattern recognition approach. Some of the techniques are tested for real time systems which show the robustness of the proposed protection schemes.

Chapter-2

Time-frequency Transform and its variations in distance relaying

2.1 Introduction

A powerful time-frequency analysis known as S-Transform that has found applications in geosciences and power engineering [27-30, 35], is used for fault detection, classification and location in distance relaying. The S-Transform is an invertible time-frequency spectral localization technique that combines elements of Wavelet Transforms and short-time Fourier transform. The S-Transform uses an analysis window, whose width is decreasing with frequency providing a frequency dependent resolution. This transform may be seen as a continuous Wavelet Transform with a phase correction. It produces a constant relative bandwidth analysis like wavelets while it maintains a direct link with Fourier spectrum. The S-Transform has an advantage in that it provides multiresolution analysis while retaining the absolute phase of each frequency. This has led to its application for detection and interpretation of events in a time series like the power quality disturbances [35]. Further to tackle the effects of noise and distortions, the original signal samples are passed through a Hanning window before they are processed by the S-Transform.

2.2 S-Transform for faulted power network

The S-Transform [29] has an advantage in that it provides multiresolution analysis, which retaining absolute phase of each frequency. This has led to its application for time series analysis and pattern recognition in power networks and other engineering systems. The expression for S-Transform of a continuous signal $x(t)$ is given as

$$S(\tau, f) = \int_{-\infty}^{\infty} x(t) \left\{ \frac{|f|}{\alpha \sqrt{2\pi}} \right\}. \exp\left(\frac{-f^2(\tau-t)^2}{2\alpha^2} \right). \exp(-2\pi i f t) dt \qquad (2.1)$$

Here f is the frequency, t is the time and τ is a parameter that controls the position of the gaussian window on the t-axis.

The factor α controls the time and frequency resolution of the transform and lower α means higher time resolution. The converse is true if higher value of α is chosen for the analysis. A suitable value of α, however, lies between $0.2 \leq \alpha \leq 1$. A value of 0.7 gave the best result for fault analysis.

Also
$$\int_{-\infty}^{\infty} S(\tau, f) d\tau = X(f) \tag{2.2}$$

where $X(f)$ is the Fourier transform of $x(t)$.

The discrete version of the continuous S-Transform is obtained as

$$S(j,n) = \sum_{m=0}^{N-1} X(m+n).\exp\left(\frac{-2\pi^2 m^2 \alpha^2}{n^2}\right).\exp(i2\pi mj) \tag{2.3}$$

and $j = 1.........N-1$, $n = 0, 1...N-1$.

Here j and n indicate the time samples and frequency step, respectively and

$$X(n) = \frac{1}{N}\sum_{k=0}^{N-1} x(k).\exp(-i2\pi nk) \tag{2.4}$$

where $n = 0, 1........., N-1$

Computation of $X(m+n)$ is done in a straight forward manner from (2.4). The Fourier spectrum of the gaussian window at a specific n (frequency) is called a voice gaussian and for a frequency $f_1(n_1)$, the voice is obtained as

$$S(j,n_1) = A(j,n_1).\exp(j\phi(j,n_1)) \tag{2.5}$$

Hence the peak value of the voice is

$$\max(S(j,n_1)) = \max(A(j,n_1)) \tag{2.6}$$

and

$$\phi(j,n_1) = a\tan\left\{\frac{imag(S(j,n_1))}{real(S(j,n_1))}\right\} \tag{2.7}$$

The energy E of the signal is obtained from S-Transform as

$$E = \left\{abs(S(j,n))\right\}^2 \tag{2.8}$$

From the above analysis it is quite evident that not only S-Transform localizes the faulted event but also peak amplitude and phase information of the voltage and current

signals can be obtained, which are required for impedance trajectory calculations. The signal energy obtained from S-Transform can be used to detect and classify the fault on the transmission line. To reduce calculations, only the fundamental voice of the S-Transform can be used as

$$E_{fund} = abs(S(j, n_{fund}))^2 \tag{2.9}$$

The succeeding sections describe the detailed simulation study of the distance protection of single circuit and double circuit transmission lines using the approach presented in the above formulations.

2.2.1 Distance relaying of single-circuit transmission line

The proposed protection scheme consists of three basic parts. The first part includes the fault detection from the change in energy content of the S-Transform of the voltage and current signal. After fault detection, the impedance to the fault point is calculated from the estimated current and voltage phasors. The phasors are estimated from the S-matrix generated from S-Transform for respective faulted current and voltage signal with and without noise. The S-Transform provides accurate phasor estimation even with SNR 20 dB unlike Wavelet Transform, which is susceptible to noise. The last part includes the fault location determination using polynomial curve fitting with a devised index found out from the ratio of energy content of the faulted voltage and current signal.

The time taken for fault detection is half cycle (10 samples from fault inception) and the time taken for the impedance trajectory to enter the relay operating zone, is within half cycle (6-10 samples). Thus the total time taken for the fault detection and impedance trajectory to enter the relay operating zone is less than one cycle (20 samples) from the inception of the fault which shows the fastness of the proposed protection scheme.

2.2.1.1 System Studied
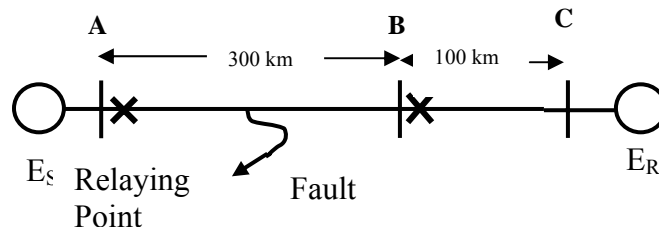
Fig. 2.1 Transmission Line Model

The transmission line model shown in Fig. 2.1 has been simulated using PSCAD (EMTDC) package. The network having two areas connected by the transmission line of 400 kV. The transmission line has zero sequence parameter Z (0) =96.45+j335.26 ohm and positive sequence impedance Z (1) =9.78+j110.23 ohm. $E_S = 400\,\text{kV}$ and $E_R = 400\angle\delta$ kV .The relaying point is shown in Fig.3.22, where data is retrieved for different fault conditions. There are two sections AB and BC of the transmission line. The fault within section BC will be considered as external fault to the relay at A. The sampling rate chosen is 1.0 kHz at 50 Hz frequency. There are 20 samples per cycle.

The S-Transform is applied to the faulted current and voltage signal to generate the S-matrix. From the S-matrix, change in energy is calculated for fault detection and phasors are estimated for impedance calculation. The S-Transform is applied to the data half cycle ahead of fault inception and half cycle during the fault. The change in energy detects the faulty phase involved. Thus, the fault detection is achieved within half cycle of the fault inception. The following section deals with the fault detection and impedance calculation.

2.2.1.2 Simulation Results

(a) Faulty Phase detection

For fault detection, the change in energy of the corresponding voltage and current signal is computed from the spectral energy content of the S-Transform coefficients (S-matrix). Change in the signal energy of the S-Transform contour are obtained as

$$ce = E_f - E_A = \left\{abs(\,h_f\,)\right\}^2 - \left\{abs(\,h_n\,)\right\}^2 \tag{2.10}$$

where h_f is the S-matrix coefficients for post-fault current signal and h_n is the S-matrix coefficients for pre- fault current signal. Change in energy of the signal is calculated by deducting the energy content of the signal half cycle ahead of the fault inception from the energy content of S-Transform of the signal half cycle during the fault. The change in energy of the S-Transform of the current and voltage signal clearly identifies the faulty

phases from un-faulted ones. Table-2.1 and Table-2.2 depict the change in energy for different types of fault for different location, fault resistances, variations in the source impedance and different inception angles. A threshold value can be set above which the line is considered as faulty.

Table-2.1 Change in energy for different fault conditions

Faults	Voltage			Current		
	a	b	c	a	b	c
a-g (R_f =0 ohm,δ=30° at 10%)	3.98	0.15	0.03	28.64	1.02	0.98
a-g (R_f =100 ohm,δ=30° at 10%)	2.51	0.21	0.23	22.64	1.02	0.68
b-g (R_f =100 ohm, δ=45° at 10%)	0.16	1.80	0.19	1.12	18.32	2.15
ab-g (R_f =100 ohm, δ=60° at 30%)	1.98	2.21	0.04	19.36	17.36	1.04
ab (R_f =0 ohm, δ=60° at 50%)	3.25	3.78	0.15	26.65	21.64	0.57
ab (R_f =10 ohm, δ=90° at 50%)	2.69	2.54	0.35	26.35	19.68	0.25
bc(R_f =10 ohm, δ=45° at 70%)	0.04	3.12	3.45	0.08	26.57	26.41
abcg(R_f =150 ohm , δ=30° at 70%)	1.65	1.39	1.45	12.39	16.45	15.87
abcg(R_f =200 ohm, δ=60° at 90%)	1.55	1.69	1.23	11.69	10.98	14.25
abcg(R_f =150 ohm, δ=90° at 70%) with source impedance changed(increased 10%)	1.11	1.23	1.09	9.23	8.25	7.26
abcg (R_f =150 ohm at 70%) with source impedance changed (increased 30%)	0.89	0.99	0.84	8.36	10.98	9.99

Table-2.2 Change in energy for different fault conditions with SNR 20 dB

Faults	Voltage			Current		
	a	b	c	a	b	c
a-g(R_f =0 ohm,δ=30° at 10%)	3.42	0.11	0.01	26.69	1.03	0.58
a-g(R_f =100 ohm,δ=30° at 10%)	2.54	0.22	0.14	20.36	0.98	1.55
b-g(R_f =100 ohm, δ=45° at 10%)	0.11	1.58	0.14	1.02	16.98	2.11
ab-g(R_f =100 ohm, δ=60° at 30%)	1.69	1.98	0.01	18.36	16.35	0.98
ab(R_f =0 ohm, δ=60° at 50%)	3.12	3.45	0.01	25.64	20.36	0.41
ab(R_f =10 ohm, δ=90° at 50%)	1.69	1.89	0.03	19.62	16.68	0.01
bc(R_f =10 ohm, δ=45° at 70%)	0.02	2.98	3.45	0.03	25.36	24.65
abcg(R_f =150 ohm, δ=30° at 70%)	1.45	1.51	1.59	11.36	15.68	14.69
abcg(R_f =200 ohm, δ=60° at 90%)	1.49	1.52	1.23	11.69	10.98	14.25
abcg(R_f =150 ohm, δ=90° at 70%) with source impedance changed (increased 10%)	1.10	1.21	1.11	8.96	7.98	6.98
abcg (R_f =150 ohm at 70%) with source impedance changed (increased 30%)	0.79	0.89	0.98	7.98	9.68	8.69

From Table-2.1 and Table-2.2 it is clearly seen that the faulty phase has maximum change in energy compared to un-faulted phase. For a-g fault with fault resistance R_f =0 ohm, inception angle δ=30° at 10% of the transmission line, the change in energy in the voltage signal are 3.98, 0.15 and 0.03 for a, b, c phases, respectively. Similarly the change in energy in the current signal are 28.64, 1.02 and 0.98 for a, b, c phases, respectively. Similar observation for a-g fault with R_f =100 ohm and δ=30° at 10% the line, the change in energy in the voltage signal are 2.51, 0.22 and 0.23 for a ,b, c phases, respectively. Similarly the change in energy in the current signal are 22.64, 1.02 and 0.68 for a, b, c phases, respectively. For a-b fault with R_f =0 ohm, δ=60°   at 50% of line, the change in energy in the voltage signal are 3.25, 3.78 and 0.15 for a, b, c phases, respectively. Similarly the change in energy in the current signal are 26.65, 21.64 and 0.57 for a, b, c phases, respectively. The faulty phase will have a higher change of change in energy than the un-faulted one and this criterion is used to detect the faulty .The change in energy for different types of fault with various operating conditions with different fault resistance, source impedance and inception angles are shown in the Table.2.1. Table.2.2 shows the change in energy for different types of faults with various operating conditions with noise up to SNR 20 dB.

It is found that the change in energy of the signals with SNR 20 dB produces very accurate results for fault detection. Thus the fault is detected very accurately within half cycle (10 samples) from the inception of the fault. After the fault detection, the impedance to the fault point is calculated. For impedance calculation, the phasor estimation is done for both voltage and current signal from the derived S-matrix of the faulted voltage and current signal. The next section deals with the phasor estimation and impedance calculation.

(b) Phasor Estimation

The amplitude and phase of the faulted current and voltage signals are calculated from the S-matrix. After calculating the S-matrix, the amplitude of the signal is found out by

$$Amplitude = \max(abs(S)) \tag{2.11}$$

Where *'S'* is the S-Transform matrix, *'abs'* is the absolute value and *'max'* is the maximum one.

The S-matrix provides the frequency-amplitude relationship. From the frequency-amplitude relationship, the voice frequency at which maximum amplitude occurs is found out. The instantaneous phase of the signal is found out at the exact frequency voice where amplitude is maximum. The S-matrix provides the coefficients in complex domain at a particular voice frequency. Then the phase can be calculated as

$$ph = a\tan(imag(S)/real(S)) \tag{2.12}$$

Figs. 2.2, 2.3, 2.4 and 2.5 show the magnitude and phase of the fault current and voltage for a single-line-to-ground fault (a-g) at 10% of the line length without noise and with noise (SNR=20 dB), respectively. From the figures it is found that the peak magnitudes and phase angle of the voltage and current signals are hardly influenced by the presence of 20 dB noise.
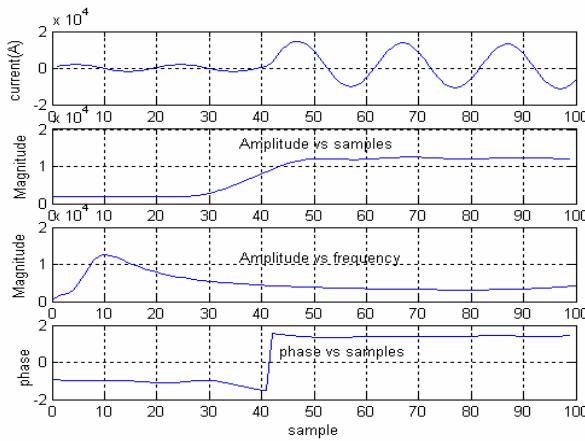
Fig. 2.2. Magnitude and phase of current at a-g fault at 10 %, R$_f$ =20ohm

Fig. 2.4.Magnitude and phase of voltage at a-g fault at 10 %, R$_f$ =20 ohm
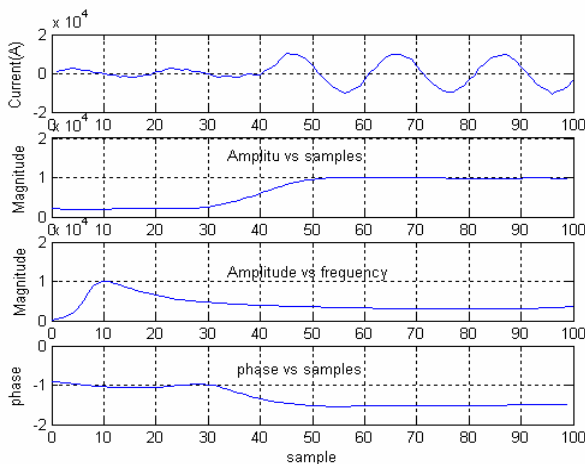
Fig. 2.3.Magnitude and phase of current at a-g fault at 10 %, R$_f$ =20ohm with SNR 20 dB
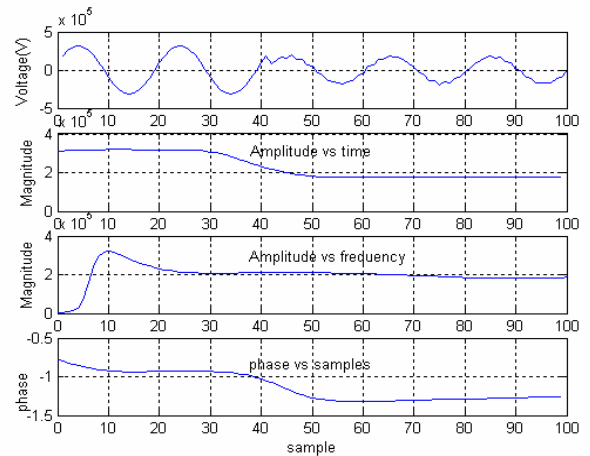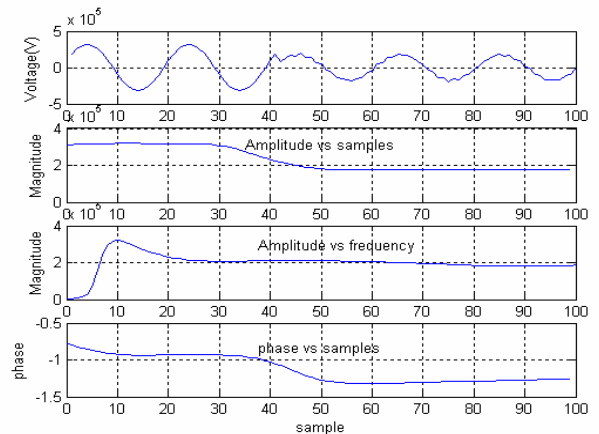
Fig. 2.5.Magnitude and phase of voltage at a-g fault at 10 %, R$_f$ =20 ohm with SNR 20 dB

(c) Impedance Calculation

The impedance to the fault point is calculated by using the phasor information. The impedance trajectories (R-X plot) for different operating conditions are found out and the circuit breaker is tripped when the trajectory enters in to the relay operating zone and thus protects the line. The impedance is calculated [17] as follows:

1. For phase-earth fault

$$Z_{ph} = \frac{V_{ph}}{I_{ph}(1) + I_{ph}(2) + KI_{ph}(0)} \qquad (2.13)$$

where V_{ph} is the estimated amplitude of the phase voltage, $I_{ph}(1)$, $I_{ph}(2)$, $I_{ph}(0)$ are positive , negative and zero sequence currents of estimated amplitude. Factor 'K' is chosen as 0.7

2. For phase-phase fault

$$Z_{ab} = \frac{V_a - V_b}{I_a - I_b} \qquad (2.14)$$

where V_a and V_b are estimated voltage amplitude and I_a and I_b are estimated current amplitude.

(i) Fault within the protected zone (Section AB)

From the above impedance trajectory it is clearly seen that in case of faults the trajectory come within the relay operating zone. Fig.2.6 through Fig.2.17 show the impedance trajectory for L-G, LL-G, LL, LLL-G faults with different operating conditions. Fig. 2.6 through Fig. 2.10 shows the impedance trajectory for different kinds of faults at 10% of the line. Fig. 2.11 shows the impedance trajectory for fault at 50% of the line. Fig. 2.12 through Fig. 2.15 shows the impedance trajectory for different kinds of faults at remote end of the line (90% of line length). It is seen that the impedance trajectory for the fault at remote end of the line also enters the relay operating zone within 10 samples of fault detection. It is seen that in Fig. 2.6 for LLL-G fault, the trajectory comes within the tripping area of the relay within 6 samples, and this indicates the fastness of the proposed algorithm.

Also in case of faults with high fault resistance, the proposed method gives accurate result. Fig. 2.7 and Fig. 2.11 show the impedance trajectory for faults with fault

resistance of 50 ohm and 100 ohm, respectively. It is found that the impedance trajectory enters within the tripping zone of the relay within 9 samples from the fault detection in case of fault with fault resistance 100 ohm.

The impedance trajectory is found out for the charging condition (steady state) of the line without fault. Fig. 2.16 shows the impedance trajectory for charging condition and the impedance trajectory is away form the tripping area of the relay, which doesn't isolate the line under consideration. From the above results, it is found out that the impedance trajectory enters in the relay operating zone within 10 (6-9 samples) samples after the fault detection. The total time taken for the protection scheme is 20 samples or one cycle (10 samples for fault detection and 10 samples for impedance trajectory to enter the relay zone) from the inception of fault.

(ii) External faults (Section BC)

The fault in the section BC is considered as external fault for the relay at 'A'. Fig. 2.17 shows the impedance trajectory. The comparison of the impedance trajectory for the faults within section AB(50% of the line AB)) and within section BC(20% of line BC) clearly shows that in case of faults in section 'BC', the trajectory doesn't come inside the zone-1 tripping area of relay 'A', but it enters in the zone-2 tripping area of the relay at 'A'. This indicates that for the external fault, the relay at 'A' acts as a back-up protection scheme. The relay at 'B' will provide primary protection for any faults within the section BC.
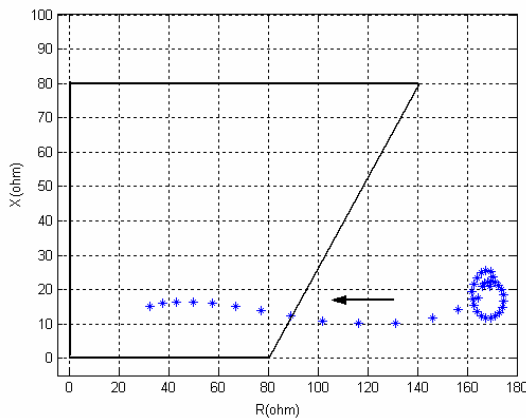
Fig. 2.6 R-X trajectory for abc-g (LLL-G) fault at 10% of line with R_f =20 ohm
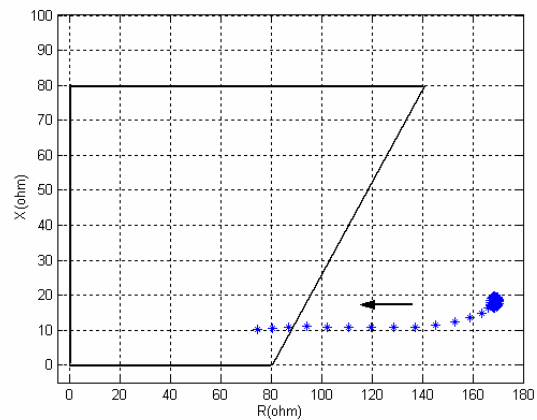
Fig. 2.7 R-X trajectory for abc-g (LLL-G) fault at 10% of line with R_f =50 ohm
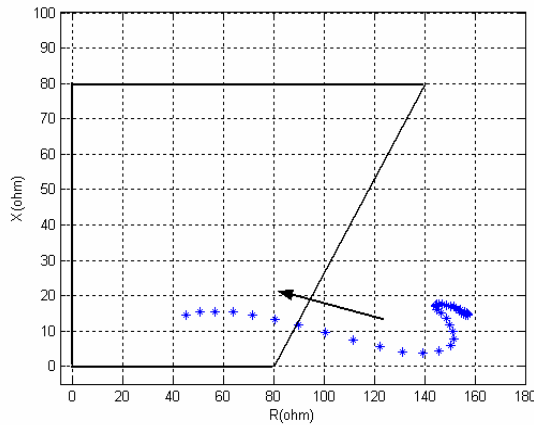
Fig. 2.8 R-X trajectory for a-g(L-G) fault at 10% of line with R$_f$ =20 ohm
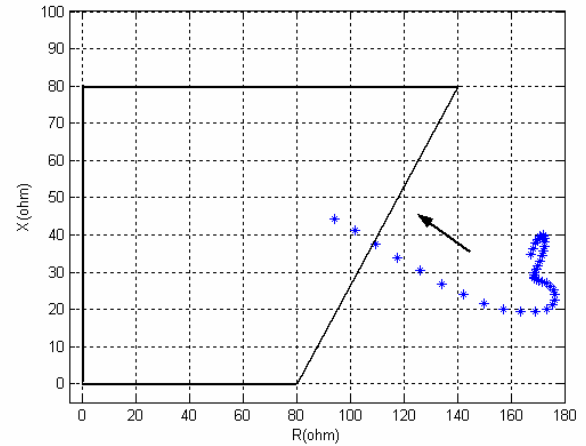
Fig. 2.11 R-X trajectory for abc-g(LLL-G) fault at 50% of line with R$_f$ =100 ohm
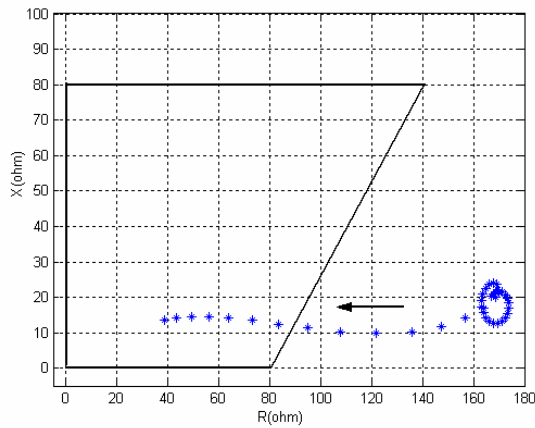
Fig. 2.9 R-X trajectory for ab-g(LL-G) fault at 10% of line with R$_f$ =20 ohm
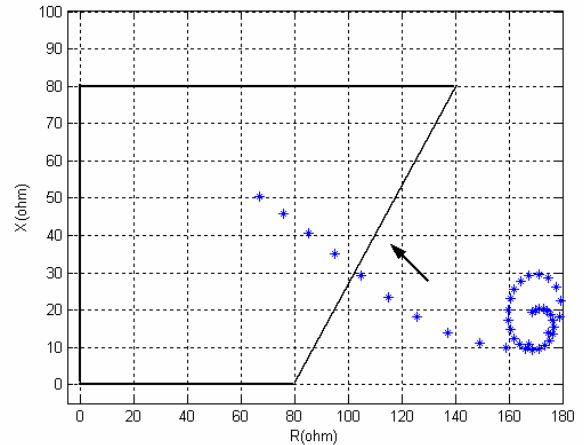
Fig. 2.12 R-X trajectory for abc-g (LLL-G) fault at 90% of line with R$_f$ =50 ohm
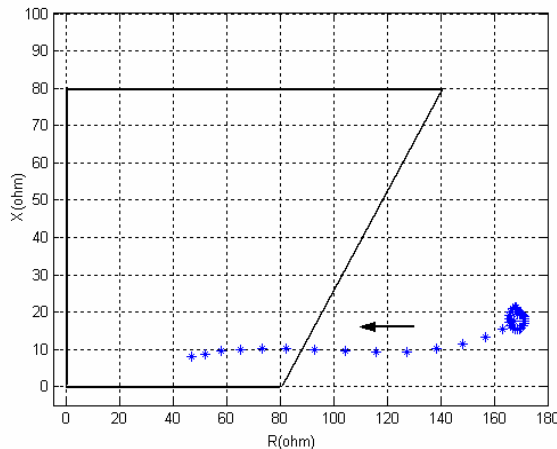
Fig. 2.10 R-X trajectory for b-phase at a-b (LL) fault at 10% of line with R$_f$ =20 ohm
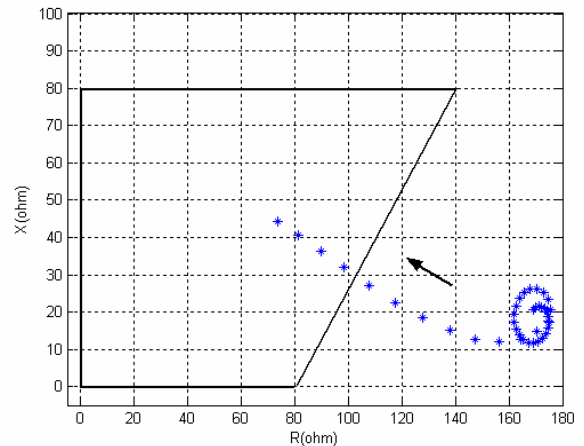
Fig. 2.13 R-X trajectory for ab-g(LL-G) 90% of line with R$_f$ =50 ohm
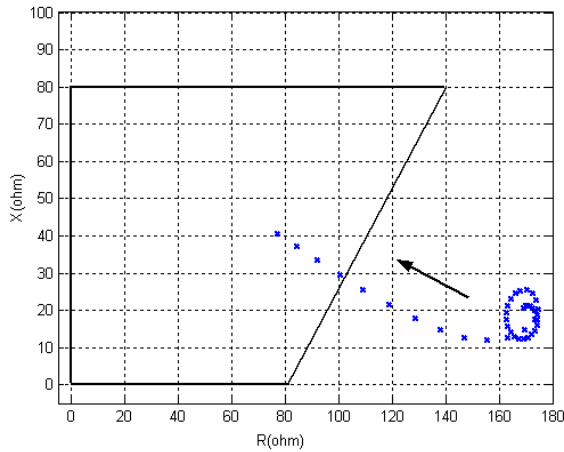
Fig. 2.14 R-X trajectory for ab (LL) 90% of line with R_f =50 ohm
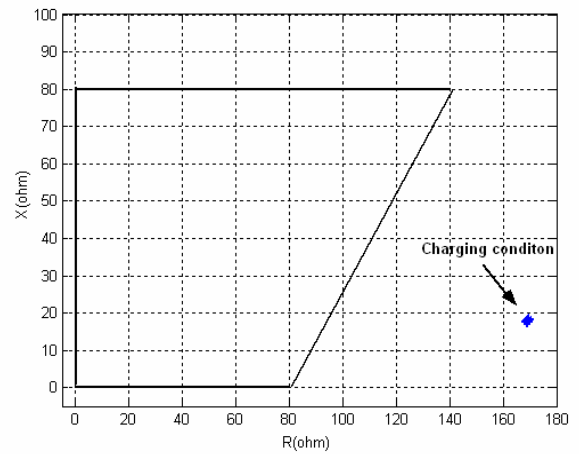
Fig. 2.16 R-X trajectory for the line in charging condition without fault.
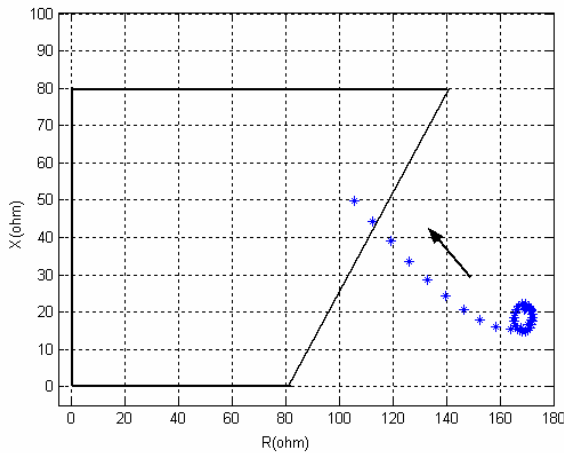
Fig. 2.15 R-X trajectory for ab (L-G) 90% of line with R_f =100 ohm
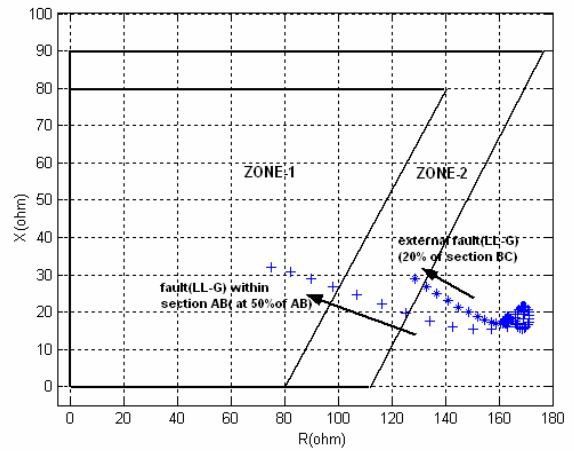
Fig. 2.17 R-X trajectory comparison for L-G fault with R_f =50 ohm within section AB (50%) and fault in section BC (10%) seen by the relay at 'A'.

2.2.1.3 Fault Location

The proposed scheme also includes the fault location determination from the relaying point. In the proposed work polynomial curve fitting is used for finding out fault location. The curve fitting is done on a proposed *index*.

$$index = \frac{|E_V|}{|E_I|} \tag{2.15}$$

where E_V and E_I are spectral energy of the S-Transform of the faulted voltage and current signal of half cycle from the inception of fault for different operating conditions. The *index* is calculated at different location (10%, 20%, 30%, 50%, 70%, and 90%) with different fault resistance (10 ohm to 200 ohm), source impedance and incident angles. The polynomial used here is

$$y = a_0 + a_1 x + a_2 x^2 + a_3 x^3 + a_4 x^4 + a_5 x^5 \qquad (2.16)$$

where 'y' is represents the location and 'x' represents the *index* as defined earlier. The 5th degree polynomial is derived from the respective curve fitting.

The coefficients of the polynomial are found out for each curve fitting based on data (*index*) with different operating conditions like different fault resistance, incident angles, changed source impedance. The mean values of these corresponding coefficients are determined to form an optimized polynomial to be used as fault locator which determines the fault location from the relaying point. After the polynomial is ready, the *index* for random location with different operating conditions is used as input to get the exact fault location. The error in fault location is given as

$$error(\%) = \frac{\left|actual \quad dis\tan ce - calculated \quad dis\tan ce\right|}{protected \quad line \quad length} * 100 \qquad (2.17)$$

For finding the polynomial coefficients for fault location, different fault data sets are used for curve fitting. The total number of fault cases simulated is 800, and 500 cases are used for finding corresponding polynomial coefficients for each curve fitting based on data (*index*) with different operating conditions like different fault resistance, incident angles, changed source impedance . The mean values of the corresponding coefficients are then found out to get the optimized polynomial. The polynomial is tested for the rest 300 cases (*index*) with various operating conditions. Table-2.3 through Table-2.6 provides the location calculation for L-G, LL-G, and LL and LLL-G faults at various conditions. The polynomial has been tested for other power networks with different operating conditions. Maximum error is 2.63% in LLL-G fault at 15% line length with fault resistance of 10

ohm and minimum 0.25% in LL at 95% of line length with fault resistance of 200 ohm faults, respectively.

Table-2.3 Fault Location for L-G faults

Distance (%)	Fault Resistance (R_f)	Error (%)
15	10	1.29
	200	2.10
35	10	0.98
	200	1.23
55	10	1.14
	200	1.28
75	10	0.99
	200	1.03
95	10	1.42
	200	1.47

Table-2.4 Fault Location for LL-G faults

Distance (%)	Fault Resistance(R_f)	Error (%)
15	10	1.36
	200	1.41
35	10	0.98
	200	1.01
55	10	1.23
	200	1.25
75	10	0.98
	200	1.05
95	10	0.96
	200	0.99

Table-2.5 Fault Location for LL faults

Distance (%)	Fault Resistance(R_f)	Error (%)
15	10	2.25
	200	2.32
35	10	1.23
	200	1.05
55	10	1.52
	200	0.99
75	10	0.64
	200	0.84
95	10	0.67
	200	0.25

Table-2.6 Fault Location for LLL-G faults

Distance (%)	Fault Resistance(R_f)	Error (%)
15	10	2.63
	200	1.63
35	10	2.12
	200	0.38
55	10	1.11
	200	1.56
75	10	0.99
	200	0.67
95	10	0.87
	200	0.95

2.2.2 Distance relaying of double-circuit transmission line

Transmission line protection is a key issue in power system network operation. Generally distance protection algorithm is used to protect transmission lines under different fault conditions. Distance relaying techniques based on the measurement of the impedance at the fundamental frequency between the fault location and the relaying point have attracted wide spread attention. Impedance is calculated from the phasor values of voltage and current signals retrieved at the relaying point. The value of the calculated impedance depicts whether the fault is internal or external to the protection zone. The above method works satisfactorily for the protection of single circuit lines. But when applied for the protection of parallel lines, the performance is affected by mutual coupling between two lines. In this work, however, compensation due to mutual coupling between lines is not included as it can lead to a first zone tripping for faults beyond the remote end of the parallel lines.

Different approaches have been attempted for protection of parallel lines by comparison of line currents of corresponding phases and positive and zero sequence current for fault detection. Also traveling wave based parallel line protection has already been presented [36] and impedance comparison between two lines has been used to detect the faulty phase [37]. As the voltage and current signals contain the DC offset and harmonics in comparison to the fundamental component, it affects accuracy of the phasor

estimation. Fourier Transforms, Differential equations, Waveform modeling, Kalman filters, and Wavelet Transforms are some of the techniques used for digital distance protection of transmission lines. Some of the recent papers in this area [38-39] have used only the sampled current values at the relaying point during faults for classification of fault types and distance calculations. Another pattern recognition technique based on Wavelet Transform has been found to be an effective tool in monitoring and analyzing power system disturbances including power quality assessment and system protection against faults. Although Wavelet Transform provides a variable window for low and high frequency components in the   voltage and current waveforms during faults, special threshold techniques are needed under noisy conditions. Moreover, the scalograms obtained from DWT and multiresolution signal decomposition presents only the average information of each frequency band rather than the detailed amplitude, frequency or instantaneous phase of the fundamental components that are essential for protection tasks.

Voltage and current signals are processed through the S-Transform to yield a complex S-matrix. From the S-matrix the spectral energy is calculated for the pre-fault cycle and post fault cycle. The pre fault and post fault boundary is detected by using the fault detector which uses a short data window (four samples) algorithm [40]. The final indication of the fault is only given when three consecutive comparisons give the difference more than a specified threshold value. After knowing the fault instance, the change in energy which is the difference between the spectral energy of pre-fault current signal for half cycle and post fault current signal for half cycle is calculated .The change in energy gives an indication of the occurrence of a fault in a particular phase or more than one phase. Second part includes finding out the difference in magnitude and phase of the estimated phasors to identify the faulty phase as well as the faulty line.

The proposed approach includes three main parts. In the first part, the faulty phase is detected by finding the change in energy of the prefault and post fault current signals. The second part describes the identification of the faulty phase and line simultaneously from the differences in magnitude and phase of the estimated current phasors. In the third part, the impedance to the fault point is calculated in case of similar types of faults on both the lines where the first and second approach fails substantially. The impedance trajectory is then obtained from the estimated voltage and current phasors clearly

showing the tripping characteristics of the relay for different fault conditions within the zone and also for the external faults. For providing a robust protection scheme for the parallel transmission lines, the change in energy and phasors estimation are then carried out under noisy conditions with SNR up to 20 dB and it is observed that in most cases S-Transform provides significantly accurate results.

2.2.2.1 Simulation Study
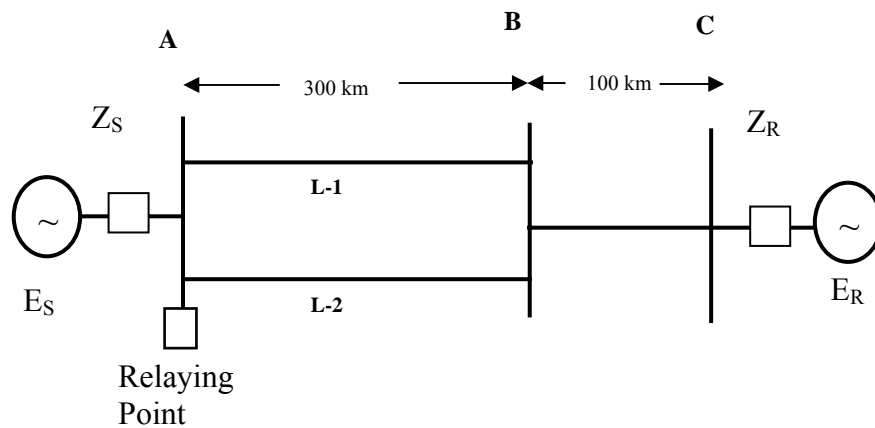
Fig. 2.18 Transmission Line Model

The model network shown in Fig. 2.18 has been simulated using PSCAD (EMTDC) software package. The relaying point is as shown in Fig. 2.18, where data is obtained for different fault conditions. The fault within the section BC will be considered as an external fault to the relay at A. The network consists of two areas connected by two 400 kV, 300 km long parallel transmission lines in section AB and an equivalent 100 km transmission line in section BC, respectively.

The parameters of the transmission line are:

Zero sequence impedance of each parallel line (Z_{L0}) = 96.45 + j 335.26 ohms

Positive sequence impedance of each parallel line (Z_{L1})=9.78 + j 110.23 ohms

Source impedances: $Z_S = 6 + j\,28.5$ ohms, $Z_R = 1.2 + j11.5$ ohms

Source voltages: $E_S = 400$ kV, $E_R = 400\angle\delta$ kV

where δ = load angle in degrees.

For fault studies, all the three line voltage signals and six line current signals of the parallel lines are sampled at a sampling frequency of 1.0 kHz with base frequency of 50 Hz. The fault detection algorithm is initiated by collecting a one cycle sampled data window for each signal. Based on a base frequency of 50 Hz and sampling frequency of 1 KHz, one cycle of the faulted voltage or current signal contains 20 samples. For each new sample that enters the window, the oldest sample is discarded, and difference between the two is noted for three consecutive samples. If this difference exceeds a threshold, the occurrence of a fault or an abnormal condition is assumed and the fault calculation algorithm starts from the point of occurrence of deviation of the data sample. The data window used for fault analysis comprises half cycle data backward and half cycle data forward from the detection of an abnormality. The S-Transform calculates the time-frequency contours from which the peak amplitude and phase of the voltage and current signals along with the change in energy values are derived.

2.2.2.2 Proposed Method and Simulation Results

(a) Faulty phase selection based on change in energy

The fault current signal is considered for faulty phase detection for different types of faults on one line or both the lines. . From the S-Transform matrix, the energy content of the respective current signals is calculated. Change in energy of the signal is calculated by deducting the energy content of S-Transform of the signal after half cycle of fault inception from the energy content of the signal half cycle before the fault inception. The change in energy of the S-Transform of the current signal clearly indicates the faulty phase from the un-faulted one. cei_{a1}, cei_{b1}, cei_{c1} are changes in energy for the three phases of line-1 and cei_{a2}, cei_{b12}, cei_{c2} are changes in energy for the three phases for line-2, respectively. Tables-2.7 and 2.8 depict the changes in energy for various types of faults for different locations, various fault resistances, source impedances, and different inception angles.

Change in the signal energy of the S-Transform contour are obtained as given in (2.10). The relay is set with all the six values of change in energy with a threshold value

and the calculated change in energy is compared with that of the threshold value and the faulty phase is identified when the calculated value exceeds the threshold value.

From Table-3.7, it is clearly seen that the faulty phase has maximum change in energy compared to un-faulted phases. For a-g fault with fault resistance R_f =20 ohms, inception angle $\delta=30°$ at 10% of the transmission line, cei_{a1}=26.40 while cei_{b1}=1.49, cei_{c1} =1.80, cei_{a2}=2.01, $cei_{b12,}$=1.09 and cei_{c2} =1.00, which clearly shows that there is a-g(line to ground fault) on line-1.The threshold value chosen here is 5.0 above which the phase is identified as faulty phase.

The change in energy values for different types of faults has been found out with various operating conditions including different   fault resistances, inception angles, source impedances, and different locations with all 11 types of shunt faults and is shown in Table-2.7 and 2.8. Also the proposed method is tested under noisy conditions when a white gaussian noise of SNR 20dB is added to the voltage or current signals. A higher value of change in energy for a particular phase indicates the occurrence of the fault in that phase. Table 2.8 shows the calculated energy values under noisy condition and the results given in this table shows that the proposed method provides satisfactory results under noisy conditions.

Table-2.7 Change in energy for different fault conditions

Faults	Change in energy					
	cei_{a1}	cei_{b1}	cei_{c1}	cei_{a2}	cei_{b2}	cei_{c2}
a-g on line-1(R_f =20 ohm,$\delta=30°$ at 10%)	26.40	1.49	1.80	2.01	1.09	1.00
b-g on line-2(R_f =100 ohm, $\delta=45°$ at 10%)	2.35	1.98	3.01	1.04	19.32	1.96
ab-g on line-2(R_f =30 ohm, $\delta=60°$ at 30%)	2.98	1.39	1.67	23.56	18.35	1.24
ab on line-1 and line-2(R_f =50 ohm, $\delta=90°$ at 50%)	22.12	18.36	0.02	20.36	19.38	0.01
bc on line-2(R_f =120 ohm, $\delta=45°$ at 70%)	0.01	0.14	0.18	0.03	16.89	15.25
abc on line-2(R_f =150 ohm, $\delta=30°$ at 70%)	1.23	0.25	1.05	12.49	16.24	14.89
abc-g on line-1 and line-2(R_f =200 ohm, $\delta=60°$ at 90%)	10.98	11.21	13.15	11.69	10.98	14.25
abc-g on line-1(R_f =150 ohm, $\delta=90°$ at 70%) with source impedance changed (increased 10%)	9.23	8.25	7.26	0.21	0.65	0.98
abc-g on line-2(R_f =150 ohm at 70%) with source impedance changed (increased 30%)	0.84	0.24	0.58	8.36	10.98	9.99

Table-2.8 Change in energy for different fault conditions with SNR 20 dB

Faults	Change in energy					
	cei_{a1}	cei_{b1}	cei_{c1}	$cei_{a2,}$	$cei_{b2,}$	cei_{c2}
a-g on line-1(R_f =20 ohm,δ=30° at 10%)	28.69	2.65	1.00	2.11	1.12	1.05
b-g on line-2(R_f =100 ohm, δ=45° at 10%)	2.45	1.92	2.01	1.23	20.12	1.69
ab-g on line-2(R_f =30 ohm, δ=60° at 30%)	3.01	1.56	1.74	25.64	19.68	1.54
ab on line-1 and line-2(R_f =50 ohm, δ=90° at 50%)	23.12	20.02	0.12	21.32	19.36	0.02
bc on line-2(R_f =120 ohm, δ=45° at 70%)	0.11	0.15	0.28	0.18	17.36	18.65
abc on line-2(R_f =150 ohm, δ=30° at 70%)	1.35	0.68	1.21	13.56	17.36	15.64
abc-g on line-1 and line-2(R_f =200 ohm, δ=60° at 90%)	11.23	12.36	14.32	12.36	12.65	16.28
abc-g on line-1(R_f =150 ohm, δ=90° at 70%) with source impedance changed (increased 10%)	10.36	9.36	8.64	0.25	0.98	1.02
abc-g on line-2(R_f =150 ohm at 70%) with source impedance changed (increased 30%)	0.98	0.25	0.87	9.36	11.54	11.23

(b) Faulty line selection based on phasor comparison

After detecting the disturbance on the faulty phase from change in energy, the corresponding faulty line can be detected and trip signal can be sent to the circuit breaker by calculating the difference in magnitude of the faulted current signal from the estimated phasors. The amplitude and phase of the fault current and voltage signal are calculated from the S-Transform matrix(S) as given in (2.11) and (2.12) and as shown in Fig.3.2 through Fig.3.5.

The differences in the magnitude and phase of the current signals in the two parallel transmission lines are obtained as

$$Imagdiff = Imag1 - Imag2 \qquad\qquad (2.18)$$

$$Iphdiff = Iph1 - Iph2 \qquad\qquad (2.19)$$

where *Imag1* and *Imag2* are the estimated magnitude of fault current signal for line-1 and line-2, respectively. Similarly *Iph1* and *Iph2* are the estimated phase of fault current signal of line-1 and line-2, respectively. Likewise the difference in magnitude and phase of the current signal for other phases of the lines can be calculated. For positive values of *Imagdiff* above a threshold value, the relay trips the circuit breaker of line-1 and for negative value below the threshold the relay trips the circuit breaker of line-2. Similarly a trip signal for the circuit breakers in liners 1 and 2 can be generated.

Fig. 2.19 depicts the line-ground fault (a-g) on line-1, where the *Imagdiff* increases from the 0 to 6000. The threshold value is chosen as +/-1000 taking into all operating conditions of fault resistance, source impedance, fault location and inception angles. When the *Imagdiff* exceeds the threshold value of +1000 the relay trips line-1 and when the value is -1000 the relay trips line-2 circuit breaker. Fig. 2.20 shows *Imagdiff* for line-ground fault (a-g) at 30 % of the line-1 and b-g fault at 30% of the line-2 with 100 ohms fault resistance for section AB. Fig. 2.21 shows the value of *Imagdiffs* for line-line-ground fault (ab-g) at 50% of the line-1 with 150 ohms and 200 ohms fault resistance for section AB, respectively. Similarly Fig. 2.22 shows the *Imagdiff* for line-ground fault (a-g) at 90 % of the line-1 with 200 ohm fault resistance for section AB. Figs.2.23 and 2.24 show the *Imagdiff* for line-ground fault (a-g) at 30 % of the line-1 and b-g fault at 80% of line-2 with 20 ohms fault resistance for section AB and for line-ground fault (a-g) at 30% of the line-1 with 50 ohms fault resistance for section AB with SNR 20 dB, respectively. The above results clearly identify the faulty phase as well as the line involved under widely varying operating conditions.

Figs.2.25 and 2.26 show *Iphdiff* for line-ground fault (a-g) at 30 % of the line-1 with 20 ohms fault resistance for the section AB and for line-ground fault (a-g) on line-1 and b-g fault on line-2 at 90% of lines with 200 ohms fault resistance for the same section. The threshold limits for *Iphdiff* are chosen as $I_{phdiff1}$ = +0.25, $I_{phdiff2}$ = -0.25, taking all operating conditions into consideration.
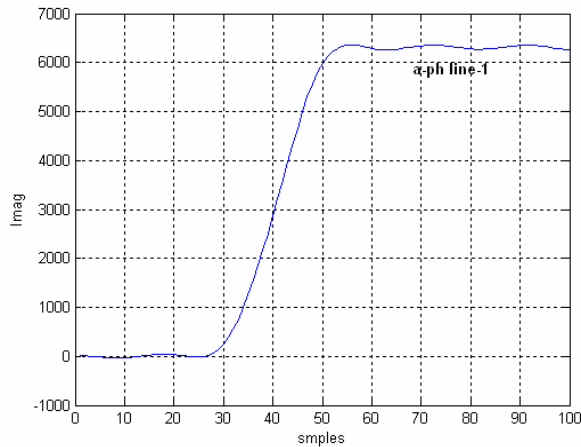
Fig. 2.19.*Imagdiff* **for line-ground fault (a-g) at 10 % of the line-1 with 50 ohm fault resistance for section AB**
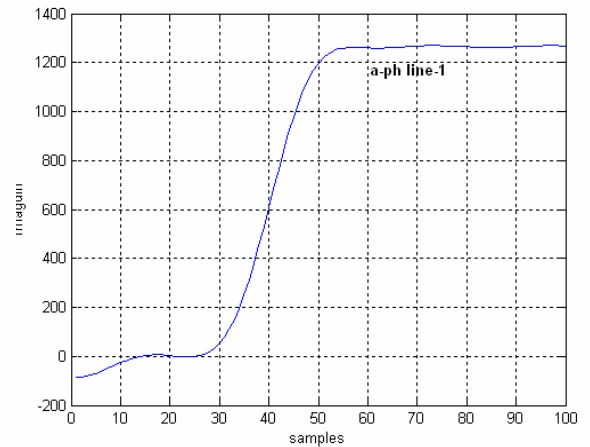
Fig. 2.22 *Imagdiff* **for line-ground fault (a-g) at 90 % of the line-1 with 200 ohm fault resistance for section AB**
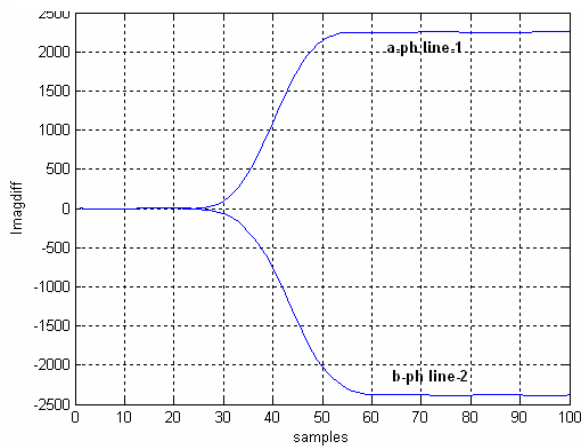
Fig. 2.20.*Imagdiff* **for line-ground fault (a-g) at 30 % of the line-1 and b-g fault at 30% of the line-2 with 100 ohm fault resistance for section AB**
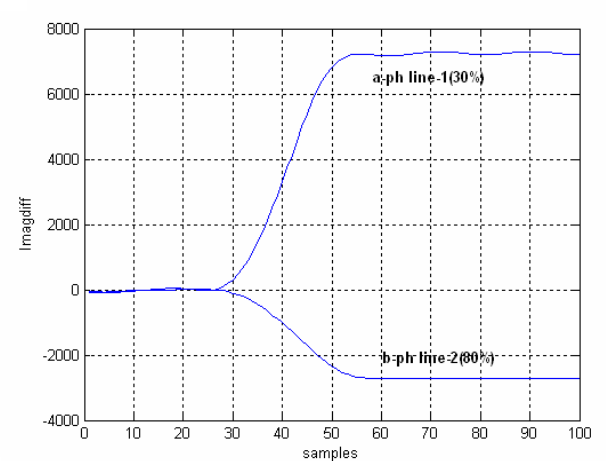
Fig. 2.23 *Imagdiff* **for line-ground fault (a-g) at 30 % of the line-1 and b-g fault at 80% of line-2 with 20 ohm fault resistance for section AB**
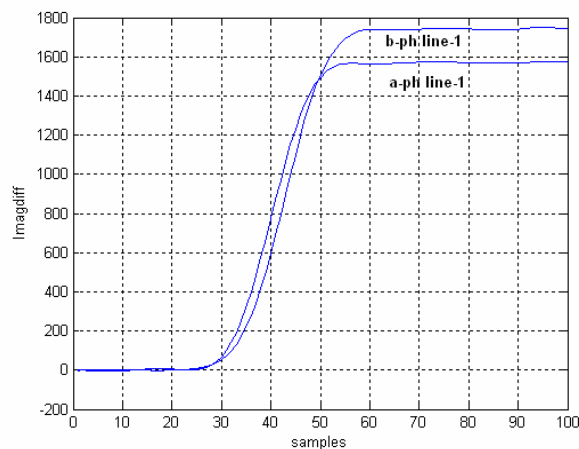
Fig. 2.21 *Imagdiff* **for line-line-groun fault (ab-g) at 50 % of the line-1 with 15 ohm fault resistance for section AB**
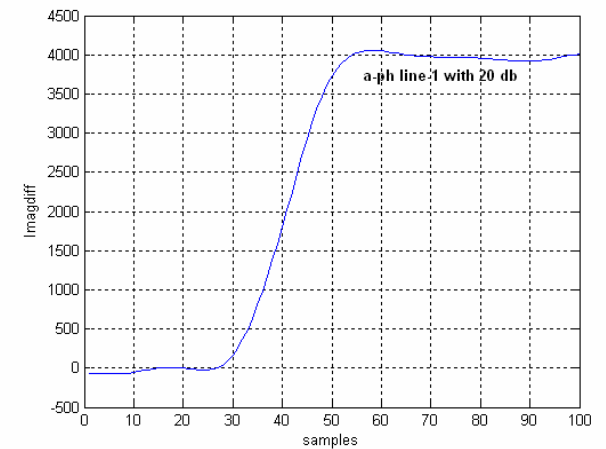
Fig. 2.24 *Imagdiff* **for line-ground fault (a-g) at 30 % of the line-1 with 50 ohm fault resistance for section AB with SNR 20 dB**

35
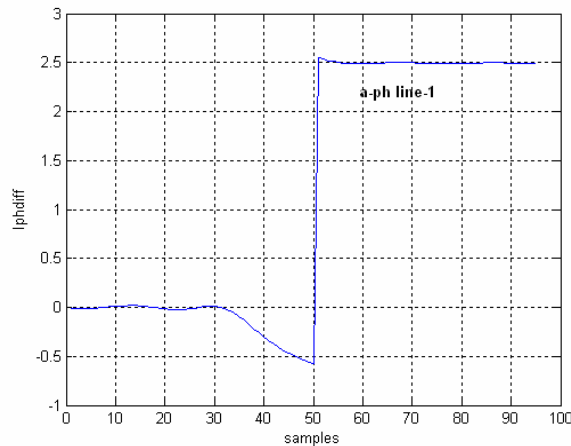
Fig. 2.25 *Iphdiff* for line-ground fault (a-g) at 30 % of the line-1 with 20 ohm fault resistance for section AB
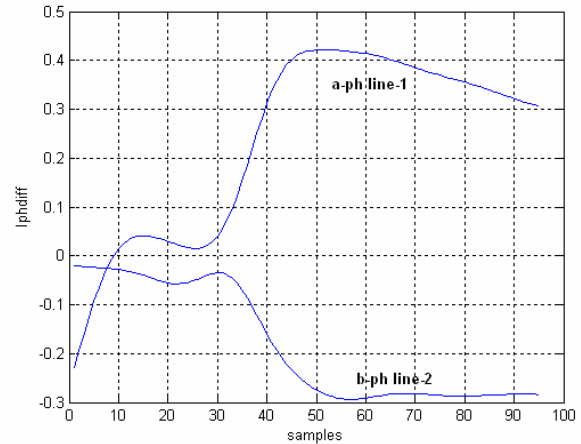
Fig. 2.26 *Iphdiff* for line-ground fault (a-g) on line-1 and b-g fault on line-2 at 90 % of lines with 200 ohm fault resistance for section AB

(c) Impedance trajectory

The magnitude and phase difference of the fault voltage and current in different phases works successfully in case of different types of faults on either of lines. But for similar types of faults on both lines simultaneously, the above method doesn't work. This problem arises in case of a-g fault on line-1 and a-g fault on line-2, ab-g fault on line-1 and ab-g fault on line-2, a-b fault on line-1 and a-b fault on line-2, abc-g fault on line-1 and abc-g fault on line-2 simultaneously. Because in the above cases the difference in magnitude and phase does not provide adequate information regarding the faulted condition, as the difference may give the values nearly zero or much below the threshold value set for the relay to respond to the magnitude difference in identifying the faulty phase as well as faulty line. The above problem can only be solved by calculating the impedance of the line to the fault point. The impedance trajectory provides the information whether the line is under fault condition or line is healthy and accordingly the circuit breaker is tripped if the impedance trajectory enters the tripping zone of the relay.

After the phasor calculation, impedance to the fault point is calculated by using the phasor information. The R-X trajectory is found out from the impedance information which clearly shows how the trajectory enters within the relay operating zone for

different fault conditions to protect the line and does not enter the relay zone in case of un-faulted condition. The impedance is calculated as given in (2.13) and (2.14).

(i) Fault within the protected zone (Impedance seen by the relay at 'A')

The impedance is calculated from the methods depicted in Appendix-A and from the impedance trajectory it is clearly seen that in case of faults, the trajectory comes within the relay operating zone. Fig. 2.27 shows the R-X plot for a-g (line-ground) fault on lines -1 and 2 simultaneously with fault resistance of 10 ohms, and the trajectory enters the tripping zone within 8 samples after the fault detection. It is found that the R-X plots for the a-g fault on line-1 and R-X plot for a-g fault on line-2 overlap each other as the operating conditions for both the lines remain same. Similarly Fig. 2.28 depicts the R-X plot for b-g (line-ground) fault on line-1 at 20% of line length and b-g fault on line-2 at 50% of line length with 10 ohms fault resistance.

Also the algorithm has been tested for various operating conditions with 0-200 ohms fault resistance, variable source impedance (up to 130%), various inception angles and at various locations for all the 11 types of shunt faults. Also the R-X trajectory enters the tripping characteristics within 8 samples after the fault on a particular phase is detected and thus the total fault tripping time is less than 18 samples (less than one cycle), which proves the fastness of the proposed method. The speed of the proposed algorithm can be further improved if the identification of the faulty phase can be achieved in less than half a cycle say a quarter of a cycle for instance.

(ii) External faults (Impedance seen by the relay at 'A')

For external faults, *Imagdiff* and *Iphdiff* are almost zero for the corresponding phase. Thus determination of the impedance trajectory provides the necessary protection to the line. The fault in the section BC is considered as an external fault for the relay at 'A'. Fig. 2.29 shows the impedance trajectory for a-b fault (line-line) at 20% on line-1(AB) , 70% on line-2(AB) and at 20% on line in section BC with fault resistance of 50 ohms in all the cases. From Fig. 2.29, it is clearly seen that for fault on line-1(AB) and fault on line-2(AB), the impedance trajectory enters into the tripping zone of the relay

within 8 samples from the detection of fault and less than one cycle from the inception of the fault. The impedance trajectory for the faults within section BC (20% of line BC) doesn't come inside the zone-1 tripping area of relay 'A', but it enters in the zone-2 tripping area of the relay at 'A'. This indicates that for external faults, the relay at 'A' provides back-up protection.
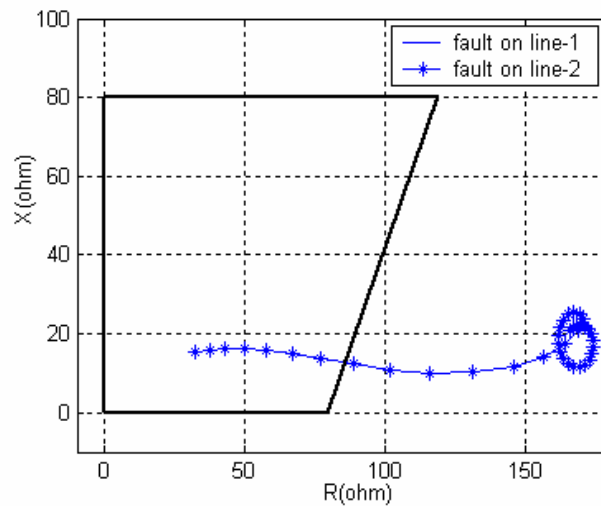
Fig. 2.27 R-X plot for a-g fault on line-1 and line-2 at 10% of both the line with 10 ohm fault resistance. ⎯⎯ represents R-X plot for line-1 and ✱✱✱ R-X plot for line-2.
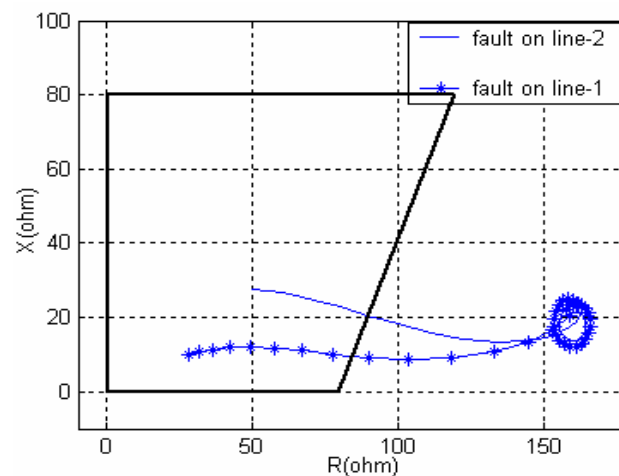
Fig. 2.28 R-X plot for b-g fault on line-1 at 20% of line-1 and b-g fault at 50% of line-2 with 10 ohm fault resistance. ⎯⎯ represents R-X plot for line-1 and ✱✱✱ R-X plot for line-2.
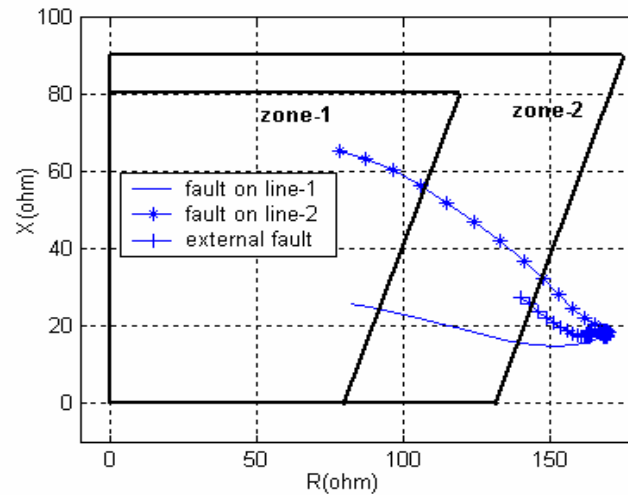
Fig. 2.29 R-X plot for a-b fault on line-1, line-2 and line-3. —— shows the R-X plot for a-b fault at 20% of line-1(AB), *** shows R-X plot for a-b fault at 70% of line-2(AB) and +++ shows the a-b fault at 20% of section BC with 50 ohm fault resistance in all cases.

2.2.2.3 Results from Laboratory Power Network Simulator

The proposed algorithm has been tested on a physical transmission line model. The transmission line consists of two parallel lines (section AB), each consists of 150 km π -sections and another 100 km π-section (section BC) of 100 km length. The line is charged with 400 volt, 5 kVA synchronous machines at one end and 400 volt at the load end. The three phase voltage and current are steeped down at the relaying end with potential transformer (PT) of 400/10 V and current transformer (CT) of 15/5 A respectively. Data collected using PCL-208 Data Acquisition Card (DAC) which uses 12-bit successive approximation technique for A/D (Analog to Digital) conversion. The card is installed on a with PC (P-4) with a driver software routine written in C++. It has 6 I/O channels with input voltage range of +/- 5 Volts. Data colleted with a sampling frequency of 1.0 KHz.

The results are shown in Fig. 2.30 through Fig. 2.34. Fig. 2.30 shows the Imagdiff for line-ground (L-G) fault at 50km of the line-1 and Fig. 2.31 shows the Imagdiff for line-line (L-L) fault at 100km on line-1 and line-2, respectively. The phase difference for the same L-L fault is shown in Fig. 2.32.The threshold for Imagdiff is +/-3.0 and for Iphdiff is +/-0.25. The impedance trajectory for L-G fault at 50 km on line-1 is shown in Fig. 2.33. Also the impedance trajectory for LL-G fault on both lines at 100 km is depicted in Fig. 2.34. It is found that the trajectory enters into the relay operating zone within 8 samples of the fault detection (18 samples after the fault inception). As the operating voltage range is 400 volt, the relay zone and threshold values are selected accordingly. From the above result it is seen that the proposed method works satisfactorily in laboratory environments.
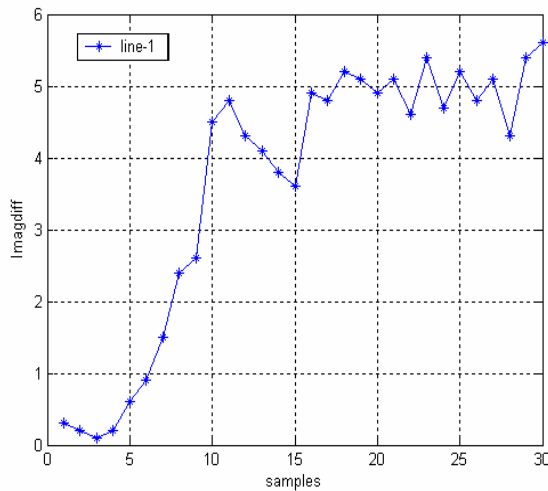
Fig. 2.30 *Imagdiff* for L-G fault at 50km on line-1.
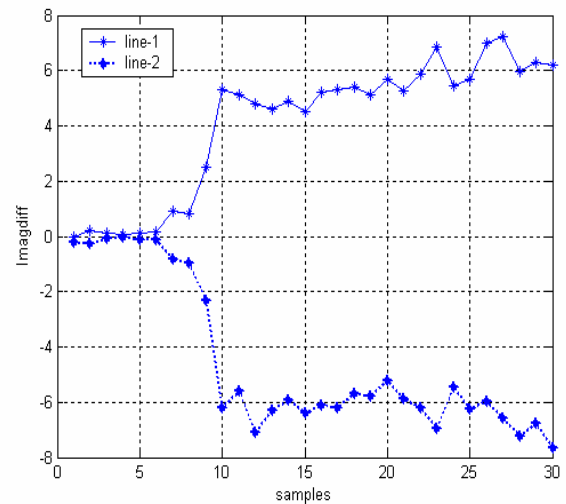
Fig. 2.31 *Imagdiff* for L-L fault at 100 km on line-1 and line-2, respectively.
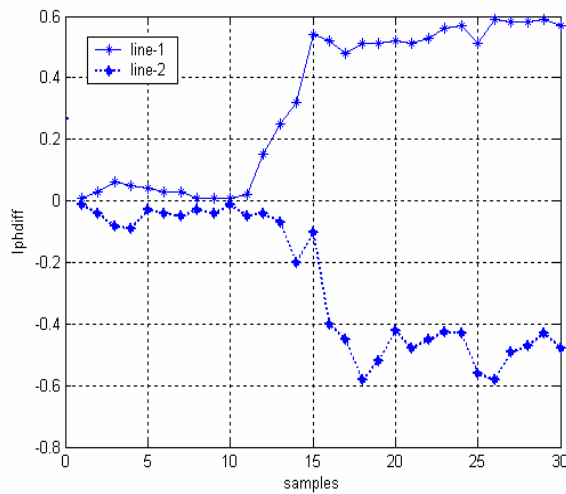
Fig. 2.32 *Iphdiff* for e for L-L fault at 100 km on line-1 and line-2, respectively.
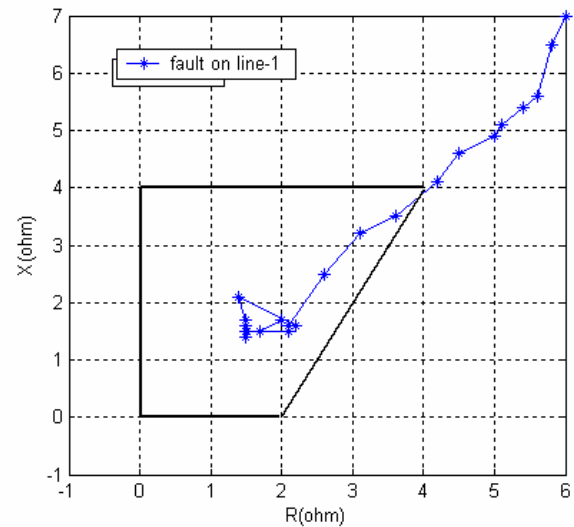
Fig. 2.33 R-X plot for L-G fault at 50km on line-1.
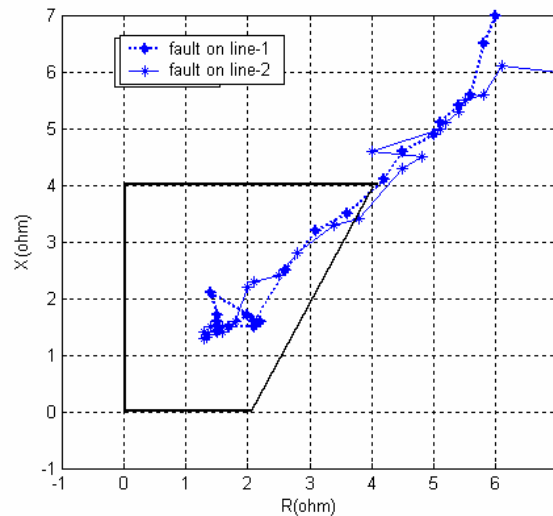
Fig. 2.34 R-X plot for LL-G fault at 100km on line-1 and line-2. respectively.

2.3 A variant of S-Transform: HS-Transform.

A pseudo-gaussian hyperbolic window is used to provide better time and frequency resolutions at low and high frequencies unlike the S-Transform using the Gaussian window. Here the hyperbolic window has frequency dependence in its shape in addition to its width and height. The increased asymmetry of the window at low

frequencies leads to an increase in the width in the frequency domain, with consequent interference between major noise frequencies.

The original S-Transform [29] is defined as

$$S(\tau, f) = \int_{-\infty}^{\infty} h(t) \left\{ \frac{|f|}{\sqrt{2\pi}} exp\left\{ -f^2(\tau-t)/2 \right\} exp(-2\pi ft) \right\} dt \tag{2.20}$$

where S denotes the S-Transform of *h(t)*, which is the actual fault current or voltage signal varying with time, frequency is denoted by *f*, and the quantity τ is a parameter which controls the position of gaussian window on the time-axis. A small modification of the gaussian window has been suggested for better performance.

$$W_{gs}(\tau-t, f, \alpha_{gs}) = \frac{|f|}{\sqrt{2\pi\alpha_{gs}}} exp\frac{\left[-f^2(\tau-t) \right]}{2\alpha_{gs}^2} \tag{2.21}$$

and the S-Transform with this window is given by

$$S(\tau, F, \alpha_{gs}) = \int_{-\infty}^{\infty} h(t)\omega(\tau-t, f, \alpha_{gs}) \cdot exp(-2\pi ift) dt \tag{2.22}$$

where α_{gs} is to be chosen for providing suitable time and frequency resolution. The value of α_{gs} selected in the proposed study is 0.6.

In applications, which require simultaneous identification time-frequency signatures of different faulted phase currents and voltages, it may be advantageous to use a window having frequency dependent asymmetry. Thus, at high frequencies where the window is narrowed and time resolution is good, a more symmetrical window needs to be chosen. On the other hand, at low frequencies where a window is wider and frequency resolution is less critical, a more asymmetrical window may be used to prevent the event from appearing too far ahead on the S-Transform. Thus an hyperbolic window of the form given below is used.

$$W_{hy} = \frac{2|f|}{\sqrt{2\pi(\alpha_{hy} + \beta_{hy})}} \cdot exp\left\{ \frac{-f^2X^2}{2} \right\} \tag{2.23}$$

where

$$X = \frac{\alpha_{hy} + \beta_{hy}}{2\,\alpha_{hy}\beta_{hy}}(\tau - t - \xi) + \frac{\alpha_{hy} - \beta_{hy}}{2\,\alpha_{hy}\beta_{hy}}\sqrt{(\tau - t - \xi)^2 + \lambda_{hy}^2} \qquad (2.24)$$

In the above expression $0\langle\alpha_{hy}\langle\beta_{hy}$ and ξ is defined as

$$\xi = \frac{\sqrt{(\beta_{hy} - \alpha_{hy})^2 \lambda_{hy}^2}}{4\alpha_{hy}\beta_{hy}} \qquad (2.25)$$

The translation by ξ ensures that the peak W_{hy} occurs at $\tau - t = 0$. At $f = 0$, W_{hy} is very asymmetrical, but when f increases, the shape of W_{hy} converges towards that of the symmetrical gaussian window W_{gs} given in (2.21). For different values of α_{hy} and β_{hy} and with $\lambda_{hy}^2 = 1$, Fig. 2.35 shows the nature of the window as the function of time $\tau - t$. As seen from the figure the change in the shape from an asymmetrical window to a symmetrical one occurs more rapidly with increasing f. The discrete version of the Hyperbolic S-Transform of the faulted voltage and current signal samples at the relaying point is calculated as

$$S[n, j] = \sum_{m=0}^{N-1} H[m + n]\,G(m, n)\,exp(i2\pi mj) \qquad (2.26)$$

where N is the total number of samples and the indices n, m, j are $n = 0,1....N - 1, m = 0,1.....N - 1,$ and $j = 0,1.......N - 1$.

The $G(m, n)$ denotes the Fourier transform of the Hyperbolic window and is given by

$$G(m, n) = \frac{2|f|}{\sqrt{2\pi(\alpha_{hy} + \beta_{hy})}}\,exp\left(\frac{-f^2 X^2}{2n^2}\right) \qquad (2.27)$$

where

$$X = \frac{(\alpha_{hy} + \beta_{hy})}{2\alpha_{hy}\beta_{hy}}t + \frac{\beta_{hy} - \alpha_{hy}}{2\alpha_{hy}\beta_{hy}}(\sqrt{t^2 + \lambda_{hy}}) \qquad (2.28)$$

and $H(m,n)$ is the frequency shifted discrete Fourier transform $H[m]$ and is given by

$$H(m) = \frac{1}{N}\sum_{m=0}^{N-1}h(k)\exp(-i2\pi nk) \qquad (2.29)$$

The computational steps of the hyperbolic S-Transform (HS-Transform) are:

(i) $H[m]$ of the faulted voltage and current waveform samples are calculated and shifted to give $H[n+m]$

(ii)   The localizing Hyperbolic gaussian window $G[m,n]$ is evaluated.

(iii) $H[n+m]$ and $G[m,n]$ are multiplied and the inverse Fourier transform of the product is found out to give the rows of $S[n,j]$ corresponding to the frequency n.

The Hyperbolic S-Transform is found to be a complex matrix $S[\frac{N}{2},N]$ .Fig. 2.36 shows the flow chart for HS-Transform.
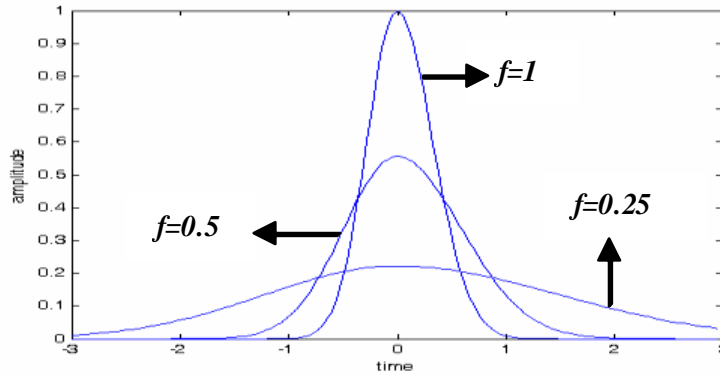
Fig. 2.35 Varying window W_{hy} at $f=1$, $f=0.5$ and $f=0.25$.

```
                              ┌─────────┐
                             (   Start   )
                              └────┬────┘
                    ┌──────────────┴──────────────┐
                    ▼                              ▼
         ┌────────────────────┐       ┌────────────────────┐
         │ Current or Voltage │       │  Gaussian Window   │
         │    Signal h(t)     │       │  function Why       │
         └─────────┬──────────┘       └─────────┬──────────┘
                   ▼                             ▼
         ┌────────────────────┐       ┌────────────────────┐
         │  H (m, n)=FFT(h(t)) │       │  G(m, n)=FFT(Why)   │
         └─────────┬──────────┘       └─────────┬──────────┘
                   ▼                             │
         ┌────────────────────┐                 │
         │      H (m+ n))      │                 │
         │ (shifting H (m, n)) │                 │
         └─────────┬──────────┘                 │
                   ▼                             ▼
         ┌───────────────────────────────────────────────┐
         │             H (n +m) * G(m ,n)                 │
         └───────────────────────┬───────────────────────┘
                                 ▼
         ┌───────────────────────────────────────────────┐
         │       S (n, j)=IFFT(H(n, m) * G(m, n))          │
         └───────────────────────┬───────────────────────┘
                                 ▼
                            ┌─────────┐
                           (    End    )
                            └─────────┘
```

Here the mathematical expressions in the flow chart are:

- Current or Voltage Signal $h(t)$
- Gaussian Window function W_{hy}
- $H(m, n)=FFT(h(t))$
- $G(m, n)=FFT(W_{hy})$
- $H(m+n))$ (shifting $H(m, n)$)
- $H(n+m) * G(m, n)$
- $S(n, j)=IFFT(H(n, m) * G(m, n))$
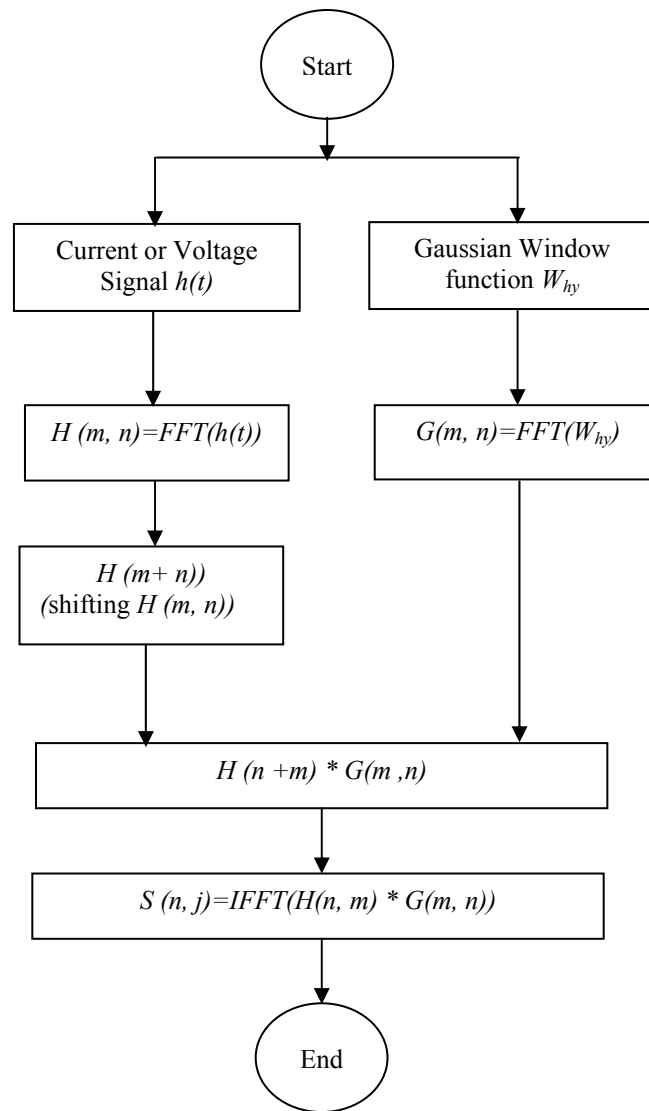
Fig. 2.36 Flow chart for HS Transform

2.3.1 Distance protection of single-circuit transmission line using HS-Transform.

The proposed technique consists of preprocessing the fault current and voltage signal sample using Hyperbolic S-Transform to yield the change in energy and standard deviation at the appropriate window variation. After extracting these two features, a decision of fault or no-fault on any phase or multiple phases of the transmission line is detected, classified, and its distance to the relaying point found out using RBFNN (Radial Basis Function Neural Network) with RLS(Recursive Least Square) algorithm. The ground detection is done by a proposed indicator '*index*'. As HS-Transform is very less sensitive to noise compared to Wavelet Transform, the proposed method provides very accurate and robust relaying scheme for distance protection.

2.3.1.1 System Studied
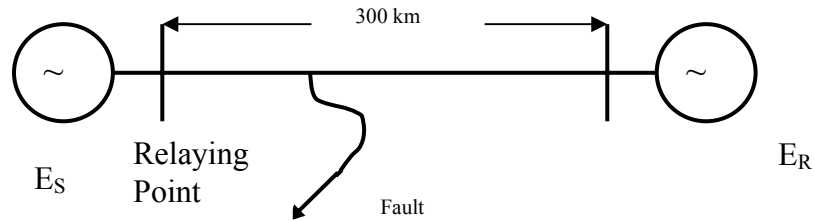
Fig. 2.37 Transmission Line Model

The model network shown in Fig. 2.37 has been simulated using PSCAD (EMTDC) package. The network having two areas connected by the transmission line of 400 kV. The transmission line has zero sequence impedance Z (0) =96.45+j335.26 ohm and positive sequence impedance Z(1)=9.78+j110.23 ohm and $E_S = 400\,\text{kV}$, $E_R = 400\angle\delta\,\text{kV}$. The relaying point is as shown in the Fig. 2.37, where data is retrieved for different conditions. Isolation of over voltage and high frequency components can be performed according to the required level of decomposition and reconstruction. The sampling rate is 1.0 kHz   at 50 Hz base frequency. The change in energy and standard deviation are calculated from the S-Transform of the current and voltage signal one cycle

ahead and one cycle back from the fault inception. The proposed scheme is depicted as in Fig. 2.38.
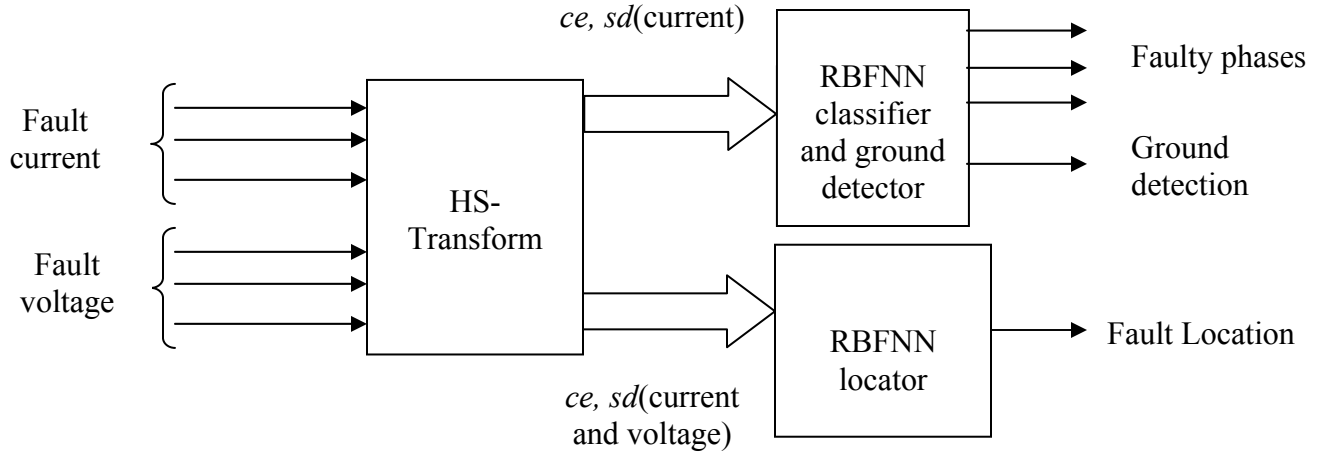
Fig. 2.38 Protection scheme for proposed method

2.3.1.2 Feature extraction for Fault Classification and Location

For faulty phase identification or fault classification only current signal is preprocessed through HS-Transform to find out the features. The HS-Transform outputs of the faulted current signal for different types of faults at 10% to 90% of the line with different incidence angles, source impedance and fault resistances are used to provide the following pertinent features, which can be used to classify the type of fault. Change in the signal energy and standard deviation of the HS-Transform contour are obtained as

$$ce = E_f - E_A = \{abs(hs_f)\}^2 - \{abs(hs_n)\}^2 \qquad (2.30)$$

and

$$sd = std\{abs(hs_f)\} \qquad (2.31)$$

Where hs_f is the HS-Transform coefficient is for one cycle ahead of fault inception and hs_n is the HS-Transform coefficients for one cycle before the inception of the fault. For faulted phase identification, simulations are carried out for faults at intervals of 10 km from the sending end for a total line length of 300 km. For each of these fault locations

inception angles (δ) and fault resistance (R_f) and source impedance (Z_s) are varied to provide the change of energy and standard deviation are presented in Tables-1 to 2. From the tables, it is seen that the faulted phases exhibit high output in the form of change in energy (*ce*) and standard deviation (*sd*) in comparison to the un-faulted phases.

Various types of faults are simulated on the system shown in Fig. 2.37 with varying inception angle, fault location and fault resistance R_f in the fault path to ground. Fig. 2.39 through Fig. 2.42 show the time frequency contours of the HS-Transform output for different fault and no-fault condition. From these figures, it can be seen that the faulted phase exhibits the distinct contours and the time at which it occurs. The phase, which is not faulted, exhibits no such contours, thus clearly classifying the type of fault visually. For recognizing this fault pattern, the change in energy of the signal (*ce*) and standard deviation (*sd*) are used and the detailed results for different types of fault inception angles distance and fault resistance.

Table-2.9 through Table-2.14 show the change energy (*ce*) and standard deviation (*sd*) for all the three phases in faulted condition. It can be clearly seen that, in case of L-G(a-g) fault at 10% of line, 20 ohm fault resistance and 30º inception angle, the *ce* and *sd* value for a-phase are 49.6137 and 0.6269 ,respectively, while for phase b , *ce* and *sd* are 3.3263 and 0.0698 and for c-phase *ce* and *sd* are 1.0416 and 0.0481, respectively. The value of *ce* and *sd* in a- phase clearly shows that there is fault in a-phase. Likewise in case of LL-G (ab-g) fault, *ce* and *sd* for a phase are 49.7764 and 0.6724, respectively. For b-phase *ce* and *sd* are 18.90 and 0.29, respectively and for c-phase *ce* and *sd* are 2.01 and 0.06 respectively. The above result clearly shows that the phase involving fault is having very high value of *ce* and *sd* compared to un-faulted phase. Table-4 provides *ce* and *sd* for fault at 50 % location, 200 ohm fault resistance and 90º inception angle. In case of L-L (ab) fault, *ce* and *sd* values for a-phase are 8.8929 and 0.1422, respectively and for b phase ce and sd are 7.7138 and 0.1231 while for c-phase *ce* and *sd* are 0.0000 and 0.0350 respectively. For above location and fault resistance, for LLL-G(abc-g), *ce* and *sd* values for a-phase are 12.7833 and 0.1799, *ce* and *sd* values for b-phase are 8.132 and 0.1327 and *ce* and *sd* values for c-phase are 11.5229 and 0.1965, respectively, which indicates that all three phases are in faulted condition. The *ce* and *sd* values for different phases at different fault resistance, fault inception angle, fault location and for

different types of fault have been shown in Table-1 through Table-6.From the above analysis fault classification can easily done to detect the faulty phase. A general rule can be formulated for change in energy (*ce*)>5.0 and standard deviation (*sd*)>0.1 for the phase involving fault otherwise the phase is un-faulted.

For a line-to-line ground (LG) type, it is found from Table-2.9 and Table-2.14 that the change in energy *ce* depends on the magnitude of the fault resistance, R_f, the value of *ce* is less for higher values of R_f. It is found from these tables that the current signals in the faulted phases exhibit greater *ce* and standard deviation (*sd*) values in comparison to the un-faulted phases. Here ce_a, ce_b, ce_c represent change energy and sd_a, sd_b, sd_c represent standard deviation in a, b and c phases, respectively.
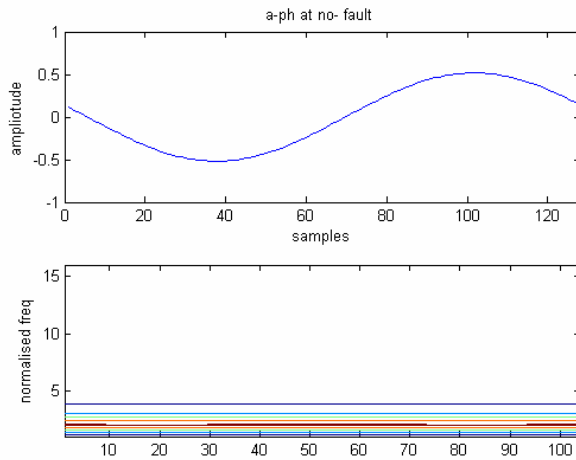
Fig. 2.39 a-ph at no-fault
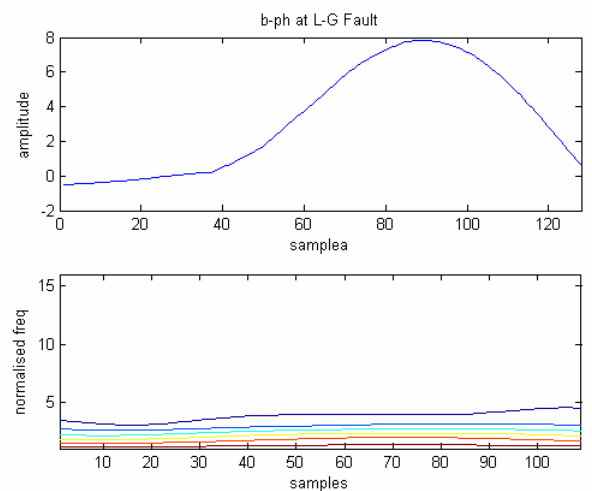
Fig. 2.41 b-ph at L-G fault at 50% of line, R$_f$ 150 ohm
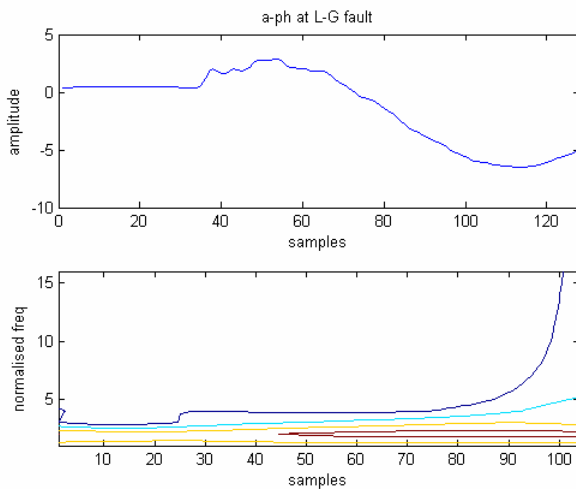
Fig. 2.40.a-ph at L-G fault at 50% of line, R$_f$ 150 ohm
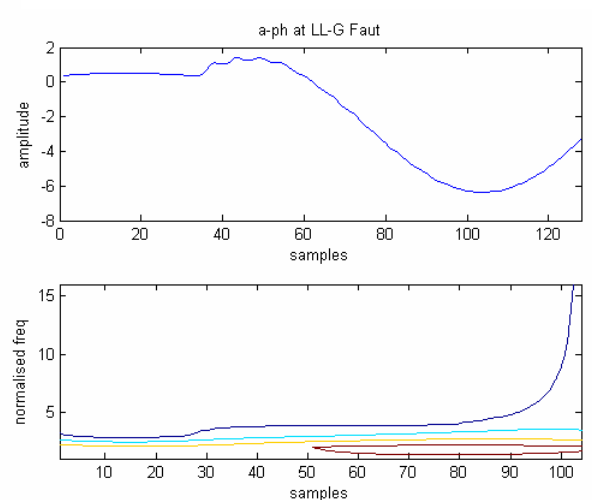
Fig. 2.42 a-ph at LL-G fault at 70% of line, R$_f$ 200 ohm

Table-2.9 R$_f$=20 ohm, Fault at 10 %, Inception angle 30º

FAULT		a		b		c	
		ce_a	sd_a	ce_b	sd_b	ce_c	sd_c
LG	ag	49.6137	0.6269	3.3263	0.0698	1.0416	0.0481
	bg	1.7655	0.0859	24.9729	0.3148	3.1497	0.0920
	cg	2.1833	0.0592	1.0604	0.0538	34.9404	0.5415
LLG	abg	49.7764	0.6724	18.9028	0.2907	2.0117	0.0610
	bcg	3.3505	0.0703	36.7778	0.4392	43.9432	0.6116
	cag	42.5899	0.5139	2.4216	0.0841	24.9239	0.4324
LL	ab	24.2053	0.3070	22.2882	0.2856	0.0001	0.0350
	bc	0.0001	0.0350	11.5396	0.2076	10.1772	0.2003
	ca	26.7541	0.3909	0.0001	0.0350	28.0509	0.4028
LLLG	abcg	33.7419	0.4424	16.2684	0.2178	23.1498	0.3767

Table-2.10 R$_f$=200 ohm, Fault at 30 %, Inception angle 45º

FAULT		a		b		c	
		ce_a	sd_a	ce_b	sd_b	ce_c	sd_c
LG	ag	15.8385	0.2117	0.2464	0.0396	0.0230	0.0378
	bg	0.9986	0.0647	11.2101	0.1739	1.1876	0.0647
	cg	0.4431	0.0475	0.2272	0.0442	14.9927	0.2370
LLG	abg	16.4559	0.2231	8. 9539	0.1491	0.1174	0.0415
	bcg	0.2905	0.0323	11.7237	0.1727	12.5895	0.1969
	cag	13.4441	0.1825	0.4681	0.0559	15.3726	0.2517
LL	ab	9.9518	0.1473	8.1618	0.1281	0.0000	0.0350
	bc	0.0000	0.0350	8.2121	0.1577	7.1622	0.1526
	ca	13.1622	0.1526	0.0001	0.0350	12.3702	0.1854
LLLG	abcg	13.4585	0.1874	8.5023	0.1370	12.1127	0.2046

Table-2.11 R$_f$=0 ohm, Fault at 30 %, Inception angle 60º

FAULT		a.		b		c	
		ce_a	sd_a	ce_b	sd_b	ce_c	sd_c
LG	ag	53.6753	0.6884	2.0811	0.0572	0.4064	0.0410
	bg	2.3987	0.0757	26.8833	0.3412	3.2008	0.0800
	cg	1.6748	0.0562	0.9305	0.0504	35.25	0.5514
LLG	abg	52.8872	0.7219	18.8112	0.2796	1.1625	0.0489
	bcg	1.7182	0.0512	41.0512	0.4916	48.2312	0.6806
	cag	48.2917	0.5965	2.2728	0.0718	22.5077	0.3926
LL	ab	26.6698	0.3360	24.7842	0.3158	0.0001	0.0350
	bc	0.0001	0.0350	11.2606	0.1976	9.8353	0.1896
	ca	28.7006	0.4210	0.0001	0.0350	29.9979	0.4328
LLLG	abcg	36.7997	0.4865	17.7464	0.2351	23.9085	0.3904

Table-2.12 R$_f$=200 ohm, Fault at 50 %, Inception angle 90º

		a		b		c	
FAULT		ce_a	sd_a	ce_b	sd_b	ce_c	sd_c
LG	ag	14.2844	0.1947	0.0551	0.0365	0.3697	0.0419
	bg	1.1669	0.0667	10.4977	0.1615	0.9766	0.0645
	cg	0.3176	0.0443	0.4479	0.0453	13.5935	0.2180
LLG	abg	15.0194	0.2062	8.2011	0.1365	0.116	0.0421
	bcg	0.116	0.0421	10.773	0.1639	11.2391	0.1818
	cag	12.3907	0.1708	0.5111	0.0583	14.4228	0.2366
LL	ab	8.8929	0.1422	7.7138	0.1231	0.0000	0.0350
	bc	0.0000	0.0350	7.862	0.1522	6.816	0.1471
	ca	10.5525	0.1664	0.0000	0.0350	11.7686	0.1781
LLLG	abcg	12.7833	0.1799	8.132	0.1327	11.5329	0.1965

Table-2.13 R$_f$=200 ohm, Fault at 10 %, Inception angle 45º

		a		b		c	
FAULT		ce_a	sd_a	ce_b	sd_b	ce_c	sd_c
LG	ag	17.4713	0.2295	0.6927	0.0451	0.2538	0.0350
	bg	0.8430	0.0648	12.5204	0.1861	1.4074	0.0681
	cg	0.6854	0.0463	0.1306	0.0437	16.4686	0.2574
LLG	abg	18.0017	0.2406	9.7721	0.1632	0.1512	0.0405
	bcg	0.2849	0.0335	12.8119	0.1819	14.0022	0.2124
	cag	14.5258	0.1944	0.5134	0.0594	16.4302	0.2684
LL	ab	10.4262	0.1525	8.6269	0.1332	0.0001	0.0350
	bc	0.0001	0.0350	8.5845	0.1634	7.5322	0.1584
	ca	11.769	0.1811	0.0001	0.0350	12.992	0.1929
LLLG	abcg	14.1534	0.1952	8.8947	0.1413	12.719	0.2129

Table-2.14 R$_f$=200 ohm, Fault at 100 % ,Inception angle 30º

		a		b		c	
		ce_a	sd_a	ce_b	sd_b	ce_c	sd_c
FAULT							
LG	ag	13.0008	0.1752	0.5925	0.0717	2.9957	0.0891
	bg	2.4032	0.0725	12.1988	0.1611	0.4849	0.0587
	cg	0.2494	0.0351	2.1859	0.0581	15.0271	0.2869
LLG	abg	14.7122	0.1912	9.0009	0.1296	1.7841	0.0532
	bcg	1.9142	0.0760	14.3503	0.1830	12.5379	0.1727
	cag	10.3315	0.1448	1.5882	0.0628	17.0525	0.2311
LL	ab	10.3064	0.1464	7.8023	0.1178	0.0003	0.0350
	bc	0.0002	0.0350	12.0526	0.1645	10.4153	0.1539
	ca	10.7793	0.1575	0.0002	0.0350	13.1282	0.1774
LL LG	abcg	12.4227	0.1658	11.4536	0.1561	14.7028	0.2014

2.3.1.3   Fault Classification using RBFNN

Even if HS-Transform gives information regarding the faulty phase involved, the RBFNN classifier is used to classify faults in the proposed method to overcome the error due to assigning threshold value to the parameters for fault identification including all operating conditions. After feature extraction using HS-Transform, RBFNN is used to detect the faulty phase or multiple phases involving fault. The RBFNN [41] used here has an input layer, a hidden layer consisting of gaussian node function, a set of weights W, to connect the hidden layer and output layer. Let x be the input vector $x = (x_1, x_2, \ldots \ldots x_D)^T$, where D represents input dimension. The output vector $o = (o_1, o_2, \ldots \ldots o_N)^T$, where N is the numbers of output node. For P training patterns, RBFNN approximates the mapping from the set of input $X = \{x(1), x(2), \ldots \ldots x(P)\}$, to the set of outputs, $O = \{o(1), o(2), \ldots \ldots o(P)\}$. For an input vector $x(t)$, the output of j th output node produced by an RBF is given by

$$o_j(t) = \sum_{i=1}^{m_{tot}} w_{ij} \phi_i(t) = \sum_{i=1}^{m_{tot}} w_{ij} e^{\frac{-\|x(t) - c_i\|}{2\sigma_i}} \tag{2.32}$$

where c_i is the center of the 'i' th hidden node, σ_i is the width of the 'i' th center, and m_{tot} is the total number of hidden nodes.

If output of the hidden neurons, by vector notation

$$\varphi = (\phi_1(t), \phi_2(t), \ldots \ldots, \phi_{tot}(t)) \tag{2.33}$$

and weight vector

$$w_j = (w_{1j}, w_{2j}, \ldots \ldots \ldots, w_{totj})$$

RBFNN output can be written as

$$o_j = w_j \varphi^T \tag{2.34}$$

In our implementation these sets of centers are trained with K-means clustering approach, where the centers are initially defined as the first training m_c inputs that correspond   to a specific class c. The Center vector is given by

$$C_c(i = 0) = \{x(c_1), x(c_2), \ldots \ldots, x(c_{mc})\} \tag{2.35}$$

At each iteration 'i', following a new input $x(i)$ is presented, the distance for each of the centers is denoted by

$$\rho_j(i) = \left\| x(i) - c_{j(i-1)} \right\|, \text{ where } j = 1,2,............,m_c \tag{2.36}$$

The *kth* center is updated by the following equation:

$$C_k(i) = C_k(i-1) + \alpha \left| \rho_k(i) \right| \tag{2.37}$$

where k that is chosen as the k that minimizes $\rho_j(i)$, as

$$k = \arg(\min(\rho_j(i)) \tag{2.38}$$

and α is the learning rate.

The width associated with the k th center is adjusted as

$$\sigma_k(i) = \sqrt{\frac{1}{N_a} \sum_{j=1}^{N_a} \left\| C_k(i) - C_j(i) \right\|^2} \tag{2.39}$$

where N_a is number of the hidden neurons.

The weights of the RBF classifier can be trained using the linear RLS (Recursive Lease Square) algorithm. The RLS is employed here since it has a much faster rate of convergence compared to the gradient search and least means square (LMS) algorithms.

$$k(i) = \frac{P(i-1)\varphi^T(i)}{\lambda + P(i-1)\varphi^T(i)} \tag{2.40}$$

$$w_j = w_j(i-1) + k(i)\left[d_j(i) - w_j(i-1)\varphi^T(i) \right] \tag{2.41}$$

$$P(i) = \frac{1}{\lambda}\left[P(i-1) - k(i)\varphi(i)P(i-1) \right] \tag{2.42}$$

where λ is real number between 0 and 1, $P(0) = a^{-1}I$, and a is a small positive number and $w_j(0) = 0$

The computational steps involved in implementing of RBFNN for fault classification are:

1. For each class c initial centers are first input sets that is $m_c = m_{init}$ (initialization)

2. Train the RBFNN using current set of centers to get cross validation error for class $c, e = \{e_1, e_2....., e_{N_c}\}$ (Clustering of centers)

3. $e_m(mean(e)) \leq e_{t\,\arg et}$ that is e_m has not decreased by 0.15 % over last iteration, go to step 5(convergence test

4. Add e_{inc} centers to N_c classes with highest error, to get a new m, then go to step 2.

5. The RBFNN is used with the one with the current m.

The learning rate of the RBFNN is 0.1 and the center and the weights are updated in every iteration that is by new training input to the RBFNN. Here only fault current signal is considered for feature extraction. Six inputs to the RBFNN fault classifier consisting of *ce(i)* and *sd(i)* values of all the three phases ('*i*' represents only current signal) are presented to the RBFNN and correspondingly three output are generated from the RBFNN, which gives the faulty phases involved. The RBFNN architecture for fault classification is shown in Fig. 2.43.
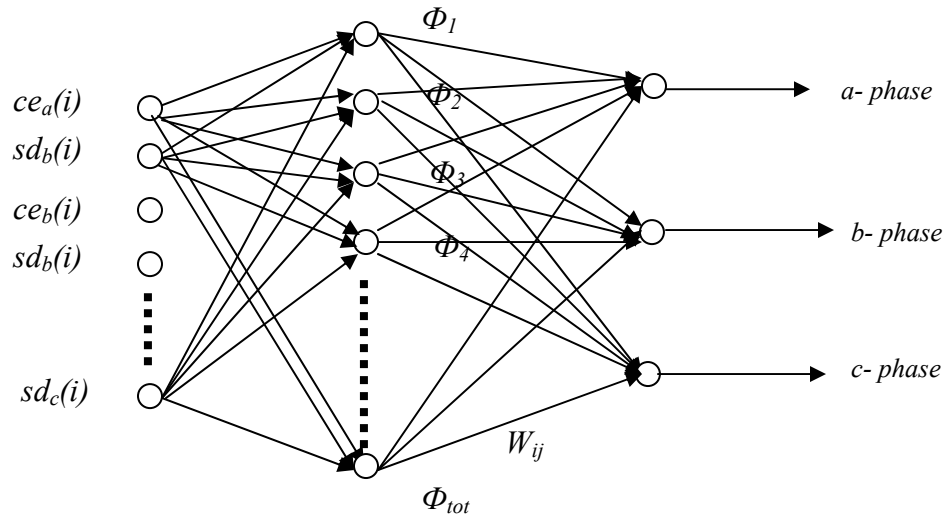
Fig. 2.43 RBFNN architecture for Fault Classification

The RBFNN consists of three outputs representing 'a', 'b', 'c', phases. During training these outputs are assigned '1' or '0' considering whether the fault is involved with that phase or not. For example 'ab-g' fault case the output will be assigned '1 1 0'. The training set include data (ce and sd) for 5%, 15%, 25%, 35%, 45%, 55%, 65%, 75%, 85%, 95% fault location for different fault inception angles , fault resistance ,different source impedance for 11 types of faults (ag, bg, cg, abg, bcg, cag, ab, bc, ca, abc, abcg). The flow chart for fault classification is shown in Fig. 2.44.

The performance of the RBFNN is tested for *ce* and *sd* values of different faults with varying location and fault resistance.Table-2.15 through Table-2.18 present some of the classification results for faulted transmission line.Table-2.15 shows the performance of RBFNN for 10% of the line and 45° inception angle for R_f =20 Ω and R_f =200 Ω. The, respective, values in a, b, c column for 'ab' case with R_f =20Ω, a=1.0098, b=0.9947, c=0.0298 depicts the phases involved with the fault are 'a' and 'b' only. The classification approach takes a particular phase to be involved with fault if it's corresponding values greater than a threshold value of 0.5 else it categorizes the phase to be 'undisturbed'. Similarly Table-2.16 provides the fault classification results for different faults at 30% of line with 60° inception angle. Also Table-2.17 provides the fault classification results for different faults at 50% of line with 90° inception angle where as Table-2.18 presents fault classification at 70% of line with 30° inception angle. The RBFNN has been trained by 3000 sets of data which comprises *ce* and *sd* for faulted current signals of every kind of fault at various locations, fault resistance, and inception angle. Observation of all test results ascertains that the RBFNN performs excellent even at different inception angles, fault location, fault resistance and pre-fault loading conditions.

Start

Fault current retrieved at relaying end

HS-Transform

ce and *sd* values computed

RBFNN
(output for a, b, c phase)

Ground Detector

If a ph≈ 1.0
If b ph≈ 1.0
If c ph≈ 1.0
(either combinations)

Index
>=0.005

No

No

Yes

Yes

No Fault

Fault detected

Ground Involved

Ground not Involved

a-g, b-g, c-g, ab-g, bc-g, ca-g, abc-g fault

ab, bc, ca, abc fault
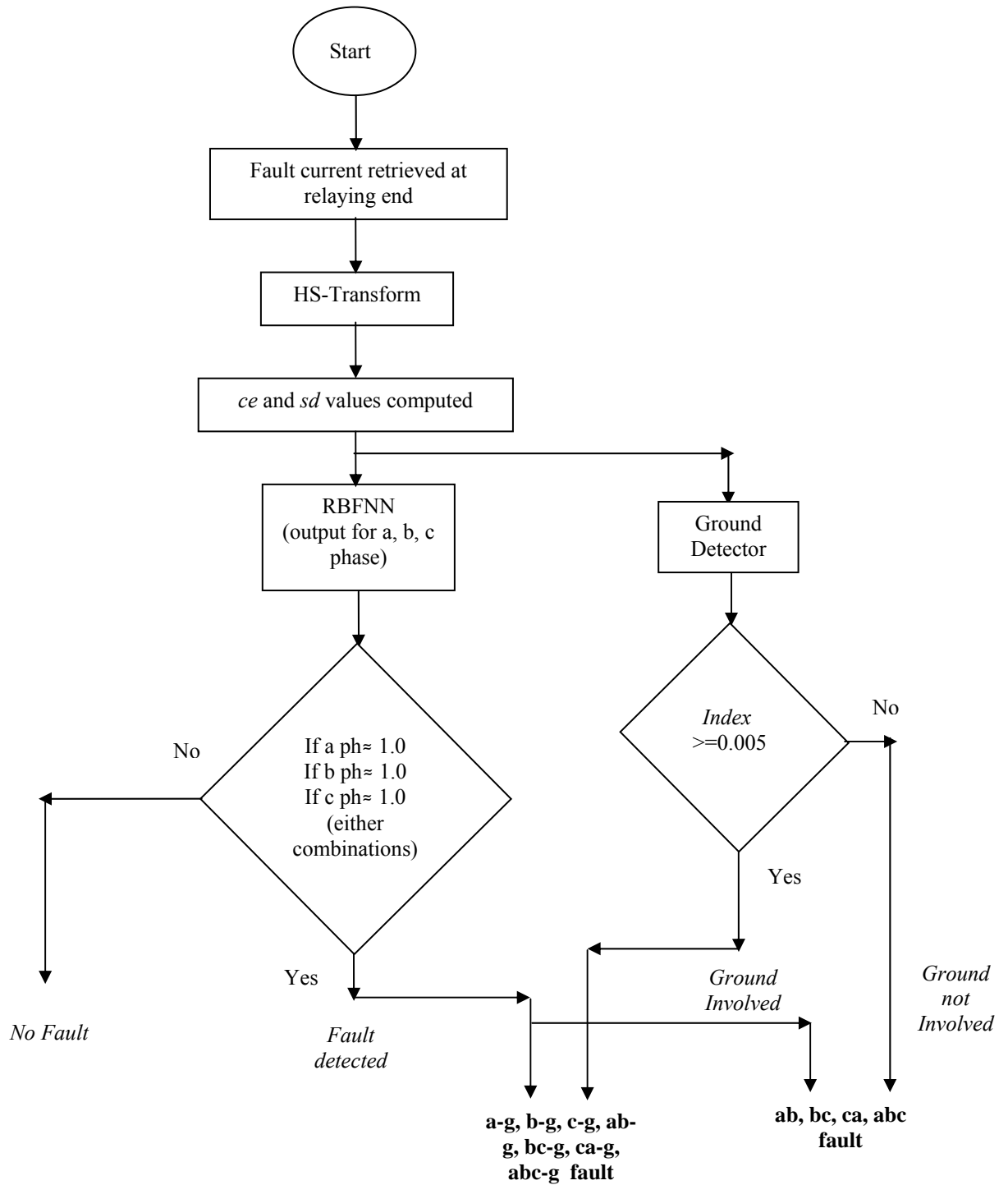
Fig. 2.44 Flow chart for Fault classification

Table-2.15 Fault at 10% of line with 45° inception angle

Fault Type	R_f=20 Ω			R_f=200 Ω		
	a	b	c	a	B	c
ag	0.9995	0.0025	0.0321	0.9987	0.0125	0.0241
bg	0.0325	1.0012	0.0125	0.9847	0.0541	0.0287
cg	0.0124	0.0354	1.0035	0.0354	0.0412	1.0036
abg	1.0048	0.9968	0.0014	1.0003	0.9974	0.0254
bcg	0.0036	1.0051	0.9874	0.0025	0.9964	0.9984
cag	1.0012	0.0041	1.0065	1.0041	0.0069	1.0954
ab	1.0098	0.9947	0.0298	1.0089	1.0074	0.0541
bc	0.0036	1.0051	0.9857	0.0041	0.9874	0.9968
ca	0.9945	0.0054	1.0087	1.0069	0.0654	1.0658
abc	1.0052	0.9998	0.9999	1.0023	0.9986	0.9979
abcg	1.0095	0.9991	0.9984	0.9948	0.9874	1.0019

Table-2.16 Fault at 30% of line with 60° inception angle

Fault Type	R_f=20 Ω			R_f=200 Ω		
	a	b	c	a	b	c
ag	1.0025	0.0002	0.0013	0.9995	0.0026	0.0014
bg	0.0041	1.0098	0.0054	0.9987	0.0036	0.0254
cg	0.0254	0.0369	1.0008	0.0256	0.0036	1.0095
abg	1.0056	0.9995	0.0024	1.0096	0.9996	0.0025
bcg	0.0089	1.0009	1.0004	0.0012	0.9956	1.0236
cag	0.9996	0.0365	0.9996	1.0006	0.0065	0.9954
ab	1.0025	0.9968	0.0214	1.0006	1.0068	0.0036
bc	0.0006	0.9985	0.9965	0.0036	1.0069	1.0063
ca	1.0548	0.0698	1.0057	0.9958	0.0365	0.9968
abc	1.0028	0.9965	1.0026	0.9947	0.9968	0.9998
abcg	1.0026	1.0058	1.0008	0.9965	1.0045	0.9968

Table-2.17 Fault at 50% of line with 90° inception angle

Fault Type	R_f=20 Ω			R_f=200 Ω		
	a	b	c	a	b	c
ag	1.0089	0.0045	0.0125	0.9989	0.0126	0.0123
bg	0.0214	1.0254	0.0654	0.9954	0.0254	0.0058
cg	0.0047	0.0096	1.0025	0.0214	0.0236	0.9954
abg	1.0048	0.9987	0.0125	1.0258	0.9965	0.0036
bcg	0.0012	1.0857	0.9954	0.0415	0.9854	1.0254
cag	0.9995	0.0254	0.9914	1.0032	0.0052	1.0063
ab	1.0025	0.9912	0.0041	1.0897	1.0036	0.0213
bc	0.0032	0.9965	0.9912	0.0024	0.9863	0.9995
ca	1.0065	0.0354	1.0069	1.0025	0.0032	1.0069
abc	0.9996	0.9994	1.0058	1.0023	0.9948	1.0054
abcg	1.0056	1.0002	1.0036	0.9968	1.0025	0.9997

Table-2.18 Fault at 70% of line with 30° inception angle

Fault Type	R_f=20 Ω			R_f=200 Ω		
	a	b	c	a	b	c
ag	1.0095	0.0023	0.00254	0.9987	0.0254	0.0036
bg	0.0014	1.0001	0.0025	0.9994	0.0058	0.0254
cg	0.0065	0.0045	1.0001	0.0254	0.0036	1.0058
abg	1.0048	0.9987	0.0012	1.0025	0.9925	0.0012
bcg	0.0125	1.0024	1.0025	0.0254	0.9958	1.0026
cag	0.9998	0.0125	0.9968	1.0032	0.0036	1.0254
ab	1.0012	0.9998	0.0125	1.0045	10.365	0.0025
bc	0.0254	0.9945	0.9941	0.0145	0.9968	0.9958
ca	1.0025	0.0654	1.0254	0.9995	0.0036	1.0025
abc	0.9945	1.0023	1.0045	1.0254	0.9991	0.9967
abcg	0.9985	1.0025	1.0014	0.9968	1.0065	0.9995

2.3.1.4 Ground Detection

Usually RBFNN may not give ground detection properly. Therefore ground detection task is not included in the RBFNN classifier. For detecting the involvement of ground, an *index* is proposed as given below:

$$index = \min(ce_a, ce_b, ce_c) / \max(ce_a, ce_b, ce_c) \tag{2.43}$$

The ground detection is carried out in conjunction with the RBFNN classification. Test result showing the values of *index* for ag, abg, ab, abcg faults at 10% of line and fault resistance of 0Ω and 200Ω are given in Table-2.19. When the *index* value exceeds the threshold value of 0.005, it indicates the involvement of fault with ground. This value of index has been tested for different types of fault with various operating conditions.

**Table-2.19 Index values for fault at 10% of
the line at different Fault Resistance**

Fault Type	*index* ($R_f = 0Ω$)	*index* ($R_f = 200Ω$)
ag	0.0365894	0.1258974
abg	0.0251478	0.1548695
ab	0.0000005	0.0000003
abcg	0.4587925	0.4258974

2.3.1.5 Fault Location using RBFNN

Once the fault is classified, the control unit activates the fault locating RBFNN to locate the fault. Here RBFNN with RLS algorithm is used to build the fault locator. In this case the learning rate of the RBFNN is 0.1 and the center and the weights are updated in every iteration that is by new training input to the RBFNN. Here for fault location, both faulted voltage and current signals are considered and tuned through HS-Transform to yield change in energy and standard deviation. There are 12 inputs consisting of 6 for current signal (*ce(i)* and *sd(i)* for each phase) and 6 for voltage signal (*ce(v)* and *sd(v)* for each phase) are fed to the RBFNN and correspondingly one output is generated from the RBFNN, which is the distance of the fault from the relaying point. The RBFNN has been trained using 3000 sets of data that comprises *ce* and *sd* for faulted current and voltage signals of every kind of fault at various locations (15%,25%,35%,45%,55%,65%, 75%,85%,95% of transmission line), fault resistance, and inception angle. The RBFNN architecture for fault location determination is given in Fig.2.45. The percentage error is computed as given in (2.17).
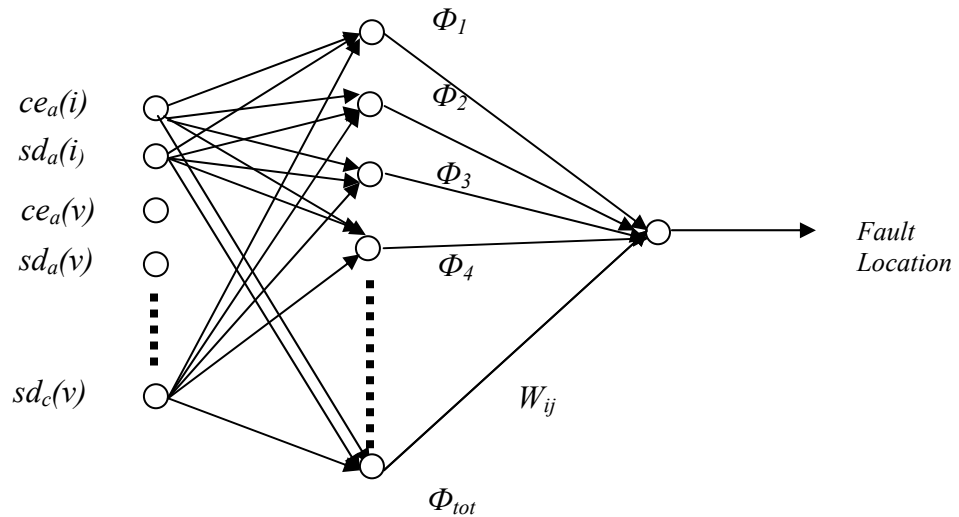
Fig. 2.45 RBFNN architecture for Fault Location

The location error shown in the Table-2.20 through Table-2.24 for 10%, 30%, 50%, 70%, 90% and L-G, LL-G, LL, LLL, LLL-G fault with   fault resistance R_f from 0 ohm to 200 ohm.. The location error for 10% of line with L-G fault with R_f=0Ω is 1.01 % and with R_f=200Ω is 0.89%. Likewise Tables -2.21, Table-2.22, Table-2.23 and Table-2.24 show the % error for LL-G, LL, LLL and LLL-G fault respectively. The error is the least in case of L-G fault that is 0.89% at 10% of line and goes up to 1.89% in case of LL-G fault at 70 % of the transmission line.

Table-2.20 Fault Location for L-G faults

Distance (%)	Fault Resistance(R_f)	Error (%)
10	0	1.01
	200	0.89
30	0	0.99
	200	1.12
50	0	1.11
	200	1.03
70	0	0.99
	200	0.96
90	0	1.00
	200	1.06

Table-2.21 Fault Location for LL-G faults

Distance (%)	Fault Resistance(R_f)	Error (%)
10	0	1.23
	200	1.11
30	0	1.26
	200	1.11
50	0	1.02
	200	1.12
70	0	1.89
	200	0.96
90	0	1.00
	200	1.23

Table-2.22 Fault Location for LL faults

Distance (%)	Fault Resistance(R_f)	Error (%)
10	0	1.23
	200	1.23
30	0	0.98
	200	1.03
50	0	1.02
	200	0.98
70	0	0.97
	200	1.03
90	0	0.99
	200	1.08

Table-2.23 Fault Location for LLL faults

Distance (%)	Fault Resistance(R_f)	Error(%)
10	0	0.99
	200	1.32
30	0	1.08
	200	1.01
50	0	0.96
	200	1.26
70	0	0.94
	200	1.12
90	0	1.11
	200	1.22

Table-2.24 Fault Location for LLL-G faults

Distance (%)	Fault Resistance(R_f)	Error (%)
10	0	1.36
	200	1.41
30	0	0.98
	200	1.12
50	0	1.45
	200	1.36
70	0	0.96
	200	1.11
90	0	0.98
	200	1.02

2.4 Conclusions

Protection scheme for single circuit line using time-frequency transform is presented in the proposed research work. Fault is detected from change in energy of S-Transform of faulted current and voltage signals for the respective phases within half cycle of fault inception. After the fault detection, the impedance to the fault point is calculated from the estimated phasor. In fault condition the impedance trajectory enters in to the relay operating zone within 10 samples (6-9 samples) after the fault detection. Thus the total time taken for the proposed scheme is less than 20 samples (one cycle based on a 50 Hz fundamental frequency) from the inception of the fault. The proposed approach also includes the fault location determination using polynomial curve fitting technique. The error in fault location is found to be below 3%, which indicates the accuracy of the proposed method for fault location determination.

Also distance relaying scheme using S-Transform for protection of parallel transmission line is presented in the proposed study. The faulty phase on either of the lines is detected by finding out the change in energy for the corresponding phase. After the faulty phase detection, the corresponding faulty line is identified by finding out the magnitude and phase difference of the estimated current phasor. But in the case of similar types of faults on both the lines simultaneously and external faults on the line, the difference in magnitude and phase cannot be used to identify the faulty line. In that case the impedance to the fault point is calculated from the estimated phasors of the faulted current and voltage signals. The relay trips the circuit breaker when impedance trajectory enters the tripping zone of the relay. Thus the proposed method provides protection of parallel lines which includes all 11 types of shunt faults on both the lines with different operating conditions. The algorithm detects the fault and identifies the line within one cycle of inception of fault and provides accurate results even in the presence of white noise of low SNR values.

An efficient fault classification and location determination using a variant of S-Transform known as HS-Transform is presented in the proposed research work. HS-Transform based time frequency analysis is used for feature extraction by computing the standard deviation and change in energy at varying window. The change in energy and standard deviation are the input to the RBFNN for fault classification and fault location

determination respectively. RBFNN locator gives the distance of the fault from the relaying point and the error calculated for all kinds of faults is below 2%. By comparing the maximum error in fault location in the original S-Transform and the S-Transform variant (HS-Transform), it is observed that the later produces a more accurate fault location scheme. From the above studies, it is quite clear that the trained neural networks are capable of providing fast and precise classification and location of different types faults with various inception angle and fault resistance.

Chapter-3

Distance relaying using machine intelligence techniques

3.1 Introduction

The proposed research includes machine intelligence techniques such as Support Vector Machine (SVM) [32-34, 42-45] for distance relaying of transmission line including FATCS. SVM is a relatively new computational learning method based on the statistical learning theory. In SVM, original input space is mapped into a high-dimensional dot product space called a feature space, and in the feature space the optimal hyperplane is determined to maximize the generalization ability of the classifier. The optimal hyperplane is found by exploiting the optimization theory, and respecting insights provided by the statistical learning theory. SVMs have the potential to handle very large feature spaces, because training of SVM is carried out so that the dimension of classified vectors does not have as distinct influence on the performance of SVM as it has on the performance of conventional classifiers. That is why it is noticed to be especially efficient in large classification problems. This will also benefit in fault classification, because the number of features to be the basis of fault diagnosis may not have to be limited. Also, SVM-based classifiers are claimed to have good generalization properties compared to conventional classifiers, because in training the SVM classifier the so-called structural misclassification risk is to be minimized, whereas traditional classifiers are usually trained so that the empirical risk is minimized.

3.2 Support Vector Machine for Classification

Let n-dimensional input x_i $(i = 1.....M), M$ is the number of samples) belong to class-I or Class-II and associated labels be $y_i = 1$ for Class I and $y_i = -1$ for Class II, respectively. For linearly separable data, we can determine a hyperplane $f(x) = 0$ that separates the data

$$f(x) = w^T x + b = \sum_{j=1}^{n} w_j x_j + b = 0 \tag{3.1}$$

where 'w' is an n-dimensional vector and 'b' is a scalar. The vector 'w' and the scalar 'b' determine the position of the separating hyperplane. Function *sign(f(x))* is also called the decision function. A distinctly separating hyperplane satisfies the constraints $f(x_i) \geq 1$ if $y_i = +1$ and $f(x_i) \geq -1$, if $y_i = -1$. These results in

$$y_i f(x_i) = y_i (w^T x_i + b) \geq 1 \text{ for } i = 1......, M. \tag{3.2}$$

The separating hyperplane that creates the maximum distance between the plane and the nearest data, i.e., the maximum margin, is called the optimal separating hyperplane. An example of the optimal separating hyperplane of two datasets is presented in Fig. 3.1. From the geometry the geometrical margin is found to be $\|w\|^{-2}$. Taking into account the noise with slack variables ξ_i and error penalty C, the optimal hyperplane can be found by solving the following convex quadratic optimization problem,

minimize $\qquad \dfrac{1}{2}\|w\|^2 + C \sum_{i=1}^{M} \xi_i$

subject to

$$y_i (w^T x_i + b) \geq 1 - \xi_i, \text{ for } i = 1......M$$
$$\xi_i \geq 0, \text{ for } \quad all \quad i \tag{3.3}$$

Where ξ_i is measuring the distance between the margin and the examples x_i lying on the wrong side of the margin. The calculations can be simplified by converting the problem with Kuhn–Tucker conditions into the equivalent Lagrange dual problem, which will maximize

$$W(\alpha) = \sum_{i=1}^{M} \alpha_i - \frac{1}{2} \sum_{i,k=0}^{M} \alpha_i \alpha_k y_i y_k x^T{}_i x_k$$

subject to

$$\sum_{i=1}^{M} y_i \alpha_i = 0, C \geq \alpha_i \geq 0, i = 1....,M \tag{3.4}$$

The number of variables of the dual problem is the number of training data. Let us denote the optimal solution of the dual problem with α^* and w^*. According to the Karush–Kuhn–Tucker theorem, the equality condition in (3.2) holds for the training input–output pair *(xi, yi)* only if the associated α^* is not 0. In this case the training example x_i is a support vector (SV). Usually, the number of SVs is considerably lower than the number of training samples making SVM computationally very efficient. The value of the optimal bias *b** is found from the geometry:

$$b^* = -\frac{1}{2} \sum_{SVs} y_i \alpha^* i (s_1^T x_i + s_2^T x_i),$$

(3.5)

where s_1 and s_2 are arbitrary support vectors (SVs) for *Class I* and *Class II*, respectively. Only the samples associated with the SVs are summed, because the other elements of optimal Lagrange multiplier α^* are equal to zero.

The final decision function will be given by

$$f(x) = \sum_{SVs} \alpha_i y_i x_i^T x + b^* \qquad (3.6)$$

Then unknown data example *'x'* is classified as follows:

$$x \in \begin{cases} Class - I & if \;\; f(x) \geq 0 \\ Class - II & Otherwise \end{cases} \qquad (3.7)$$

SVM can also be used in nonlinear classification tasks with application of kernel functions. The data to be classified is mapped onto a high-dimensional feature space, where the linear classification is possible. Using a nonlinear vector function $\phi(x) = (\phi_1(x)......\phi_m(x)), m >> n$ to map the *'n'*-dimensional input vector *'x'* into the *'m'* dimensional feature space, the linear decision function in dual form is given by

$$f(x) = \sum_{SVs} \alpha_i y_i \phi^T(x_i) \phi(x) \qquad (3.8)$$

Working in the high-dimensional feature space enables the expression of complex functions, but it also generates problems. Computational problems occur due to the large vectors and the danger of overfitting also exists due to the high dimensionality. The latter problem is solved above with application of the maximal margin classifier, and so-called kernels give solution to the first problem. Notice that in (3.8) as well as in the optimization problem (3.3), the data occur only in inner products. A function that returns a dot product of the feature space mappings of original data points is called a kernel, $K(x,z) = \phi^T(x)\phi(z)$. Applying a kernel function, the learning in the feature space does not require explicit evaluation of ϕ. Using a kernel function, the decision function will be

$$f(x) = \sum_{SVs} \alpha_i^* y_i K(x_i x) \tag{3.9}$$

and the unknown data example is classified as before. The values of $K(x_i, x_j)$ over all training samples $i, j = 1.....M$, form the kernel matrix, which is a central structure in the kernel theory. Mercer's theorem states that any symmetric positive-definite matrix can be regarded as a kernel matrix.

The polynomial learning machines of degree 'n' have the inner product kernel

$$K(x,z) = (x^T z + 1)^n \tag{3.10}$$

and radial basis function machines have the inner product kernel

$$K(x,z) = exp\left\{-\frac{|x-z|^2}{2\sigma^2}\right\} \tag{3.11}$$

Where the 'σ' is the width of the Gaussian function.
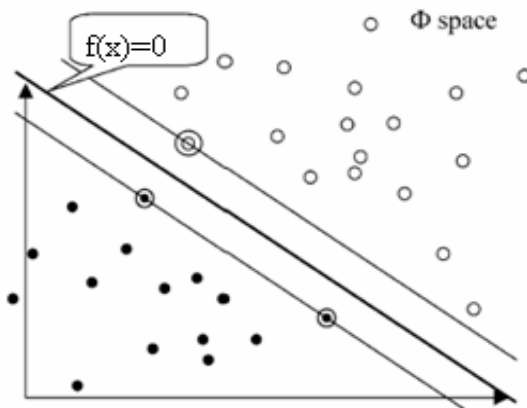
Fig. 3.1 f(x) as a separating hyperplane lying in a high-dimensional space. Support vectors are inside the circles.

3.2.1 Distance Relaying of an Advanced Series Compensated transmission Line using SVM

The use of FACTS [46-49] devices to improve the power transfer capability in high voltage transmission line is of greater interest in these days. The thyristor controlled series compensator (TCSC) is one of the main FACTS devices, which has the ability to improve the utilization of the existing transmission system. TCSC based compensation possess thyristor controlled variable capacitor protected by Metal Oxide Varistor (MOV) and an air gap. However, the implementation of this technology changes the apparent line impedance, which is controlled by the firing angle of thyristors, and is accentuated by other factors including the metal oxide varistor (MOV). The presence of the TCSC in fault loop not only affects the steady state components but also the transient components. The controllable reactance, the MOVs protecting the capacitors and the air-gaps operation make the protection decision more complex and, therefore, conventional relaying scheme based on fixed settings has its limitation. Fault classification and section identification is a very challenging task for a transmission line with TCSC. Different attempts have been made for fault classification using Wavelet Transform, Kalman filtering approach and neural network [50, 51].

The Kalman filtering approach finds its limitation, as fault resistance can not be modeled and further it requires a number of different filters to accomplish the task. Both BPNN (back propagation Neural Network), RBFNN (radial basis function neural network), FNN (Fuzzy Neural network) are employed for adaptive protection of such a line where the protection philosophy is viewed as a pattern classification problem. The networks generate the trip or block signals using a data window of voltages and currents at the relaying point. However, the above approaches are sensitive to system frequency-changes, and require large training sets and training time and a large number of neurons.

The research work presents a new approach for fault classification and section identification of TCSC based line using support vector machine (SVM). SVM, basically, is a classifier based on optimization technique. It optimizes the classification boundary between two classes very close to each other and thereby classifies the data sets even

very close to each other. Also SVM works successfully for multiclass classification with SVM regression.

The current signals for all phases are retrieved at the relaying end at a sampling frequency of 1.0 kHz. Half cycle data (10 samples) and firing angle are used as input to the SVM. The SVM is trained with input and output sets to provide most optimized boundary for classification. Also another SVM is trained for identifying the TCSC position on the transmission line. Taking the current data samples before and after the TCSC, the corresponding SVM is trained to identify whether the fault includes TCSC or not. When fault includes TCSC, the 3rd and 5th harmonic components are highly pronounced compared to the fault which doesn't include TCSC. This issue is taken care by SVMs as the total half cycle (10 samples) data of the fault current signal is taken into consideration for training and testing the SVMs.

3.2.1.1 System Studied
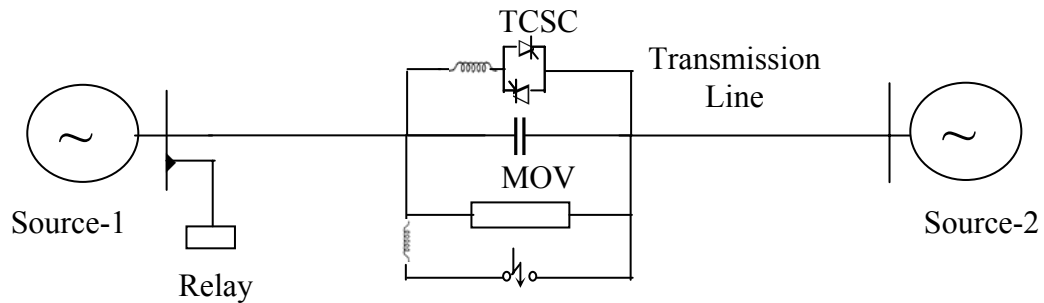
Fig. 3.2 The TCSC based line
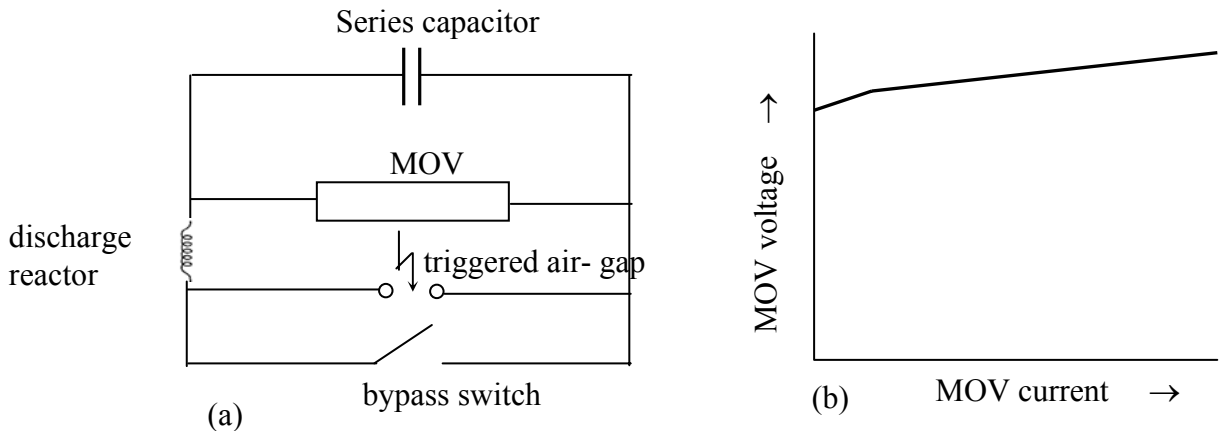
Fig. 3. 3 (a) MOV protected series capacitor
(b) MOV characteristic
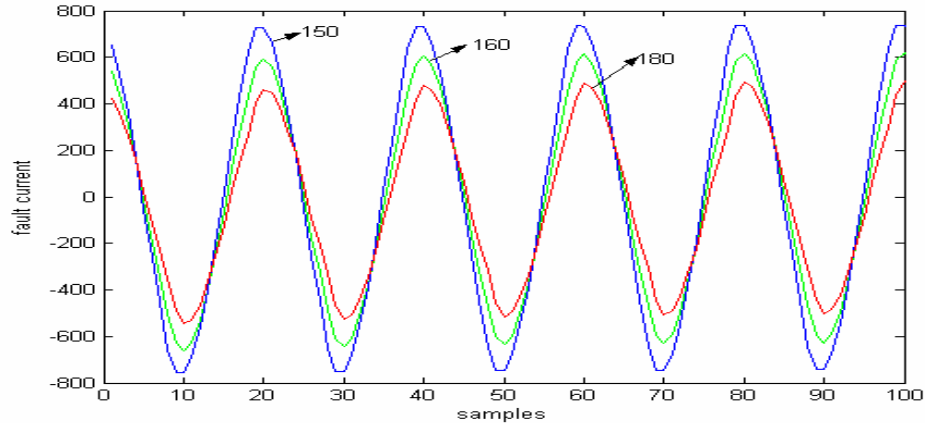
Fig. 3.4 Fault current with TCSC at different firing angles
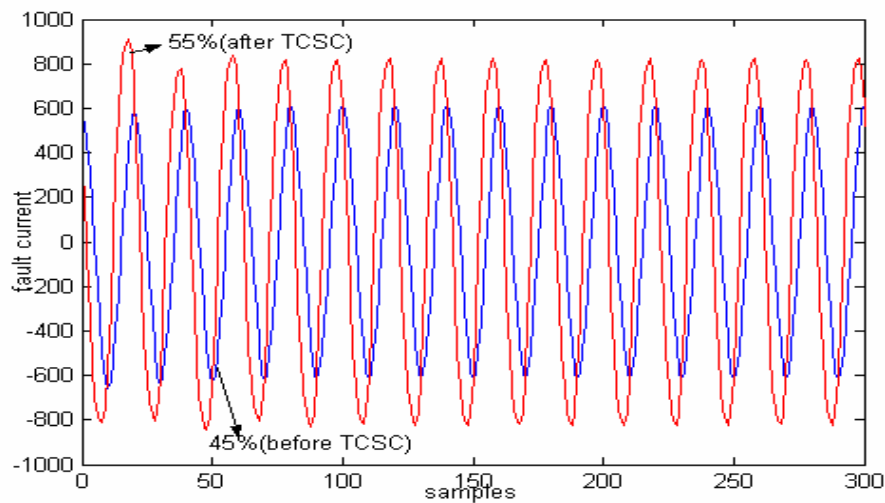
Fig. 3.5 Fault current before and after TCSC at 160⁰ firing angle

A 440 kV, 50 Hz power system is illustrated in Fig. 3.2.In this system the TCSC is located at midpoint of the transmission line, used for the distance protection study. The power system consists of two sources, TCSC and associated components and a 300 km transmission line. The transmission line has zero sequence impedance $Z(0)=96.45+j335.26$ ohm and positive sequence impedance $Z(1)=9.78+j110.23$ ohm. $E_S = 400\,\text{kV}$ and $E_R = 400\angle\delta$ kV. The TCSC is designed to provide compensation

varying form minimum 30% to maximum 40%. All   the   components are modeled using the EMTDC subroutines.

The sampling frequency is 1.0 kHz at 50 Hz base frequency. The metal oxide varistor (MOV) consists of a number of zinc oxide disks electrically connected in series and parallel. The purpose of the MOV is to prevent the voltage across the capacitor from rising to levels which will damage the capacitor. This is most likely to happen when a fault occurs at a point on the compensated line which minimizes the impedance of the fault loop. When instantaneous voltage across the capacitor approaches a dangerous level the MOV begins to draw a significant proportion of the line current thereby limiting the voltage across the capacitor at that level. This action alters the impedance in the series path and hence the fault-loop impedance. In the event that the MOV remains in conduction long enough to raise its temperature (energy) to a dangerous level an air-gap is triggered to short out both the MOV and the capacitor, again changing the fault loop impedance. The operation of the MOV can be within the first half cycle of fault and depending on the severity of the fault, it may continue to operate until the air-gap is triggered cycles later. This is precisely the time when a digital relay makes protection decision. Further, a bypass switch in parallel with the gap automatically closes for abnormal system conditions that cause prolonged current flow through the gap. Fig. 3.3 shows the components of MOV and characteristics. The fault current variation with firing angle is shown in Fig. 3.4. The fault current pattern including TCSC and without including TCSC is shown in Fig. 3.5.

The small inductance in the arrangement limits the current through the air-gap or switch circuit. The TCSC is designed such that it provides 30% compensation at 180^0 (minimum) and 40% compensation at 150^0 (maximum) firing angle and in this study the firing angle is varied within this range as shown in Fig. 3.6 .The proposed protection scheme is shown in Fig. 3.7.
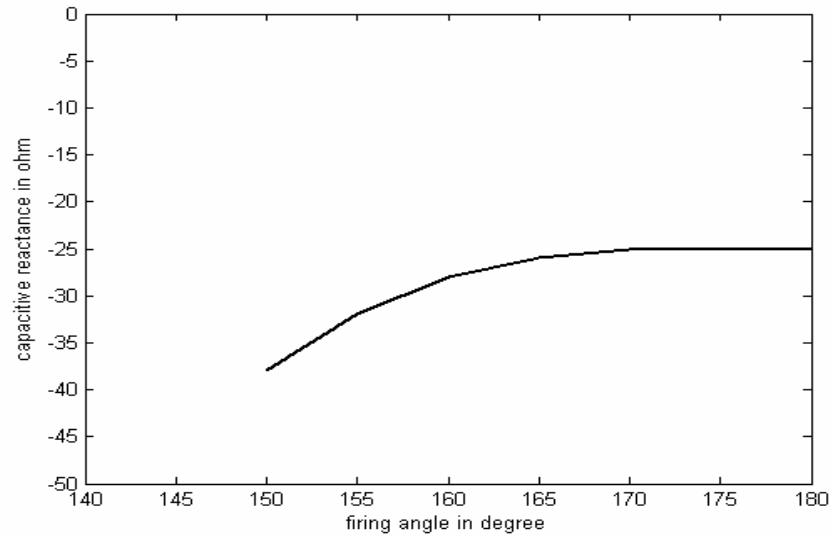
Fig. 3.6 Variation of capacitive reactance with firing angle
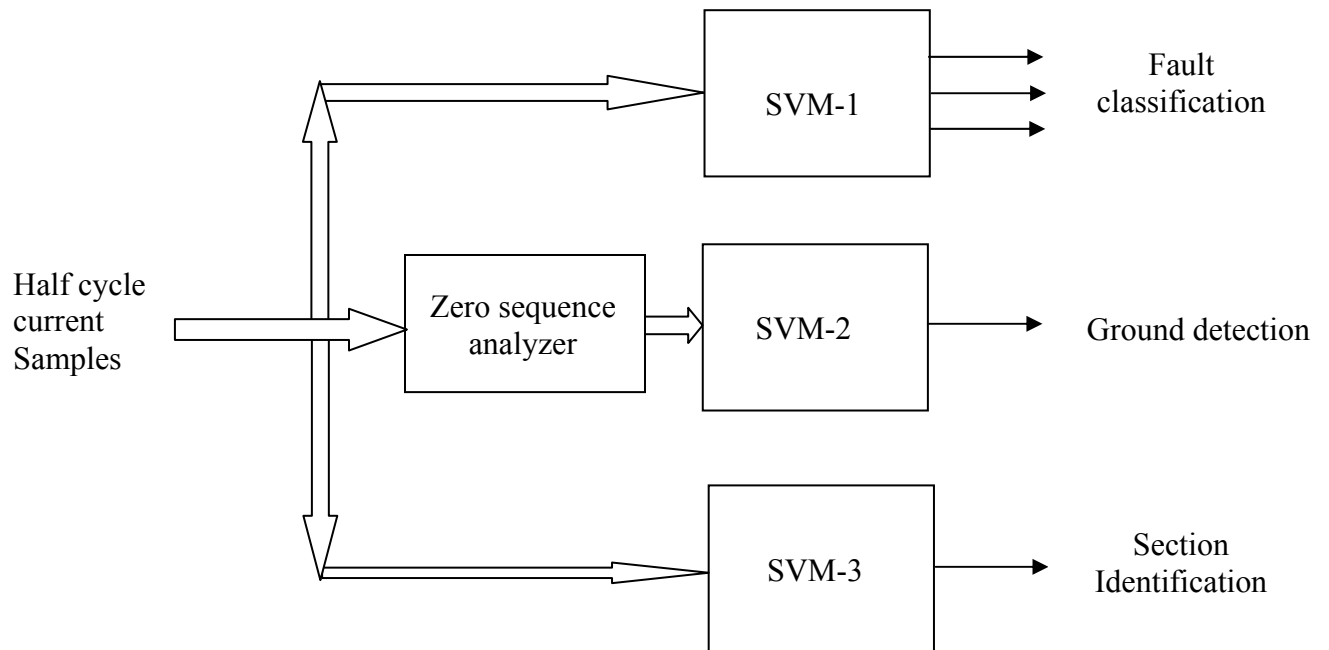
Fig. 3.7 Proposed scheme for protection. Fault classification (SVM-1), Ground detection (SVM-2) and section identification (SVM-3).

The TCSC is placed at 50% of the transmission line with 300 km line length, which is 150 km from relaying end. The simulation for all 11 types of shunt faults (L-G,LL-G,LL,LLL,LLL-G) are made on the transmission line with different fault resistance, source impedance, incident angles at different fault locations with varying the firing angle from 150º-180º with (after) and without including(before) TCSC. The half cycle signal having 10 samples from the fault inception are retrieved at the relaying end and normalized to be used as input to the corresponding SVMs.

3.2.1.2 SVM Training and testing

(a) SVM for fault classification

The half cycle fault current signal samples after the fault inception are taken as input to the SVM. The corresponding output is either fault or no-fault condition. Ten samples(half cycle at 1.0 kHz sampling frequency) of fault current form the fault inception are retrieved at the relaying end are normalized along with the firing angle of TCSC and are used as input(11-inputs) space which is termed as 'x'. 'y' is the corresponding output which results '1' for fault and '-1' for no-fault condition. The optimal marginal classifier is designed with polynomial kernel with different order and Gaussian kernel with different parameter value. Both results are compared as depicted in Table-3.1.The SVM-1 is trained with 500 data sets and tested with 200 data sets, each set comprising of 11 data points(10 for half cycle current signal and 1 for firing angle of TCSC) for 'x' as input and (1,-1) for 'y' as corresponding output.

Faults on the line are simulated with various operating conditions including different incident angles, fault resistance (10-200ohm), source capacities, and various locations with different firing angles for all 11 types of shunt faults. When the parameter values of the polynomial kernel and Gaussian kernel are changed, the numbers of support vectors on the optimized marginal plane vary accordingly as seen from the result depicted in the Table-3.2. Here 'n' stands for the order of the polynomial and 'σ' stands for width of the gaussian function. The bound on the lagrangian multipliers 'C' is selected 10 and the conditioning parameter for QP method, lambda is chosen as 1.0*e-7. Different values of 'σ' with which the SVM is trained and tested are 0.5 and 1.5. Similarly the values

selected for 'n' are 2 and 3. All the above parameters are selected after cross validation [52-54].

Table-3.1 shows the results for fault classification for various operating conditions. As seen from the table, for 'b-g' fault at 30%,$\alpha=155°$,R_f =20 ohm, the 'b' ph output is '1' but output for 'a' and 'c' phases is '-1' for both polynomial and Gaussian kernel, which depicts that fault occurs only on 'b' phase. Also for 'abc' fault at 65%,$\alpha=160°$,R_f =200 ohm, the output for all the phases is '1'. As seen, the misclassification occurs for the above operating condition with polynomial kernel with 'n'=2 resulting output of 'c' phase as '-1' instead of '1'.Table-3.2 depicts the classification rates at different faults and corresponding support vectors with polynomial and Gaussian kernel of different parameter values. The classification rate is 95.23% (minimum) at L-G fault with Gaussian kernel with σ =0.5 and the support vectors are 13. Similarly the classification rate is 97.84% (maximum) fir LL-G fault with gaussian kernel with σ =0.5 which results 7 support vectors on the hyperplane.

Table -3.1 Testing of SVM-1 for fault classification

Fault	Kernel	Parameter value	a	b	c
b-g fault at 30%,$\alpha=155°$,R_f =20 ohm	poly	n=2	-1	1	-1
	poly	n=3	-1	1	-1
	gaussian	$\sigma=0.5$	-1	1	-1
	gaussian	σ =1.5	-1	1	-1
ab-g fault at 30%,$\alpha=165°$,R_f =50 ohm	poly	n=2	1	1	-1
	poly	n=3	1	1	-1
	gaussian	$\sigma=0.5$	1	1	-1
	gaussian	σ =1.5	1	1	-1
'bc' fault at 45%,$\alpha=170°$,R_f =100 ohm	poly	n=2	-1	1	1
	poly	n=3	-1	1	1
	gaussian	$\sigma=0.5$	-1	1	1
	gaussian	σ =1.5	-1	1	1
'abc' fault at 65%,$\alpha=160°$,R_f =200 ohm	poly	n=2	1	1	-1
	poly	n=3	1	1	1
	gaussian	$\sigma=0.5$	1	1	1
	gaussian	σ =1.5	1	1	1
'abc-g' fault at 75%,$\alpha=165°$,R_f =150 ohm with source changed	poly	n=2	1	1	1
	poly	n=3	1	1	1
	gaussian	$\sigma=0.5$	-1	1	1
	gaussian	σ =1.5	1	1	1

Table -3.2 Classification rates of SVM-1 for
fault classification with 200 data sets

Fault	Kernel	Parameter value	Classification rates (%)	No.of support vectors
L-G	poly	n=2	96.52	15
	poly	n=3	97.23	12
	gaussian	σ=0.5	95.23	13
	gaussian	σ =1.5	96.85	11
LL-G	poly	n=2	96.27	9
	poly	n=3	97.36	7
	gaussian	σ=0.5	97.51	7
	gaussian	σ =0.5	97.84	7
LL	poly	n=2	96.84	11
	poly	n=3	97.29	9
	gaussian	σ=0.5	95.99	9
	gaussian	σ =1.5	96.87	6
LLL	poly	n=2	96.28	14
	poly	n=3	97.56	12
	gaussian	σ=0.5	95.68	11
	gaussian	σ =1.5	96.87	10
LLL-G	poly	n=2	97.25	12
	poly	n=3	97.68	10
	gaussian	σ=0.5	96.78	8
	gaussian	σ =1.5	97.65	5

(b) SVM for ground detection

The ground detection is done separately by training another SVM. The peak value of the zero sequence component of the fault current signal for half cycle is found out for fundamental, 3rd and 5th harmonic component. The peak value of zero sequence components and firing angle of TCSC are used as the input-'x'(4-inputs) to the SVM-2 and the corresponding output(y) is '1' for the fault involving ground and '-1' for fault without involving ground. As the zero sequence components for these three harmonic components are pronounced in case of fault involving ground compared to fault without involving ground, the SVM-2 is trained to design a optimized classifier for ground detection.

Here 'n' stands for the order of the polynomial and 'σ' stands for width of the gaussian function. The bound on the lagrangian multipliers 'C' is selected 5 and the

conditioning parameter for QP method, lambda is chosen as 1.0*e-7. Different values of 'σ' with which the SVM is trained and tested are 0.5 and 1.0. Similarly the values selected for 'n' are 1 and 2. All the above parameters are selected after cross validation [52-54].The SVM is trained with 500 data sets and tested for 200 data sets. The average classification rate for ground detection for 200 test cases is found to be 98.05% for all types of faults with different operating conditions. It is found form the Table-3.3 that for 'a-g' fault at 10%,α=160º,R_f =20 ohm, the output is'1' which shows that the fault involves ground. But 'bc' fault at 30%,α=165º,R_f =50 ohm, the output is '-1' which clearly shows that fault without involving ground. Also misclassification is observed for 'ac' fault at 45%, α=155º,R_f =200 ohm with polynomial kernel for n=2, which produces output '1' instead of '-1'. Also similar case happens for abc-g fault at 85%, α=160º,R_f =150 ohm with polynomial kernel for n=1.

Table -3.3 Testing of SVM-2 for ground detection

Fault	Kernel	Parameter value	Classification
a-g fault at 10%,α=160º,R_f =20 ohm	poly	n=1	1
	poly	n=2	1
	gaussian	σ =0.5	1
	gaussian	σ =1.0	1
bc fault at 30%,α=165º,R_f =50 ohm	poly	n=1	-1
	poly	n=2	-1
	gaussian	σ =0.5	-1
	gaussian	σ =1.0	-1
bc-g fault at 55%,α=175º,R_f =100 ohm	poly	n=1	1
	poly	n=2	1
	gaussian	σ =0.5	1
	gaussian	σ =1.0	1
abc fault at 65%,α=160º,R_f =150 ohm	poly	n=1	-1
	poly	n=2	-1
	gaussian	σ =0.5	-1
	gaussian	σ =1.0	-1
ac fault at 45%,α=155º,R_f =200 ohm	poly	n=1	-1
	poly	n=2	1
	gaussian	σ =0.5	-1
	gaussian	σ =1.0	-1
abc-g fault at 30%,α=165º,R_f =50 ohm	poly	n=1	1
	poly	n=2	1

	gaussian	$\sigma =0.5$	1
	gaussian	$\sigma =1.0$	1
bc-g fault at 85%,α=165º,R_f =100 ohm	poly	n=1	1
	poly	n=2	1
	gaussian	$\sigma =0.5$	1
	gaussian	$\sigma =1.0$	1
ab fault at 65%,α=160º,R_f =150 ohm	poly	n=1	-1
	poly	n=2	-1
	gaussian	$\sigma =0.5$	-1
	gaussian	$\sigma =1.0$	-1
abc-g fault at 85%,α=160º,R_f =150 ohm with source changed	poly	n=1	-1
	poly	n=2	1
	gaussian	$\sigma =0.5$	1
	gaussian	$\sigma =1.0$	1

(c) SVM for section identification

Section identification for the transmission line with TCSC is done by training the SVM-3 to build up an optimized classifier. The half cycle data (10 samples) after the fault inception and firing angle of TCSC are used as input-'x' (11-inputs) to the SVM and the output-'y' is the output. The output 'y' is '1' or '-1' for faults including TCSC and without TCSC, respectively. For any fault beyond 50% of the line the output of the SVM should be '1', otherwise '-1'.The SVM is trained with the bound on the lagrangian multipliers with 'C' selected as 20 and the conditioning parameter for QP method lambda chosen as 1.0*e-7. The lagrangian parameter 'C' is selected after testing the SVM with other values. The above parameters are selected after cross validation as mentioned earlier. The SVM is trained with 500 data sets and tested for 200 data sets. The average classification rate for section identification for 200 test cases is found to be 95.09% for all types of faults with different operating conditions.

Table-3.4 depicts the results for section identification for TCSC on the transmission line. For 'ac-g' fault at 30%,α=165º,R_f =50 ohm, the output of SVM is '-1' which shows that the fault occurred before TCSC on the line. But for 'bc-g' fault at 55%,α=170º,R_f =100 ohm, the output of SVM is '1', which clearly depicts that the fault occurred after the TCSC on the line. Also misclassification is observed for 'abc-g' fault at 30%, α=175º,R_f =20 ohm with polynomial kernel with n=1 and for 'ab' fault at

15%,α=160º,R_f =20 ohm with source changed with gaussian kernel with σ =0.5. Also similar result occurs for 'abc' fault at 65%, α=155º,R_f =200 ohm with source changed for polynomial kernel with n=2.

Table-3.4 Testing of SVM-3 for section identification

Fault	Kernel	Parameter value	Classification
ab fault at 10%,α=160º,R_f =20 ohm	poly	n=1	-1
	poly	n=2	-1
	gaussian	σ =0.5	-1
	gaussian	σ =1.0	-1
ac-g fault at 30%,α=165º,R_f =50 ohm	poly	n=1	-1
	poly	n=2	-1
	gaussian	σ =0.5	-1
	gaussian	σ =1.0	-1
bc-g fault at 55%,α=170º,R_f =100 ohm	poly	n=1	1
	poly	n=2	1
	gaussian	σ =0.5	1
	gaussian	σ =1.0	1
abc-g fault at 65%,α=170º,R_f =150 ohm	poly	n=1	1
	poly	n=2	1
	gaussian	σ =0.5	1
	gaussian	σ =1.0	1
ac fault at 45%,α=165º,R_f =100 ohm	poly	n=1	-1
	poly	n=2	-1
	gaussian	σ =0.5	-1
	gaussian	σ =1.0	-1
abc-g fault at 30%,α=175º,R_f =20 ohm	poly	n=1	1
	poly	n=2	-1
	gaussian	σ =0.5	-1
	gaussian	σ =1.0	-1
bc-g fault at 75%,α=165º,R_f =100 ohm with source changed	poly	n=1	1
	poly	n=2	1
	gaussian	σ =0.5	1
	gaussian	σ =1.0	1
ab fault at 15%,α=160º,R_f =20 ohm with source changed	poly	n=1	-1
	poly	n=2	-1
	gaussian	σ =0.5	1
	gaussian	σ =1.0	-1
abc fault at 65%,α=155º,R_f =200 ohm with source changed	poly	n=1	1
	poly	n=2	-1
	gaussian	σ =0.5	1
	gaussian	σ =1.0	1

3.2.2   SVM based Distance Relaying for single circuit transmission line

The proposed research also includes fault analysis of single circuit transmission line without FATCS using Support Vector Machine (SVM). Fault classification is required to detect the line or phase involved in the fault process with or without ground. The proposed method uses post fault current and voltage samples for $1/4^{th}$ cycle (5 samples) from the inception of the fault as inputs to the SVMs to result fault classification with ground detection. Polynomial and Gaussian kernel based SVMs are trained and tested with corresponding current and voltage samples to distinguish faulty phase from un-faulted one. SVM-1 and SVM-2 are designed to provide information regarding faulty phase and ground involved in the fault process respectively. The classification test results obtained form SVMs are accurate for simulation model with wide variations in operating conditions of the faulted power network, and thus provides fast and robust protection scheme for distance relaying.

3.2.2.1   System Studied
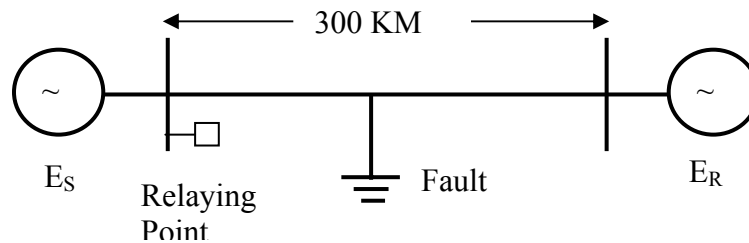
Fig. 3.8 Transmission Line Model

The network having two areas connected by the transmission line of 400 KV. The transmission line has zero sequence parameter Z(0)=96.45+j335.26 ohm and positive sequence impedance Z(1)=9.78+j110.23 ohm. $E_S = 400$ and $E_R = 400\angle\delta$. The relaying point is shown in Fig. 3.8, where data is retrieved for different fault conditions. The sampling rate chosen is 1.0 kHz at 50 Hz frequency. There are 20 samples per cycle. The model network shown in Fig. 3.8 has been simulated using PSCAD (EMTDC) package. The fault voltage and current signals are retrieved at the relaying end and fed to the

SVMs for faulty phase selection and ground detection. The proposed relaying scheme is shown in Fig. 3.9.

1/4th cycle of current signal (5 samples)

1/4th cycle of voltage signal (5 samples)

SVM-1 → Fault classification

Zero sequence analyzer → SVM-2 → Ground detection
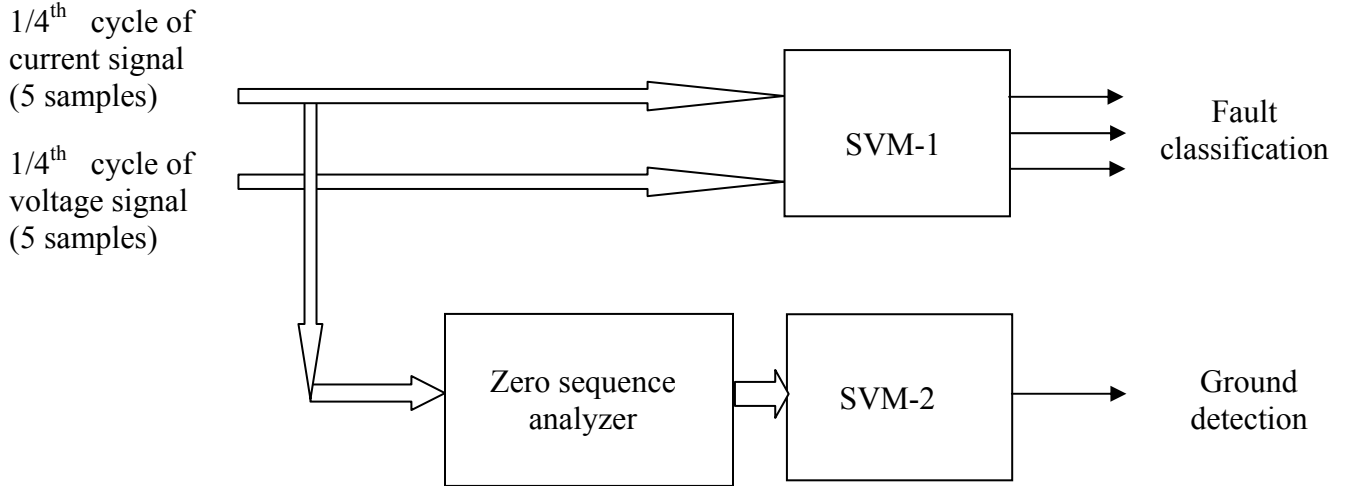
Fig.3.9 Proposed scheme for protection.
Fault classification   (SVM-1), Ground detection (SVM-2)

3.2.2.2 Simulation Results

(a) Phase selection (SVM-1)

The 1/4th cycle fault current and voltage signal samples after the fault are taken as input to the SVM. The corresponding output is either fault or no-fault condition. Ten samples (5 samples for voltage and 5 for current) of fault current form the fault inception are retrieved at the relaying end are normalized and are used as input (10-points) space which is termed as 'x'. 'y' is the corresponding output which results '1' for fault and '-1' for no-fault condition. The optimal marginal classifier is designed with polynomial kernel with different order and Gaussian kernel with different parameter value. The SVM-1 is trained with 500 data sets and tested with 200 data sets, each set comprising of 10 data points for 'x' as input and (1,-1) for 'y' as corresponding output.

Faults on the line are simulated with various operating conditions including different incident angles 'δ', fault resistance R_f (10-200ohm), source capacities and at various locations for all 11 types of shunt faults. When the parameter values of the

polynomial kernel and Gaussian kernel are changed, the numbers of support vectors on the optimized marginal plane vary accordingly as seen from the result depicted in the Table-3.6. Here 'n' stands for the order of the polynomial and 'σ' stands for width of the gaussian function. The bound on the lagrangian multipliers 'C' is selected 10 after testing the SVM for other values of 'C' and it provides better results. The conditioning parameter for QP method lambda is chosen as 1.0*e-7. The higher order polynomial is chosen for better accuracy. The above parameters are selected after cross validation as mentioned earlier.

Table-3.5 shows the results for fault classification for various operating conditions. As seen from the table, for 'ab-g' fault at 30%, $\delta=45°$ °, R_f =50 ohm, the SVM-1 outputs for 'a' and 'b' are '1' but output for 'c' phase is '-1' for both polynomial and Gaussian kernel, which depicts that fault occurs on 'a' and 'b' phases. Also for 'bc' fault at 50%,$\delta=60°$ R_f =100 ohm the output for 'b' and 'c' phases are '1' but the output is'-1' for 'a' phase. As seen, the misclassification occurs for the 'abc-g' fault at 90% ,$\delta=45°$ R_f =150 ohm with source changed, with gaussian kernel with 'σ'=1.0 resulting output of 'a' phase as '-1' instead of '1'.Table-3.6 depicts the classification rates at different faults and corresponding support vectors with polynomial and Gaussian kernel of different parameter values. The testing is done on 200 data sets. The classification rate is 97.25% (minimum) at LLL-G fault with Polynomial kernel with n =5 and the support vectors are 12. Similarly the classification rate is 98.87% (maximum) fir LL-G fault with gaussian kernel with σ =1.0 which results 9 support vectors on the hyperplane. The average classification rate for phase selection for 200 test cases is found to be 98.07% for all types of faults with different operating conditions.

Table-3.5 Testing of SVM-1 for fault phase selection

Fault	Kernel	Parameter value	a-phase	b-phase	c-phase
b-g fault at 10%,δ=30° R$_f$=10 ohm	poly	n=5	-1	1	-1
	poly	n=6	-1	1	-1
	gaussian	σ=1.0	-1	1	-1
	gaussian	σ =1.5	-1	1	-1
ab-g fault at 30%,δ=45° R$_f$=50 ohm	poly	n=5	1	1	-1
	poly	n=6	1	1	-1
	gaussian	σ=1.0	1	1	-1
	gaussian	σ =1.5	1	1	-1
'bc' fault at 50%,δ=60° R$_f$=100 ohm	poly	n=5	-1	1	1
	poly	n=6	-1	1	1
	gaussian	σ=1.0	-1	1	1
	gaussian	σ =1.5	-1	1	1
'abc' fault at 70%, δ=45° R$_f$=150 ohm	poly	n=5	1	1	-1
	poly	n=6	1	1	1
	gaussian	σ=1.0	1	1	1
	gaussian	σ =1.5	1	1	1
'abc-g' fault at 90%, δ=45° R$_f$=150 ohm with source changed	poly	n=5	1	1	1
	poly	n=6	1	1	1
	gaussian	σ=1.0	-1	1	1
	gaussian	σ =1.5	1	1	1
'ca-g' fault at 45%, δ=60° R$_f$=100 ohm	poly	n=5	1	-1	1
	poly	n=6	1	-1	1
	gaussian	σ=1.0	1	-1	1
	gaussian	σ =1.5	1	-1	1
'c-g' fault at 85%,δ=60°, R$_f$=150 ohm	poly	n=5	-1	-1	1
	poly	n=6	-1	-1	1
	gaussian	σ=1.0	-1	-1	1
	gaussian	σ =1.5	-1	-1	1
'ab' fault at 95%,δ=45°, R$_f$=200 ohm	poly	n=5	1	1	-1
	poly	n=6	1	1	-1
	gaussian	σ=1.0	1	1	-1
	gaussian	σ =1.5	1	1	-1
'abc-g' fault at 75%, δ=30°, R$_f$=200 ohm with source changed	poly	n=5	1	-1	1
	poly	n=6	1	1	1
	gaussian	σ=1.0	1	1	1
	gaussian	σ =1.5	1	1	1

Table-3.6 Classification rates of SVM-1 for phase selection with 200 data sets

Fault	Kernel	Parameter value	Classification rates (%)	No.of support vectors
L-G	poly	n=5	98.16	19
	poly	n=6	98.19	14
	gaussian	σ=1.0	98.23	15
	gaussian	σ =1.5	97.89	12
LL-G	poly	n=5	98.15	10
	poly	n=6	98.09	11
	gaussian	σ=1.0	98.87	09
	gaussian	σ =1.5	97.84	08
LL	poly	n=5	97.84	10
	poly	n=6	98.29	09
	gaussian	σ=1.0	97.99	08
	gaussian	σ =1.5	97.87	06
LLL	poly	n=5	98.01	19
	poly	n=6	97.56	14
	gaussian	σ=1.0	98.68	10
	gaussian	σ =1.5	97.87	09
LLL-G	poly	n=5	97.25	12
	poly	n=6	98.69	10
	gaussian	σ=1.0	97.86	08
	gaussian	σ =1.5	98.15	06

(b) Ground detection (SVM-2)

The ground detection is done separately by training and testing SVM-2. The peak value of the zero sequence component of the fault current signal for fundamental ,3rd and 5th harmonic are found out and are used as the input-'x'(three input) to the SVM-2 and the corresponding output(y) is '1' for the fault involving ground and '-1' for fault without involving ground. As the zero sequence components are pronounced in case of fault involving ground compared to fault without involving ground, the SVM-2 is trained to design an optimized classifier for ground detection.

The order of the polynomial is n' and width of the gaussian function is 'σ'. The lagrangian parameter is selected after testing the SVM with other values, but C=5 provide the best result compared to other values. Thus the bound on the lagrangian multipliers 'C' is selected 5 and the conditioning parameter for QP method lambda is

Table-3.7 Testing of SVM-2 for ground detection

Fault	Kernel	Parameter value	Classification
'b-g' fault at 10%, δ=30° R_f =10 ohm	poly	n=5	1
	poly	n=6	1
	gaussian	σ=1.0	1
	gaussian	σ =1.5	1
'ab-g' fault at 30%, δ=45° R_f =50 ohm	poly	n=5	1
	poly	n=6	1
	gaussian	σ=1.0	1
	gaussian	σ =1.5	1
'bc' fault at 50%, δ=60° R_f =100 ohm	poly	n=5	-1
	poly	n=6	-1
	gaussian	σ=1.0	-1
	gaussian	σ =1.5	-1
'abc' fault at 70%, δ=45° R_f =150 ohm	poly	n=5	-1
	poly	n=6	-1
	gaussian	σ=1.0	-1
	gaussian	σ =1.5	-1
'abc-g' fault at 90% , δ=45° R_f =150 ohm with source changed	poly	n=5	1
	poly	n=6	1
	gaussian	σ=1.0	-1
	gaussian	σ =1.5	1
'ca-g' fault at 45%,δ=60° R_f =100 ohm	poly	n=5	1
	poly	n=6	1
	gaussian	σ=1.0	1
	gaussian	σ =1.5	1
'c-g' fault at 85%, δ=60°, R_f =150 ohm	poly	n=5	1
	poly	n=6	1
	gaussian	σ=1.0	1
	gaussian	σ =1.5	1
'ab' fault at 95%, δ=45°, R_f =200 ohm	poly	n=5	-1
	poly	n=6	-1
	gaussian	σ=1.0	-1
	gaussian	σ =1.5	-1
'abc-g' fault at 75%, δ=30°, R_f =200 ohm with source changed	poly	n=5	-1
	poly	n=6	1
	gaussian	σ=1.0	1
	gaussian	σ =1.5	1

chosen as 1.0*e-7. The above parameters are selected after cross validation as mentioned earlier. The SVM is trained with 500 data sets and tested for 200 data sets. It is found form the Table-3.7 that for 'b-g' fault at 10%,δ=30° R_f =10 ohm, the output is '1' which shows that the fault involves ground. But for 'bc' fault at 50%,δ=60° R_f =100 ohm, the output is '-1' which clearly shows that fault without involving ground. Also misclassification is observed for 'abc-g' fault at 75%, δ=30°, R_f =200 ohm with source changed, with polynomial kernel for n=5, which produces output '-1' instead of '1'. Also similar case happens for 'abc-g' fault at 90%, δ=45° R_f =150 ohm with source changed, with gaussian kernel for σ=1.0 which results '-1' instead of '1'. Table-3.8 shows the classification rate of the SVM-2 for ground detection. The classification rate is 99.32% for LL-G fault with Gaussian kernel with σ=1.0 and the minimum is 98.02% for LLL fault with σ=1.0.The average classification rate for ground detection for 200 test cases is found to be 98.62% for all types of faults with different operating conditions.

Table-3.8 Classification rates of SVM-2 for ground detection with 200 data sets

Fault	Kernel	Parameter value	Classification rates (%)	No. of support vectors
L-G	poly	n=5	99.05	15
	poly	n=6	98.74	13
	gaussian	σ=1.0	98.98	12
	gaussian	σ =1.5	99.14	09
LL-G	poly	n=5	98.96	11
	poly	n=6	98.25	08
	gaussian	σ=1.0	99.32	10
	gaussian	σ =1.5	98.39	06
LL	poly	n=5	99.45	13
	poly	n=6	98.21	11
	gaussian	σ=1.0	98.69	09
	gaussian	σ =1.5	97.89	05
LLL	poly	n=5	98.47	17
	poly	n=6	97.98	14
	gaussian	σ=1.0	98.02	12
	gaussian	σ =1.5	98.07	09
LLL-G	poly	n=5	97.99	10
	poly	n=6	98.77	07
	gaussian	σ=1.0	99.05	09
	gaussian	σ =1.5	99.06	04

It is found that SVM-1 and SVM-2 combined together provide very accurate results for phase selection and ground detection respectively. The SVMs separate the faulty phase data from un-faulted one with error less than 2%. As the speed and accuracy are the two important requirements for digital protection of power systems, the proposed method is found to be suitable for protection of large power transmission line.

3.3   Conclusions

A new approach for the protection of Flexible AC Transmission Line with TCSC using support vector machine is presented in this research work. Half cycle post fault current samples and firing angles are used as input to the SVMs and the output is the corresponding classification. SVM-1 is used for fault classification, SVM-2 is used for ground detection and SVM-3 is used for section identification for the TCSC on the line, respectively. It is found that SVMs are trained to result most optimized classifier and with very less numbers of training samples compared to the neural network and neuro-fuzzy systems. Also the error found is less that 5% taking all SVMs to consideration. Hence the proposed method is very accurate and robust for the protection of transmission line including TCSC.

Also Support Vector Machine based protection scheme for general transmission line without FACTS is developed. In the proposed technique, $1/4^{th}$ cycle post fault current and voltage samples are collected at the relaying point and fed to the SVMs as inputs and provides the information about the faulty phase and ground involved in the fault process. SVM-1 is trained and tested with the faulted voltage and current samples to provide fault classification accurately. Similarly, SVM-2 is trained and tested with the peak of the zero sequence currents to result the ground involvement in the fault process. The kernel parameters and bound on the lagrangian multipliers are selected after cross validation. The SVMs provide fault classification and ground detection with error less than 3%. Hence the proposed technique is very fast, accurate and robust for the protection of large power transmission networks.

Chapter-4

Differential Equation based numerical protection for transmission line including FACTS

4.1 Introduction

In the current open access environment, transmission systems are being required to provide increased bulk power transfer capability and to accommodate a much wider range of possible generation patterns. This had led to an increased focus on transmission constraints and on the means by which ouch constraints can be alleviated. FACTS [46-48] devices offer a versatile alternative to conventional reinforcement methods. One of the more intriguing and potentially most versatile classes of FACTS device is the unified power flow controller (UPFC) [49]. This device, which consists of two linked self-commutating converters, connected to the ac systems through series and shunt transformers, offers a unique combination of fast shunt and series compensation. The UPFC offers new horizons in terms of power system control, with the potential to independently control up to three power system parameters; for instance bus voltage, line active power and line reactive power. While the use of UPFC improves the power transfer capability and stability of a power system, certain other problems emerge in the field of power system protection; in particular the transmission line protection. The implementation of control strategies for FACTs devices introduces new power system dynamic problems that must be considered while selecting the issues related to protection. The presence of fault in the fault loop containing an UPFC affects both transient and steady state components of the voltage and current in the transmission line. Thus finding the fault location from the relaying point in presence of UPFC is a challenging issue to deal with.

4.2   A novel Fault location algorithm for UPFC based line using Differential Equation Approach

The proposed research presents the fault location algorithm based on differential equation approach [1] for UPFC based line. The method works on the assumption that

fault detection and section identification have been done for the transmission line including UPFC. The fault detection can be done by using the fault detector which uses a short data window (four samples) algorithm [40]. The final indication of the fault is only given when three consecutive comparisons give the difference more than a specified threshold value. Fault section identification can be done using Wavelet Transform as applied for TCSC based line [55]. After fault section is identified, the control shifts to the differential equation based fault location algorithm which estimates the line inductance up to the fault point from relaying end. Thus the fault location is determined which is directly proportional to the line inductance. There are two different fault location algorithms based on the fault occurrence before or after the UPFC in the line. The UPFC model is simulated using PSCAD and simulations are carried out for different faults with different operating conditions. The instantaneous fault current and voltage samples at sending and receiving end are fed to the designed differential equation based algorithm sample by sample which results the fault location in terms of the line inductance. The proposed method results accurately with variation in series injected voltage, phase angle, fault resistance, fault inception angle etc.

4.2.1 System Studied

The model network shown in Fig. 4.1 has been simulated using PSCAD package as given in Fig. 4.2. The network having two areas connected by the transmission line of 400 kV. The transmission line has zero sequence impedance Z(0)=96.45+j335.26 ohm and positive sequence impedance Z(1)=9.78+j127.23 ohm and $E_S = 400\,\text{kV}$, $E_R = 400\angle\delta\,\text{kV}$. The relaying point is as shown in the Fig. 4.1, where data is retrieved for different fault conditions. The sampling rate is 1.0 kHz at 50 Hz base frequency. The UPFC is placed at 50% of the line with series injected voltage varying from 10% to 20%. The SSSC and STATCOM control system circuits are shown in Fig. 4.3 and 4.4, respectively.
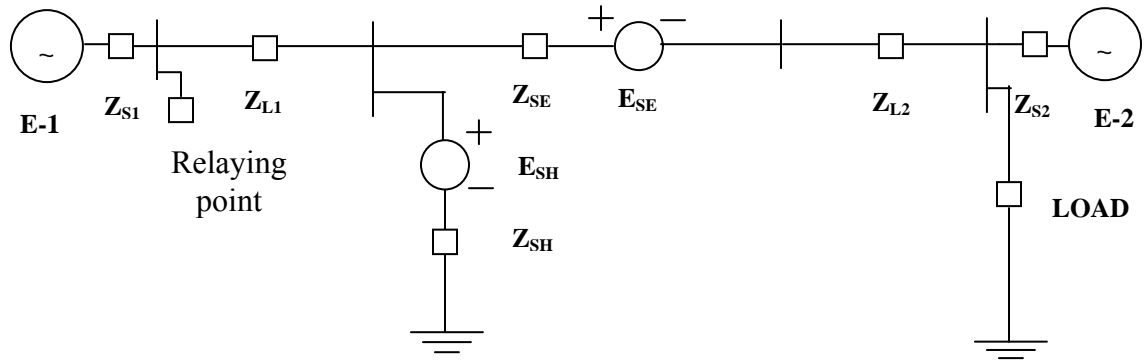
Fig. 4.1 UPFC based transmission line model
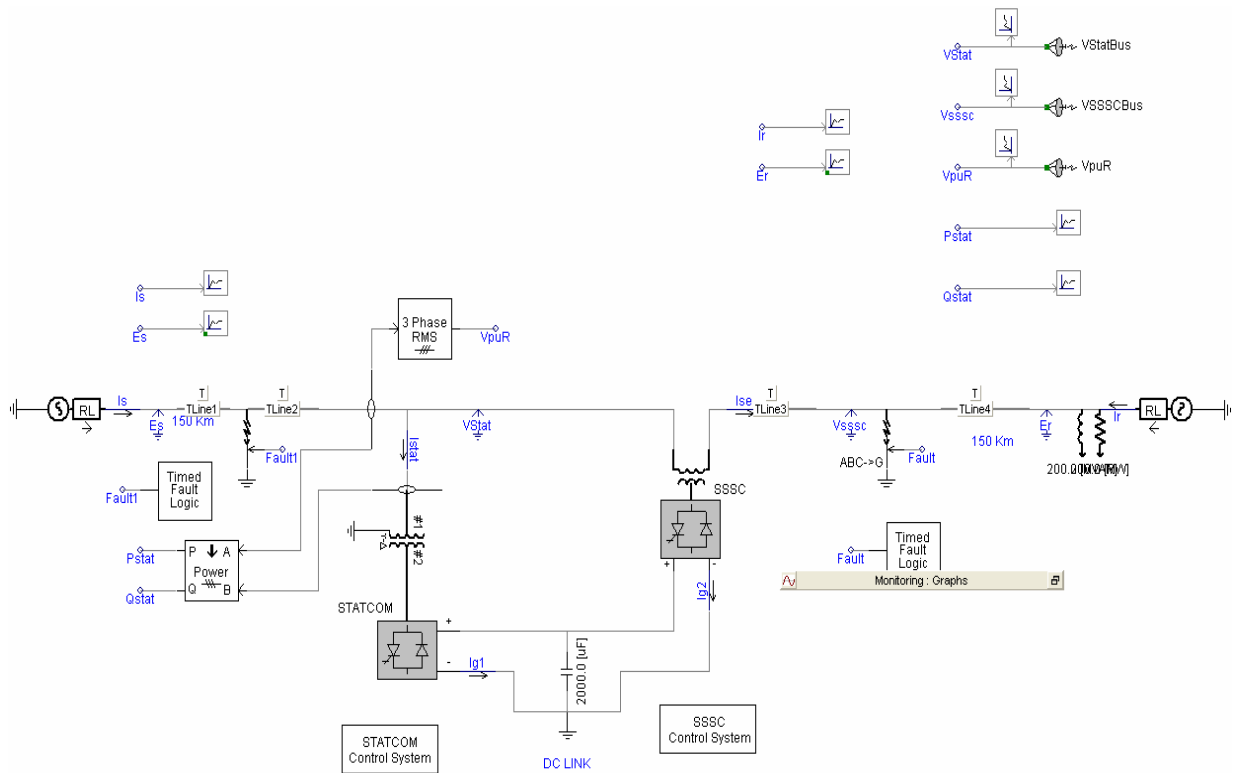
Fig. 4.2 UPFC model developed using PSCAD
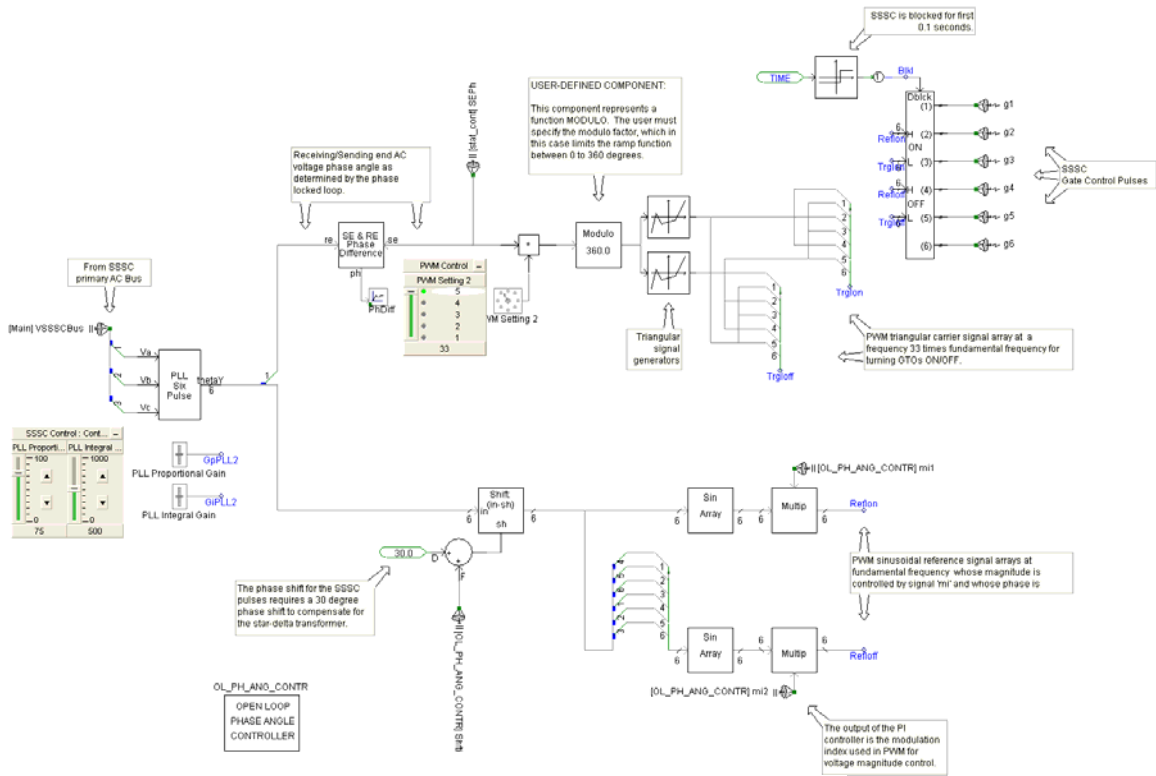
Fig. 4.3 SSSC control system
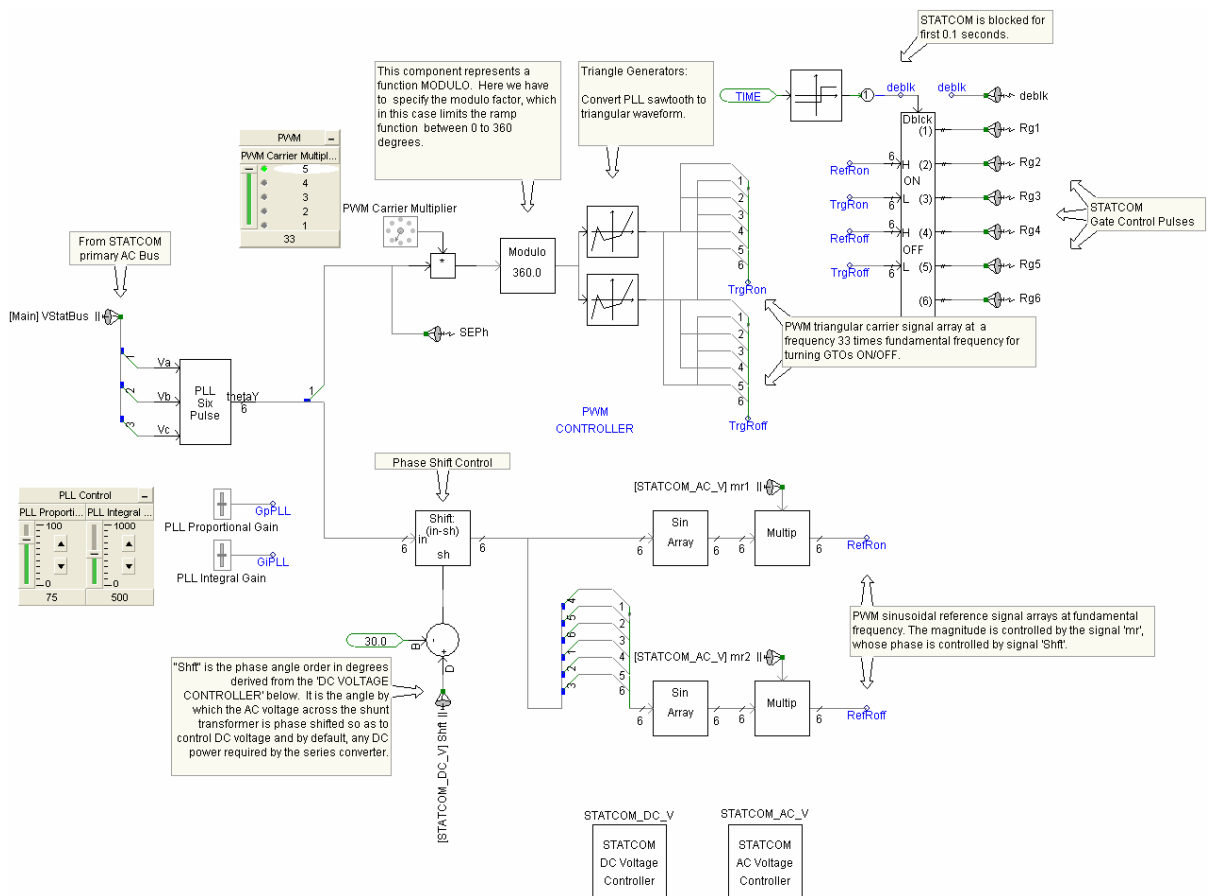
Fig. 4.4 STATCOM control system

4.2.2 Fault location determination using Differential Equation Approach

The differential equation based fault locator calculates fault location for different types of faults occurring, both before and after UPFC in the transmission line. The fault location is determined in terms of the line inductance to the fault point from the relaying end. The line inductance is determined using differential equation approach separately for faults before UPFC and after UPFC. The control shifts to the appropriate differential equation based algorithm depending upon the fault section (before or after UPFC). The following section deals with the fault location determination for faults occurring before and after UPFC.

4.2.2.1 Pre-fault parameters setting

Initially the pre-fault condition of the UPFC based line is studied. The power flow equations are formulated and solved using Newton-Raphson method. The phase angle and voltage magnitude of all the buses are found out at constant shunt voltage. Thus the series injected voltage and phase angle are resulted for specific operating pre-fault conditions. The different shunt voltage 'vsh' at which the parameters for different buses are found out are 1.0 pu (per unit), 1.05 pu and 0.95 pu. The above study was made with different loading conditions of P_L and Q_L. After getting the different values of series injected voltage and phase angle for pre-fault condition, the parameters of the UPFC model developed using PSCAD, are set and faults are created with various operating conditions like variations in fault resistance, inception angle and locations etc. The magnitude and phase angle of the series injected voltage plays vital role in the functionality of UPFC. The results obtained from the power flow solutions are given as follows for different shunt voltage 'vsh'. The UPFC model studied is given in Fig.4.5.
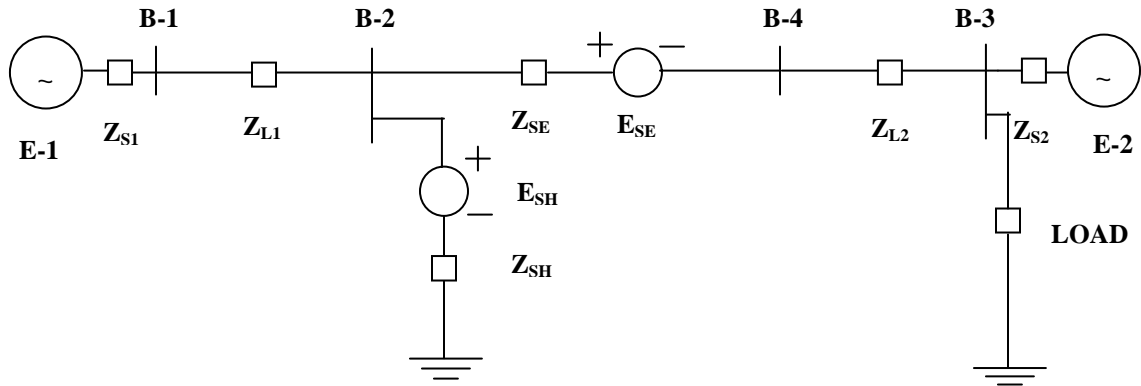
**Fig. 4.5 UPFC based transmission line model
for pre-fault power flow solution**

Where vsh--------shunt voltage
         ish---------shunt current
         vse--------series voltage
         ise---------series voltage
         thse--------series phase angle
         v2----------voltage of Bus-2
         theta2-----phase angle of Bus-2
         v3----------voltage of Bus-3
         theta3------phase angle of Bus-3
         v4----------voltage of Bus-4
         theta4------phase angle of Bus-4
         P_L Q_L------Active and Reactive part of Load

```
vsh=1.0 pu
  ish      ise      vse      thse      v2      theta2      v3
0.4475   0.2854   0.1087   -0.9714   0.9552   0.1049   0.9612
0.4475   0.3636   0.1197   -1.0244   0.9552   0.1049   0.9624
0.4475   0.5026   0.1371   -0.9864   0.9552   0.1049   0.9515
0.4475   0.5861   0.1480   -1.0321   0.9552   0.1049   0.9527
0.4477   0.7063   0.1615   -0.8878   0.9552   0.1049   0.9292
0.4475   0.9425   0.1929   -1.0134   0.9552   0.1049   0.9338
0.4475   0.7226   0.1652   -1.0012   0.9552   0.1049   0.9422


theta3      v4      theta4     PL  QL
0.0616   0.9910   0.0301   (0.2 0.2)
0.0748   0.9916   0.0276   (0.3 0.2)
0.0887   0.9948   0.0252   (0.4 0.3)
0.1018   0.9949   0.0226   (0.5 0.3)
0.1041   1.0011   0.0234   (0.5 0.5)
0.1442   1.0010   0.0154   (0.8 0.5)
0.1161   0.9980   0.0202   (0.6 0.4)
```

```
vsh=1.05 pu
  ish      ise      vse      thse      v2      theta2      v3
0.9475   0.2848   0.1097   -0.9561   0.9552   0.1049   0.9632
0.9475   0.3625   0.1211   -1.0017   0.9552   0.1049   0.9656
0.9475   0.5004   0.1391   -0.9593   0.9552   0.1049   0.9560
0.9475   0.5832   0.1501   -1.0033   0.9552   0.1049   0.9578
0.9475   0.7029   0.1645   -0.8657   0.9552   0.1049   0.9345
0.9475   0.7189   0.1676   -0.9754   0.9552   0.1049   0.9475
0.9475   0.9379   0.1951   -0.9927   0.9552   0.1049   0.9389
```

```
theta3     v4     theta4]    PL  QL
0.0615   0.9930   0.0301   (0.2  0.2)
0.0746   0.9947   0.0278   (0.3  0.2)
0.0882   0.9992   0.0253   (0.4  0.3)
0.1011   0.9998   0.0227   (0.5  0.3)
0.1030   1.0060   0.0231   (0.5  0.5)
0.1150   1.0031   0.0202   (0.6  0.4)
0.1427   1.0058   0.0152   (0.8  0.5)
```

```
vsh=0.95 pu
  ish      ise      vse      thse      v2      theta2      v3
0.0528   0.2846   0.1101   -0.9475   0.9552   0.1049   0.9643
0.0525   0.3619   0.1216   -0.9902   0.9552   0.1049   0.9671
0.0526   0.4993   0.1401   -0.9445   0.9552   0.1049   0.9584
0.0525   0.5818   0.1510   -0.9886   0.9552   0.1049   0.9603
0.0536   0.7008   0.1657   -0.8491   0.9552   0.1049   0.9377
0.0525   0.7170   0.1686   -0.9610   0.9552   0.1049   0.9504
0.0526   0.9355   0.1961   -0.9810   0.9552   0.1049   0.9416
```

```
theta3     v4     theta4     PL  QL
0.0616   0.9940   0.0303   (0.2  0.2)
0.0747   0.9962   0.0279   (0.3  0.2)
0.0882   1.0015   0.0256   (0.4  0.3)
0.1010   1.0022   0.0230   (0.5  0.3)
0.1031   1.0091   0.0237   (0.5  0.5)
0.1148   1.0058   0.0205   (0.6  0.4)
0.1422   1.0084   0.0155   (0.8  0.3)
```

4.2.2.2 Current injection based UPFC Model

The UPFC consists of shunt and series voltages with respective impedances as shown in Fig.4.6. But the proposed research uses the current injection model as shown in Fig. 4.9. The original model is reduced to current injection model as shown in Fig.4.7 through Fig. 4.9. The equivalent admittance model is shown in Fig. 4.10.
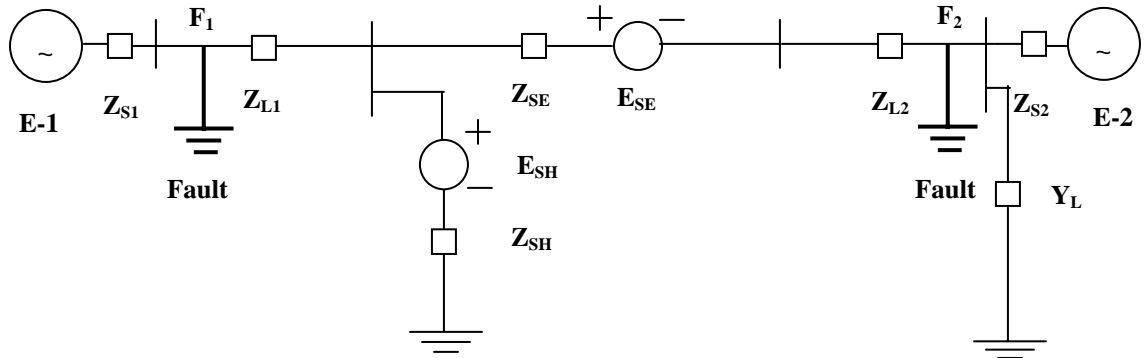
Fig. 4.6 Original UPFC based transmission line model
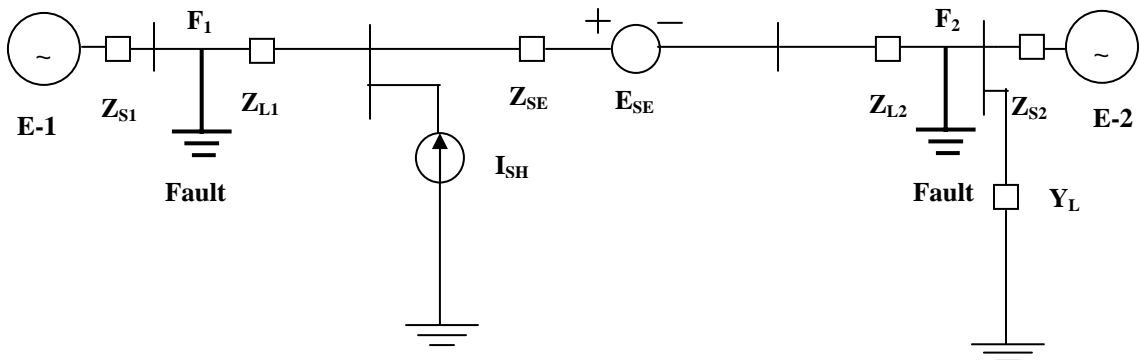
Fig. 4.7 Equivalent of Fig. 4.7
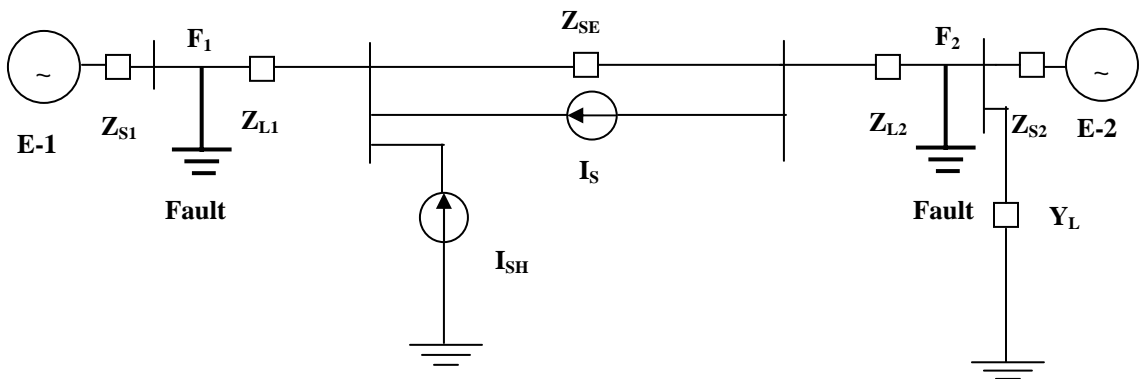
Fig. 4.8 Equivalent of Fig. 4.8
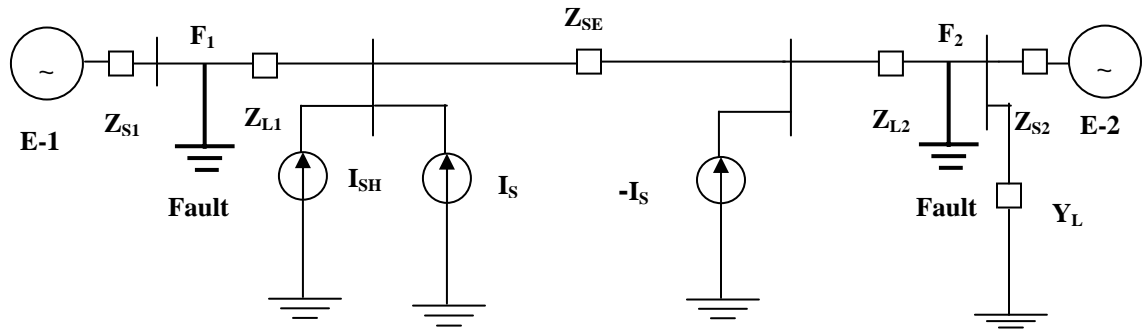
Fig. 4.9 Equivalent current injection model
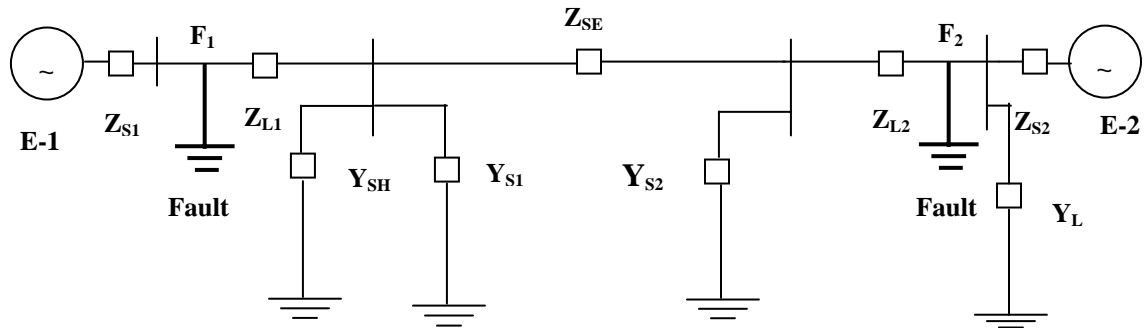
Fig. 4.10 Equivalent admittance model

4.2.2.3 Differential equation based Fault locator

(a) Fault locator for fault at F-1(Before UPFC)

For fault at F1, before the UPFC, the UPFC based line and the equivalent models are developed and are shown in Fig.4.11 and Fig.4.12 respectively. R, L, C are the line parameters and Y_F is the fault admittance. *v* and *i* are the voltage and current at the relay location. 'x' is the fraction of the line length up to fault point form the relaying end.
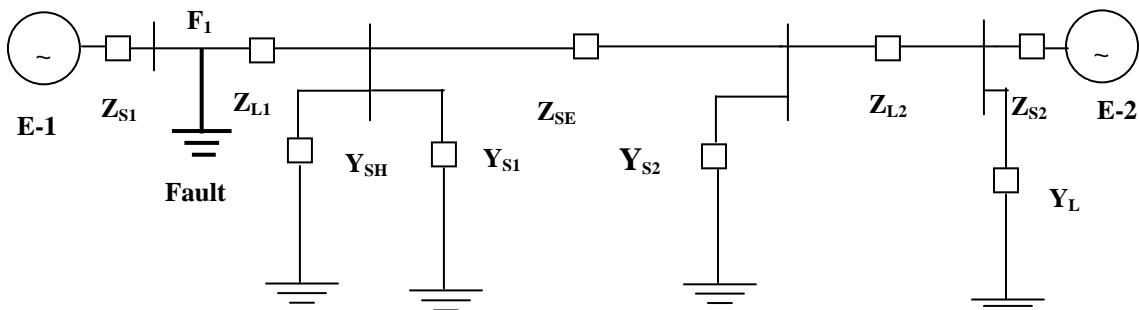
Fig. 4.11 UPFC based line for Fault at F1
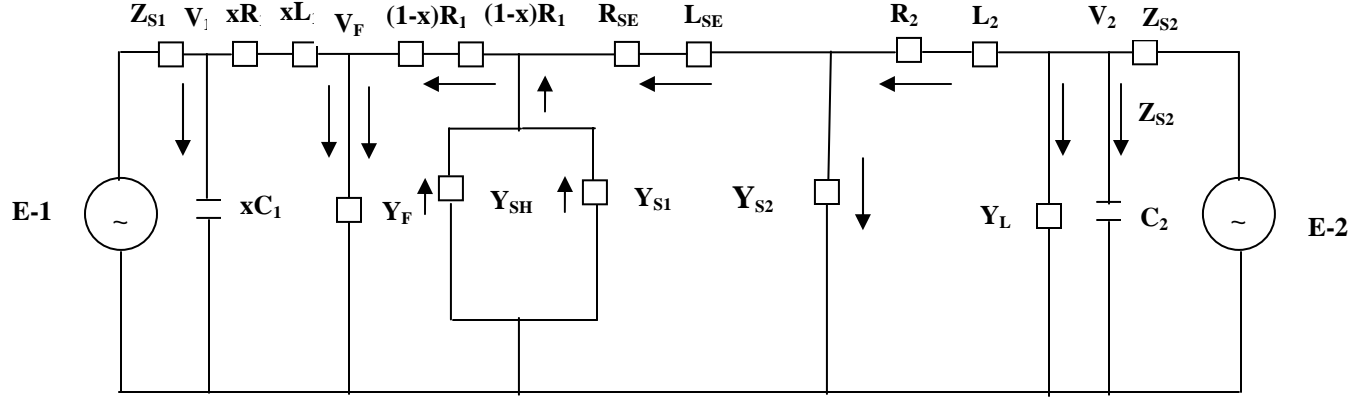
Fig. 4.12 Equivalent model for Fault at F1

If the fault occurs at F1, then the voltage equation around the fault point F1 is given as

$$xR_1(i_1 - i_{c1}) + xL_1 \frac{d}{dt}(i_1 - i_{c1}) + v_f = v_1$$

$$\Rightarrow xR_1 i_1 - x^2 R_1 C_1 \frac{dv_1}{dt} + xL_1 \frac{di_1}{dt} - x^2 L_1 C_1 \frac{d^2 v_1}{dt^2} + \frac{i_f}{Y_F} = v_1 \qquad (4.1)$$

The corresponding fault current i_f can be derived as

$$i_f = (i_1 - i_{c1}) + (i_2 - i_{c2} - i_L - i_{s2} + i_{SH}) = (i_1 - xC_1 \frac{dv_1}{dt}) + (i_2 - C_2 \frac{dv_2}{dt} - v_2 Y_L -$$

$$Y_{s2}\left[v_2 - R_2(i_2 - i_{c2} - i_L) - L_2 \frac{d}{dt}(i_2 - i_{c2} - i_L) \right] +$$

$$(Y_{SH} + Y_{S1})\begin{bmatrix} v_2 - R_2(i_2 - i_{c2} - i_L) - L_2 \dfrac{d}{dt}(i_2 - i_{c2} - i_L) - \\ R_{SE}(i_2 - i_{c2} - i_L - i_{s2}) - L_{SE} \dfrac{d}{dt}(i_2 - i_{c2} - i_L - i_{s2}) \end{bmatrix}) \qquad (4.2)$$

Equation (4.1) can be expanded to

$$(xR_1+\frac{1}{Y_F})i_1+xL_1\frac{di_1}{dt}-(x^2R_1C_1+\frac{C_1}{Y_F})\frac{dv_1}{dt}-x^2L_1C_1\frac{d^2v_1}{dt^2}+\left[\begin{array}{c}\frac{1}{Y_F}+\frac{Y_{S2}}{Y_F}-\frac{(Y_{SH}+Y_{S1})R_2}{Y_F}-\frac{(Y_{SH}+Y_{S1})R_{SE}}{Y_F}+\\ \frac{(Y_{SH}+Y_{S1})Y_{S2}R_2R_{SE}}{Y_F}\end{array}\right]i_2+$$

$$\left[\frac{(Y_{S2}L_2)}{Y_F}-\frac{(Y_{SH}+Y_{S1})L_2}{Y_F}-\frac{(Y_{SH}+Y_{S1})Y_{S2}L_2R_{SE}}{Y_F}-\frac{(Y_{SH}+Y_{S1})L_SY_{S2}R_2}{Y_F}\right]\frac{di_2}{dt}-\left[\frac{(Y_{SH}+Y_S)}{Y_F}L_{SE}Y_{S2}L_2\right]\frac{d^2i_2}{dt^2}+$$

$$\left[\frac{(Y_{S1}R_2Y_L)}{Y_F}+\frac{(Y_{SH}+Y_{S1})}{Y_F}+\frac{(Y_{SH}+Y_{S1})R_2Y_L}{Y_F}+\frac{Y_L}{Y_F}+\frac{(Y_{SH}+Y_{S1})R_{SE}Y_L}{Y_F}+\frac{(Y_{SH}+Y_{S1})R_{SE}Y_{S2}}{Y_F}-\frac{(Y_{SH}+Y_{S1})R_{SE}Y_{S2}R_2Y_L}{Y_F}\right]v_2+$$

$$\left[\begin{array}{c}\frac{C_2}{Y_F}+\frac{(Y_{S2}R_2)}{Y_F}+\frac{(Y_{S2}Y_LL_2)}{Y_F}+\frac{(Y_{SH}+Y_{S1})R_2C_2}{Y_F}+\frac{(Y_{SH}+Y_{S1})R_{SE}C_2}{Y_F}-\frac{(Y_{SH}+Y_{S1})Y_{S1}C_2R_{SE}}{Y_F}-\frac{(Y_{SH}+Y_{S1})R_{SE}Y_{S2}Y_LL_2}{Y_F}\\ -\frac{(Y_{SH}+Y_{S1})Y_{S2}R_2C_2R_{SE}}{Y_F}-\frac{(Y_{SH}+Y_{S1})R_{SE}Y_{S2}R_2Y_LL_2}{Y_F}+\frac{(Y_{SH}+Y_{S1})R_{SE}Y_{S2}R_2C_2}{Y_F}-\frac{(Y_{SH}+Y_{S1})L_{SE}Y_{S2}R_2Y_L}{Y_F}\end{array}\right]\frac{dv_2}{dt}+$$

$$\left[\frac{(Y_{SH}+Y_{S1})Y_{S2}L_2C_2}{Y_F}+\frac{(Y_{SH}+Y_{S1})Y_{S2}L_2C_2R_{SE}}{Y_F}+\frac{(Y_{SH}+Y_{S1})L_{SE}Y_{S2}C_2R_2}{Y_F}+\frac{(Y_{SH}+Y_{S1})L_{SE}Y_{S2}Y_LL_2}{Y_F}\right]\frac{d^2v_2}{dt^2}+$$

$$\left[\frac{(Y_{SH}+Y_{S1})L_{SE}Y_{S2}L_2C_2}{Y_F}\right]\frac{d^3v_3}{dt^3}\qquad=\qquad v_1$$

(4.3)

The above equation (4.3) can be represented in matrix format as given below

$$\begin{bmatrix} m_{11} & m_{12} & m_{13} & m_{14} & \dots\dots\dots\dots\dots m_{111} \\ m_{21} & m_{22} & m_{23} & m_{24} & \dots\dots\dots\dots\dots m_{211} \\ \hline m_{31} & m_{32} & m_{33} & m_{43} & \dots\dots\dots\dots m_{311} \\ . & & & & \\ . & & & & \\ . & & & & \\ . & & & & \\ m_{111} & m_{112.} & m_{113} & m_{114} & \dots\dots\dots\dots m_{1111} \end{bmatrix}\begin{bmatrix} n_1 \\ n_2 \\ \hline n_3 \\ . \\ . \\ . \\ . \\ n_{11} \end{bmatrix}=\begin{bmatrix} o_1 \\ o_2 \\ \hline o_3 \\ . \\ . \\ . \\ . \\ o_{11} \end{bmatrix}$$

(4.4)

where

$$m_{N1} = \frac{\Delta t}{2}(i_{1k+N} + i_{1k+N-1}) \, , \, m_{N2} = (i_{1k+N} - i_{1k+N-1}) \, , \, m_{N3} = -(v_{1k+N} - v_{1k+N-1}) \, ,$$

$$m_{N4} = -\frac{1}{\Delta t}(v_{1k+N} - 2v_{1k+N-1} + v_{1k+N-2}) \, , \, m_{N5} = \frac{\Delta t}{2}(i_{2k+N} + i_{1k+N-1}) \, , \, m_{N6} = (i_{2k+N} - i_{2k+N-1})$$

$$m_{N7} = -\frac{1}{\Delta t}(i_{2k+N} - 2i_{2k+N-1} + i_{1k+N-2}) \, , \, m_{N8} = \frac{\Delta t}{2}(v_{2k+N} + v_{2k+N-1}) \, ,$$

$$m_{N9} = (v_{2k+N} + v_{21k+N-1}) \, , \, m_{N10} = \frac{1}{\Delta t}(v_{2k+N} - 2v_{2k+N-1} + v_{21k+N-1}) \, ,$$

$$m_{N11} = \frac{1}{\Delta t^2}(v_{2k+N} - 3v_{2k+N-1} + 3v_{2k+N-2} - v_{21k+N-1})$$

$$O_N = \frac{\Delta t}{2}(v_{1k+N} + v_{1k+N-1})$$

$i_{1k}, i_{1k+1}, \ldots\ldots\ldots\ldots\ldots\ldots\ldots, i_{1k+11}$ samples of i_1

$i_{2k}, i_{2k+1}, \ldots\ldots\ldots\ldots\ldots\ldots\ldots, i_{2k+11}$ samples of i_2

$v_{1k}, v_{1k+1}, \ldots\ldots\ldots\ldots\ldots\ldots\ldots, v_{1k+11}$ samples of v_1

$v_{2k}, v_{2k+1}, \ldots\ldots\ldots\ldots\ldots\ldots\ldots, v_{2k+11}$ samples of v_2

k is the sample number.

Δt is the sampling interval

The divided parts of the equation can be represented as

$$\left[\begin{array}{c|c} G_1 & G_2 \\ \hline G_3 & G_4 \end{array}\right]\left[\begin{array}{c} H_1 \\ H_2 \end{array}\right] = \left[\begin{array}{c} Y_1 \\ Y_2 \end{array}\right] \qquad (4.5)$$

$$H_1 = \left[\begin{array}{c} n_1 \\ n_2 \end{array}\right] = \left[G_1 - G_2 G_4^{-1} G_3\right]^{-1}\left[Y_1 - G_2 G_4^{-1} Y_2\right] \qquad (4.6)$$

where $n_2 = xL_1$

n_1 and n_2 are found out from the equation (4.6) and n_2 is the desired estimate of the line inductance to the fault point from the relaying end. As the line inductance directly proportional to the fault location form the relaying point, the fault location is found out accurately.

(b) Fault locator for fault at F-2 (After UPFC)

For fault at F2, before the UPFC, the UPFC based line and the equivalent model is developed and is shown in Fig.4.13 and Fig.4.14 respectively. R, L, C are the line parameters and Y_F is the fault admittance. v and i are the voltage and current at the relay location. 'x' is the fraction of the line length up to fault point from the receiving end.
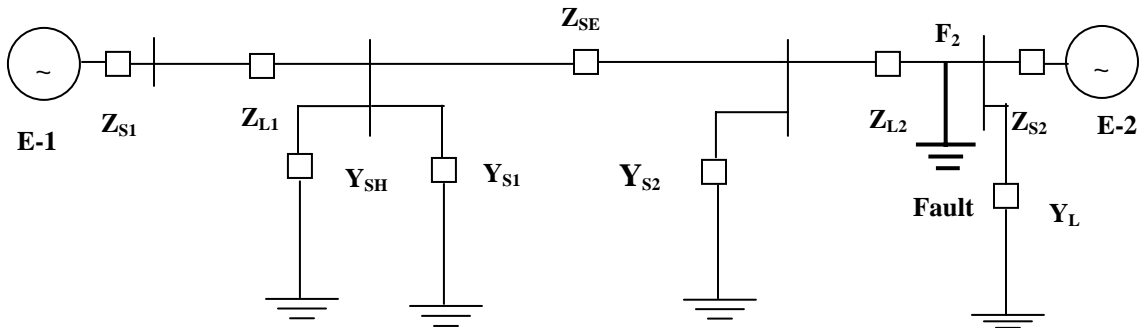
Fig. 4.13 UPFC based line for Fault at F2
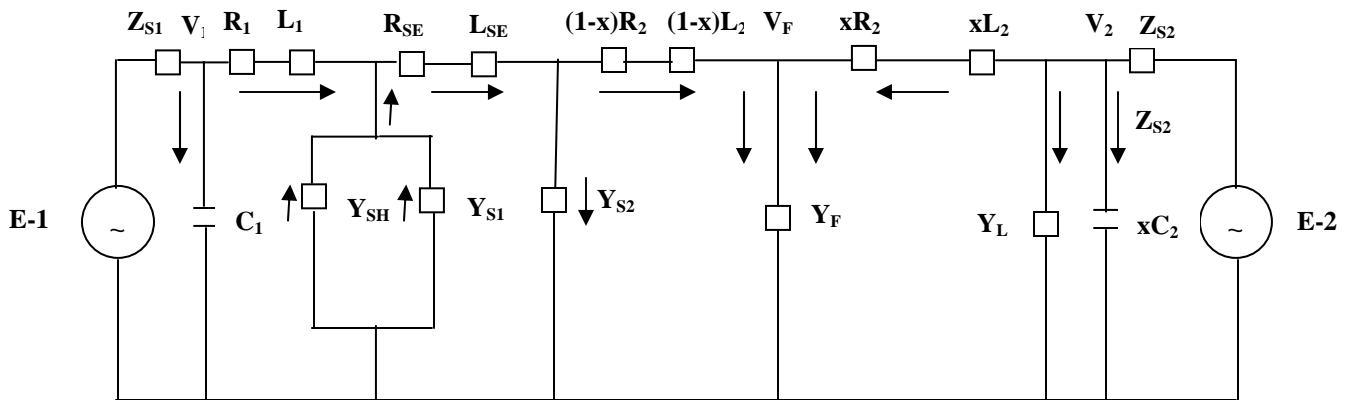
Fig. 4.14 Equivalent model for Fault at F2

If the fault occurs at F2, then the voltage equation around the fault point F2 is given as

$$xR_2(i_2 - i_{c2} - i_L) + xL_2 \frac{d}{dt}(i_2 - i_{c2} - i_L) + v_f = v_2$$

$$\Rightarrow xR_2(i_2 - xC_2 \frac{dv_2}{dt} - v_2 Y_L) + xL_2 \frac{d}{dt}(i_2 - xC_2 \frac{dv_2}{dt} - v_2 Y_L) + v_f = v_2$$

(4.7)

The fault current is derived as

$$i_f = (i_1 - i_{c1} + i_{SH} - i_{S2}) + (i_2 - i_{c2} - i_L)$$

$$= (i_1 - C_1 \frac{dv_1}{dt} + (Y_{S1} + Y_{SH})\left[v_1 - R_1(i_1 - i_{c1}) - L_1 \frac{d}{dt}(i_1 - i_{c1})\right] - i_{S2}) + (i_2 - xC_2 \frac{dv_2}{dt} - v_2 Y_L)$$

(4.8)

Equation (4.7) can be expanded to

$$\left[\frac{1}{Y_F} + \frac{Y_{S2}R_1}{Y_F} + \frac{Y_{S2}R_{SE}}{Y_F} - \frac{Y_{S2}(Y_{SH}+Y_{S1})R_{SE}R_1}{Y_F}\right] i_1 + \left[\begin{array}{c} -\frac{(Y_{SH}+Y_{S1})L_1}{Y_F} - \frac{(Y_{SH}+Y_{S1})Y_{S2}L_1R_{SE}}{Y_F} + \frac{L_1 Y_{S2}}{Y_F} + \frac{L_{SE}Y_{S2}}{Y_F} - \\ \frac{(Y_{SH}+Y_{S1})Y_{S2}L_{SE}R_1}{Y_F} \end{array}\right] \frac{di_2}{dt} -$$

$$\left[\frac{(Y_{SH}+Y_{S1})Y_{S2}L_{SE}L_1}{Y_F}\right] \frac{d^2 i_1}{dt^2} + \left[\frac{(Y_{SH}+Y_{S1})+Y_{S2}+Y_{SE}(Y_{S1}+Y_{SH})R_{SE}}{Y_F}\right] v_1 + \left[\begin{array}{c} \frac{C_1}{Y_F} - \frac{(Y_{S1}+Y_{SH})R_1C_1}{Y_F} + \frac{Y_{S2}R_1C_1}{Y_F} - \frac{Y_{S2}L_1C_1}{Y_F} + \\ \frac{Y_{S2}C_1 R_{SE}R_1(Y_{SH}+Y_1)}{Y_F} + \frac{Y_{S2}L_{SE1}(Y_{SH}+Y_1)}{Y_F} \end{array}\right] \frac{dv_1}{dt} -$$

$$\left[-\frac{L_1 C_1(Y_{SH}+Y_1)}{y_f} + \frac{Y_{S2}R_{SE}L_1C_1(Y_{SH}+Y_1)}{Y_F} - \frac{Y_{S2}L_{SE}C_1}{Y_F} + \frac{Y_{S2}L_S(Y_{SH}+Y_1)}{Y_F}\right] \frac{d^2 v_1}{dt^2} + \frac{Y_{S1}L_{SE}L_1C_1}{Y_F} \frac{d^3 v_1}{dt^3} + \frac{xR_2}{Y_F} i_2 + xL_2 \frac{di_2}{dt} -$$

$$\left[\frac{Y_L}{Y_F} + xR_2 Y_L\right] v_2 - \left[\frac{xC_2}{Y_F} + x^2 R_2 C_2 + xY_L L_2\right] \frac{dv_2}{dt} - x^2 L_2 C_2 \frac{d^2 v_2}{dt^2} \quad = \quad v_2$$

(4.9)

Equation (4.9) can be represented in matrix form as given below

$$\begin{bmatrix} m_{11} & m_{12} & m_{13} & m_{14} & \cdots\cdots\cdots & m_{112} \\ m_{21} & m_{22} & m_{23} & m_{24} & \cdots\cdots\cdots & m_{212} \\ \hline m_{31} & m_{32} & m_{33} & m_{43} & \cdots\cdots\cdots & m_{312} \\ . & & & & & \\ . & & & & & \\ . & & & & & \\ . & & & & & \\ m_{121} & m_{122.} & m_{123} & m_{124} & \cdots\cdots\cdots & m_{1212} \end{bmatrix} \begin{bmatrix} n_1 \\ n_2 \\ \hline n_3 \\ . \\ . \\ . \\ . \\ n_{12} \end{bmatrix} = \begin{bmatrix} o_1 \\ o_2 \\ \hline o_3 \\ . \\ . \\ . \\ . \\ o_{12} \end{bmatrix}$$

(4.10)

$$m_{N1} = \frac{\Delta t}{2}(i_{2k+N} + i_{2k+N-1}), m_{N2} = (i_{2k+N} - i_{2k+N-1}), m_{N3} = -\frac{\Delta t}{2}(v_{2k+N} + v_{2k+N-1}),$$

$$m_{N4} = -(v_{2k+N} - v_{2k+N-1}), m_{N5} = -\frac{1}{\Delta t}(v_{2k+N} - 2v_{2k+N-1} + v_{2k+N-2}),$$

$$m_{N6} = \frac{\Delta t}{2}(i_{1k+N} - i_{1k+N-1}), m_{N7} = (i_{1k+N} - i_{1k+N-1}), m_{N8} = -\frac{1}{\Delta t}(i_{1k+N} - 2i_{1k+N-1} + i_{1k+N-2}),$$

$$m_{N9} = -\frac{\Delta t}{2}(v_{1k+N} + v_{1k+N-1}), m_{N10} = (v_{1k+N} - v_{1k+N-1})),$$

$$m_{N11} = -\frac{1}{\Delta t}(v_{1k+N} - 2v_{1k+N-1} + v_{1k+N-1}), m_{N12} = \frac{1}{\Delta t^2}(v_{1k+N} - 3v_{1k+N-1} + 3v_{1k+N-2} - v_{1k+N-3})$$

$$O_N = \frac{\Delta t}{2}(v_{1k+N} + v_{1k+N-1}),$$

$i_{1k}, i_{1k+1}, \dots\dots\dots\dots\dots\dots\dots\dots\dots, i_{1k+12}$ samples of i_1

$i_{2k}, i_{2k+1}, \dots\dots\dots\dots\dots\dots\dots\dots\dots, i_{1k+12}$ samples of i_2

$v_{1k}, v_{1k+1}, \dots\dots\dots\dots\dots\dots\dots\dots\dots, v_{1k+12}$ samples of v_1

$v_{2k}, v_{2k+1}, \dots\dots\dots\dots\dots\dots\dots\dots\dots, v_{2k+12}$ samples of v_2

k is the sample number.

Δt is the sampling interval

The divided parts of the equation can be represented as

$$\left[\begin{array}{c|c} G_1 & G_2 \\ \hline G_3 & G_4 \end{array}\right]\left[\begin{array}{c} H_1 \\ H_2 \end{array}\right] = \left[\begin{array}{c} Y_1 \\ Y_2 \end{array}\right] \tag{4.11}$$

$$H_1 = \left[\begin{array}{c} n_1 \\ n_2 \end{array}\right] = \left[G_1 - G_2 G_4^{-1} G_3\right]^{-1}\left[Y_1 - G_2 G_4^{-1} Y_2\right] \tag{4.12}$$

where $n_2 = xL_2$

n_1 and n_2 are found out from the equation (4.12) and n_2 is the desired estimate of the line

inductance to the fault point. Here ‘ xL_2 ’ is the line inductance of the fault point from the

receiving end. Thus fault location form the relaying point can be found out by deducting

‘ xL_2 ’ form the line inductance of the complete line.

(c) Computational results for fault location

The fault location is determined in terms of inductance to te fault point. For fault at 'F1'(before UPFC), the line inductance measured is 'xL_1' for the relaying point. Similarly the 'xL_2' is measured form the receiving end and provides the fault location from the receiving end for fault at 'F2'. The fault location for fault at 'F2' from the relaying point can be found out by deducting 'xL_2' from the line inductance of the complete transmission line. The error in fault location is calculated as follows:

$$\% \quad Error \quad = \quad \frac{xL_e - xL}{L} * 100 \tag{4.13}$$

Where xL_e the estimated line inductance to the fault is point and xL is the actual line inductance to the fault point. 'L' represents the line inductance of the transmission for complete length.

Table-4.3 to 4.9 depicts the fault location for different operating conditions of the line and UPFC. 'θ_{se}' represents the series injected voltage phase angle and 'α' represents the inception angle of the fault. 'θ_{se}' also represented by 'thse' resulted form power flow solution represented in radian. Table-4.3 provides the fault location for 'a-g' fault with vse=0.1371 and thse=-0.9864 at 10% of the line. The error in fault location is 1.60% when R_F is 0 ohm. But the location error increases to 6.85% for R_F is 200 ohm for similar fault situation. Table-4.5 shows the fault location for 'ab-g' fault with vse=0.1676 and thse=-0.9754 at 65% of the line. Here the inductance is measured from the other end (receiving end) and can also be calculated form the relaying end by deducting form total line inductance. The error is 1.29% and 9.28% for R_F with 0 and 200 ohm respectively.Table-4.7 depicts the fault location for 'b-g' fault at 15% of the line with variations in series injected voltage form 0 to 15% of the line voltage. The error is 2.86% and 10.10% at 0% and 15% series injected voltage, respectively. Table-4.8 provides the fault location for variation in series injected voltage phase angle with 10% series injected voltage. The fault location error is 2.61% and 11.01% for phase angle variation form 0°

to 360°, respectively. Table-4.9 depicts the fault location for different loading conditions with variations in fault resistance. It is found that in case of different loading conditions with set pre-fault conditions of UPFC, the location error is less than 5%.

Table-4.3 Fault location for 'a-g' fault at 10% of line with different fault resistance at vsh=1.0 pu

ish	ise	vse	thse	v2	theta2	v3
0.4475	0.5026	0.1371	-0.9864	0.9552	0.1049	0.9515

theta3	**v4**	**theta4**	**P$_L$**	**Q$_L$**
0.0887	0.9948	0.0252	0.4	0.3

Fault Resistance	$\alpha = 30^0$, 10% of line, L – G Fault	
	xL_1=40.5 mH	
	xLe_1	Error(%)
$R_F = 0\ \Omega$	47.02	1.60
$R_F = 30\ \Omega$	49.36	2.18
$R_F = 70\ \Omega$	53.36	3.17
$R_F = 100\ \Omega$	56.10	3.85
$R_F = 120\ \Omega$	59.69	4.73
$R_F = 150\ \Omega$	62.98	5.55
$R_F = 170\ \Omega$	66.74	6.47
$R_F = 200\ \Omega$	68.26	6.85

Table-4.4 Fault location for 'ab-g' fault at 45% of line with different fault resistance at vsh=1.0 pu

ish	ise	vse	thse	v2	theta2	v3
0.4475	0.5861	0.1480	-1.0321	0.9552	0.1049	0.9527

theta3	**v4**	**theta4**	**P$_L$**	**Q$_L$**
0.1018	0.9949	0.0226	0.5	0.3

Fault Resistance	$\alpha = 40^0$, 45% of line, LL – G Fault	
	xL_1=182.25 mH	
	xLe_1	Error(%)
$R_F = 0\ \Omega$	185.02	0.68
$R_F = 30\ \Omega$	192.24	2.46
$R_F = 70\ \Omega$	198.68	4.05
$R_F = 100\ \Omega$	205.48	5.73
$R_F = 120\ \Omega$	209.68	6.77
$R_F = 150\ \Omega$	212.69	7.51
$R_F = 170\ \Omega$	216.47	8.44
$R_F = 200\ \Omega$	219.85	9.28

Table-4.5 Fault location for 'bc-g' fault at 65% of line with different fault resistance at vsh=1.05 pu

ish	ise	vse	thse	v2	theta2	v3
0.9475	0.7189	0.1676	-0.9754	0.9552	0.1049	0.9475

theta3	**v4**	**theta4**	**P$_L$**	**Q$_L$**
0.1150	1.0031	0.0202	0.6	0.4

Fault Resistance	$\alpha = 60^0$, 65% of line, LL $-$ G Fault	
	xL$_2$=141.75 mH (xL$_1$=263.25 mH)	
	xLe$_2$	*Error(%)*
$R_F = 0\ \Omega$	146.98	1.29
$R_F = 30\ \Omega$	153.36	2.86
$R_F = 70\ \Omega$	158.69	4.18
$R_F = 100\ \Omega$	162.35	5.08
$R_F = 120\ \Omega$	166.87	6.20
$R_F = 150\ \Omega$	171.69	7.39
$R_F = 170\ \Omega$	175.98	8.45
$R_F = 200\ \Omega$	179.36	9.28

Table-4.6 Fault location for 'ca-g' fault at 90% of line with different fault resistance at vsh=1.05 pu

ish	ise	vse	thse	v2	theta2	v3
0.9475	0.7029	0.1645	-0.8657	0.9552	0.1049	0.9345

theta3	**v4**	**theta4**	**P$_L$**	**Q$_L$**
0.1030	1.0060	0.0231	(0.5	0.5)

Fault Resistance	$\alpha = 90^0$, 90% of line, L $-$ G Fault	
	xL$_2$=40.50 mH (xL$_1$=364.5 mH)	
	xLe$_2$	*Error*
$R_F = 0\ \Omega$	49.21	2.15
$R_F = 30\ \Omega$	53.26	3.15
$R_F = 70\ \Omega$	56.45	3.93
$R_F = 100\ \Omega$	59.87	4.78
$R_F = 120\ \Omega$	62.85	5.51
$R_F = 150\ \Omega$	65.98	6.29
$R_F = 170\ \Omega$	69.41	7.13
$R_F = 200\ \Omega$	71.02	7.53

Table-4.7 Fault location for b-g fault at 15% of line with different series injected voltage vsh=1.0 pu, P$_L$=0.8 pu and Q$_L$=0.5 pu

Series Voltage injected in %	$\theta_{se} = 150^0, \alpha = 30^0, \quad 15\% \quad of \quad line, \quad L-G \; Fault$			
	$xL_1 = 60.75 \; mH$			
	$R_F = 30 \; \Omega$		$R_F = 150 \; \Omega$	
	xLe_1	Error (%)	xLe_1	Error(%)
0	63.68	0.72	72.35	2.86
2	69.85	2.24	75.69	3.68
5	71.59	2.67	81.25	5.06
7	75.69	3.68	86.25	6.29
10	79.41	4.60	90.63	7.37
12	83.64	5.65	95.63	8.61
15	89.65	7.13	101.69	10.10

Table-4.8 Fault location for c-g fault at 15% of line with different series injected voltage phase angle at vsh=1.0 pu, P$_L$=0.8 pu and Q$_L$=0.5 pu

Series injected Voltage phase angle θ_{se} in degree (Series injected voltage at 10%)	$\alpha = 30^0, \quad 15\% \quad of \quad line, \quad L-G \; Fault$			
	$xL_1 = 60.75 \; mH$			
	$R_F = 30 \; \Omega$		$R_F = 150 \; \Omega$	
	xLe_1	Error(%)	xLe_1	Error(%)
0	61.65	0.22	71.36	2.61
45	66.85	1.50	76.65	3.92
90	71.56	2.66	82.56	5.38
135	76.57	3.90	91.47	7.58
180	82.45	5.35	95.26	8.52
270	87.85	6.69	99.03	9.45
360	93.63	8.11	105.36	11.01

Table-4.9 Fault location for a-g fault at 45% of line with different loading conditions at vsh=1.0 and other conditions set as from pre fault conditions

Loading conditions	$\alpha = 30^0,\quad 45\%\quad of\quad line,\quad L-G\ Fault$			
	$xL_1 = 182.25mH$			
	$R_F = 30\ \Omega$		$R_F = 150\ \Omega$	
	xLe_1	$Error(\%)$	xLe_1	$Error(\%)$
P_L Q_L	188.75	1.60	191.65	2.32
0.2 0.2	187.64	1.33	190.63	2.07
0.3 0.2	190.53	2.04	193.75	2.84
0.4 0.3	196.63	3.55	199.65	4.30
0.5 0.3	189.56	1.80	191.23	2.22
0.6 0.4	192.06	2.42	194.65	3.06
0.8 0.5	188.63	1.58	190.65	2.07

4.3   Conclusions

In the proposed study, an attempt is made to find out the fault location in presence of UPFC in the transmission line. The current injection model of the UPFC is chosen for analysis. The fault location is determined in terms of line inductance to the fault point. The proposed method work on the assumption that the fault detection and fault section identification have been done. The fault location is determined using differential equation based approach. The inductance to the fault point is calculated for faults occurring before and after UPFC in the transmission line separately. Thus when the fault section is identified, the control shifts to the differential equation based fault location algorithm depending upon the occurrence of the fault in the transmission line (i.e. before or after UPFC). The line inductance is measured for different operating conditions of the transmission line such as variations in inception angle, fault resistance and fault location. Before the faults are created on the line, the pre-fault power flow solution is worked out using Newton-Raphson method. From the power flow solution, different parameters like voltage magnitude and phase angle are found out. After getting the parameters, the UPFC is set with resulted pre-fault series and shunt injected voltage and phase angle. Then different faults are created on the UPFC based line with different operating conditions. The maximum error resulted is 12% for fault resistance of 150 ohm and phase angle 360° with series injected voltage of 10%. Thus the proposed method provides a new approach for fault location in presence of UPFC with wide variation in operating conditions.

Chapter-5

Distance protection of compensated transmission line using time-frequency transform techniques

5.1 Introduction

The proposed research presents the protection of compensated transmission line using time-frequency analysis and pattern recognition approach. Both Wavelet Transform and S-Transform are applied to analyze faulty signals for a transmission system employing a thyristor controlled series capacitor (TCSC) at the midpoint of a line. Wavelet Transform based multi-resolution analysis is done to extract the frequency content information of the faulted current signal at appropriate decomposition level. The detailed coefficients are extracted to identify the faulty phase and faulty section involved in the fault process. Although Wavelets provide a variable window for low and high frequency currents in the voltage and current waveforms during faults, their capabilities are often significantly degraded owing to the existence of noises riding high on the signal [56]. In particular, as the spectrum of the noises coincides with that of the transient signals, the effects of noises cannot be excluded by means of some kinds of filters without affecting the performance of the Wavelet Transform. Thus another powerful time-frequency analysis known as S-Transform, an invertible time-frequency spectral localization technique that combines elements of Wavelet Transforms and short-time Fourier transform, is proposed for the same.

The S-Transform uses an analysis window whose width is decreasing with frequency providing a frequency dependent resolution. This transform may be seen as a continuous Wavelet Transform with a phase correction. It produces a constant relative bandwidth analysis like wavelets while it maintains a direct link with Fourier spectrum. The S-Transform has an advantage in that it provides multiresolution analysis while retaining the absolute phase of each frequency. The frequency contours generated form S-transform matrix provides the information of the faulty phase and faulty section involved in the fault process. The following section describes both the proposed methods for protection of TCSC line.

5.2 Wavelet Transform based multi-resolution analysis for protection of compensated (TCSC) line

Use of power electronic devices in ac powers system, to improve power transfer capability, forms the basis of flexible ac transmission systems (FACTS) [57]. TCSC is one of the main FACTS devices, which has ability to enhance utilization of existing transmission systems [58]. During a fault in a transmission line the presence of TCSC and series capacitor in fault loop affects steady state components and transient components also. Controllable reactance, metal oxide varistor (MOV) protecting capacitor and air-gap operations result in much complexity to protection design and to phase selection and fault section identification in particular. Recently an adaptive Kalman filter based approach has been proposed for phase selection and fault section identification for a transmission line that includes a TCSC [3]. However, such an approach finds its limitations as a number of Kalman filters are necessary for execution and it does not model the fault resistance in its algorithm.

Neural network based phase selection procedures [50, 51] are proposed which need large training set generation, longer training time and design of a new neural network for each transmission system. Further, such designs do not consider the presence of TCSC at midpoint of a line. Recently Wavelet Transform is proposed as a new tool to power system area for power quality monitoring [59], data compression [60] and transient analysis [61,62] using its multi-resolution feature and frequency and time domain analysis capability. Liao *et al.* [63] proposed wavelet based phase selection of an ordinary transmission line using the fault noise as signal which needs additional arrangement of stack tuner, etc. In another attempt Yu *et al.* [64] used wavelet integrated with neural network for phase selection for autoreclosing purpose of an ordinary transmission line. Morlet wavelet is utilized to detect high impedance fault (HIF) and to distinguish HIF from switching events [65].

Significant differences exist between fault signals in presence of capacitor-MOV combination for faults encountering TCSC and not encountering it. When the fault loop does not include the TCSC, like an ordinary transmission line, the current signal of the

relay contains decaying dc and high frequency components besides fundamental frequency component. In the other case of fault loop enclosing TCSC, the current signal consists of non-fundamental decaying frequency components, odd harmonics, high frequency and the fundamental frequency components. In this research work the powerful function of DWT in analyzing non-static signal is utilized to select the faulty section and to identify the faulty phase correctly for a transmission system employing a TCSC at the midpoint. New energy and standard deviation based indices are calculated for phase selection and section identification of the transmission network. The EMTDC [66] generated data are used to evaluate the performance of the DWT based approach, which needs only current information at relaying end. The new approach is tested for all types of faults at different locations and different operating conditions of the transmission system.

The proposed technique uses Discrete Wavelet Transform (DWT) to analyze faulty signals for a transmission system employing a thyristor controlled series capacitor (TCSC) at the midpoint of a line. Different frequency components of current signals are considered to select the phase(s) involved with a fault. To identify the fault-section the new approach utilizes the difference in high frequency components of the current signals. For both phase selection and section identification tasks new energy and standard deviation based indices are also calculated for the transmission system.

5.2.1 The Studied Power System

A 230kV, 50Hz power system is illustrated in Fig. 5.1 where a TCSC is located at the midpoint of the transmission sections. The power system consists of two sources, capacitors and their associated components and two transmission lines of length 150km each. The fixed capacitor provides 25% compensation and the TCSC compensates a minimum of 10%. All the components are modeled using the EMTDC subroutines and the system data used are provided in Appendix-1. For wavelet based study, only data available at relay end 'R' are used.

System Data:

System Voltage=230kV, Each source capacity =45GVA

Transmission Line:

Length=300km

The Mode Surge Impedance's (Ω)

742.98   406.09   355.79

The Mode Traveling Time (ms)

1.458   1.052   1.046

The Mode Resistance (Ω / km)

50 Hz 0.3534   0.0751   0.0749

730 Hz 1.8356   0.1671   0.1599

(a) The MOV protected series capacitor

Fig. 5.2(a) shows a typical series capacitor arrangement for one phase of a transmission line. The metal oxide varistor (MOV) consists of a number of zinc oxide discs electrically connected in series and parallel. The purpose of the MOV is to prevent the voltage across the capacitor from rising to levels, which will damage the capacitor. This is most likely to happen when a fault occurs at a point on the compensated line, which minimizes the impedance of the fault loop. When instantaneous voltage across the capacitor approaches a dangerous level the MOV begins to draw a significant proportion of the line current thereby limiting the voltage across the capacitor.

In the event that the MOV remains in conduction long enough to raise its temperature (energy) to a dangerous level, an air-gap is triggered to short circuit both MOV and capacitor, changing again the fault loop impedance. The operation of the MOV can be within the first half cycle of fault and upon the severity of the fault, it may continue to operate until the air-gap is triggered cycles later. This is precisely the time when a digital relay makes protection decision. Further, a bypass switch in parallel with the gap automatically closes for abnormal system conditions that cause prolonged current flow through the gap. The small inductance in the arrangement limits the current through the air-gap or switch circuit.
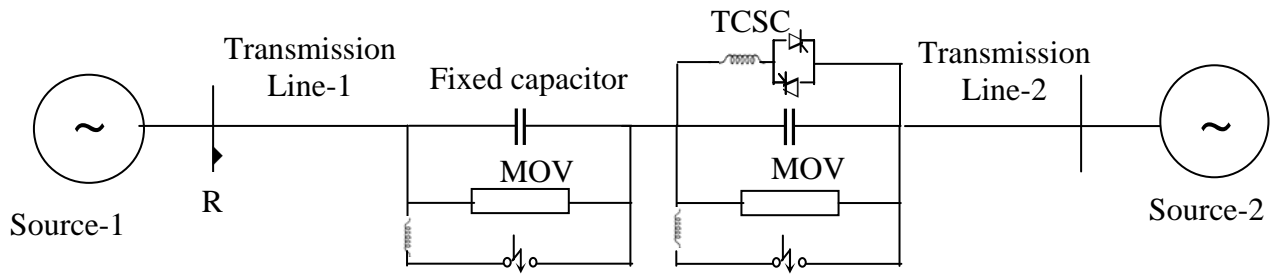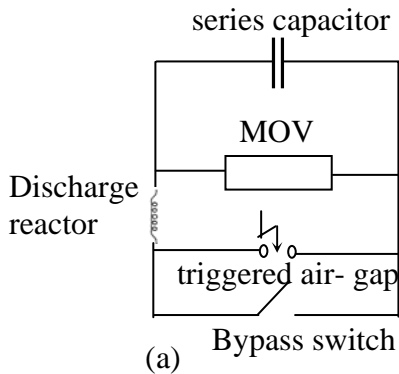
Fig. 5. 1 The Power System

(a)

(b)

**Fig. 5. 2 (a) Series Capacitor arrangement
(b) Voltage-current characteristic of MOV**
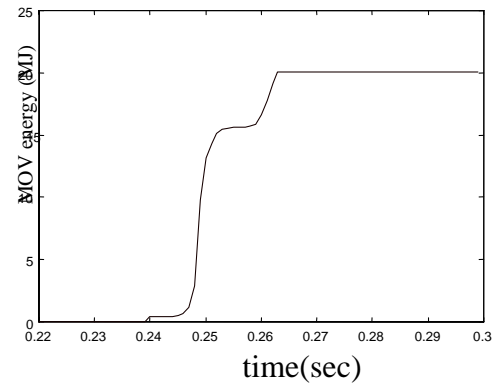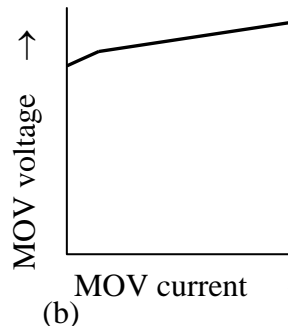

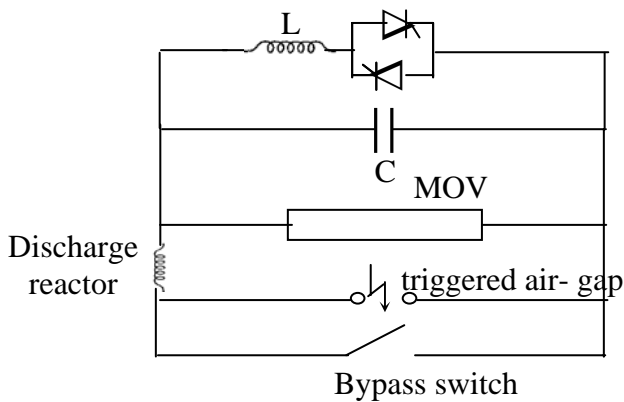**Fig. 5.3 Energy growth in the MOV during fault**
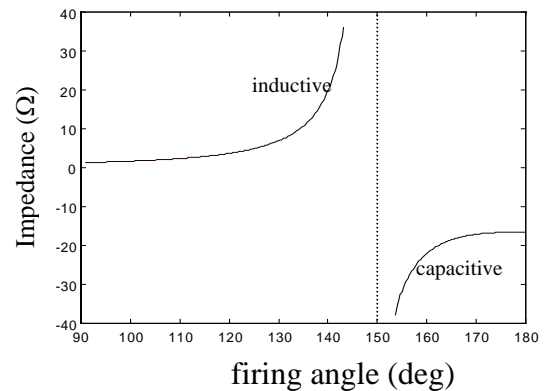

Fig. 5.4 Basic TCSC arrangement

Fig. 5.5 Impedance characteristic of the TCSC

The typical voltage-current characteristic of an MOV is shown in Fig. 5.2(b). For a particular application the major considerations for the MOV are its voltage and energy ratings. The maximum normal voltage that is anticipated across the series capacitor establishes voltage rating and related voltage-current characteristic.

The MOV protecting the fixed capacitor placed in each phase of the system accumulates energy during a faulty condition. The growth in energy during a three-phase fault at 70% of the line is shown in Fig.5.3 for 'a-phase' MOV.

(b) The Thyristor Controlled Series Compensator (TCSC)

When the energy level in the MOV increases to 20MJ the air-gap is fired and hence the curve is clamped at that energy level. TCSC can control power flow, mitigate sub-synchronous resonance, improve transient stability, damp out power system oscillations resulting increase of power transfer capability. Today, TCSC is being already included in some of the transmission systems. The basic circuit of a TCSC in one of the phases is shown in Fig. 5.4. The thyristors control the current through the reactor. The forward-looking thyristor has firing angles of 90^0 through 180^0. Firing the thyristors at this time results in a current flow through the inductor that is opposite to the capacitor current. This loop current increases the voltage across the capacitor and hence the overall series compensation.

Further, the loop current increases as firing angle decreases from 180^0. In the present study the capacitor-reactance is considered to be 10% of the line reactance. The inductance of the TCSC is 0.0038H. The impedance characteristic of the TCSC is shown in Fig. 5.5.

Different compensation levels are obtained by varying the firing angle of the reactor-circuit-thyristors. In this study the firing angle is varied within 154.6^0 to 180^0 where the degree of compensation changes from 20% to 10%. For transient waveforms during faulty situation, a three-phase fault at 70% of the line is simulated and the different currents and voltages at the relay end are shown in Fig. 5.6. The voltage and current of faulty phases are affected by the presence of MOVs and the firing angle set for the TCSC besides the system operating condition, switching instant etc.
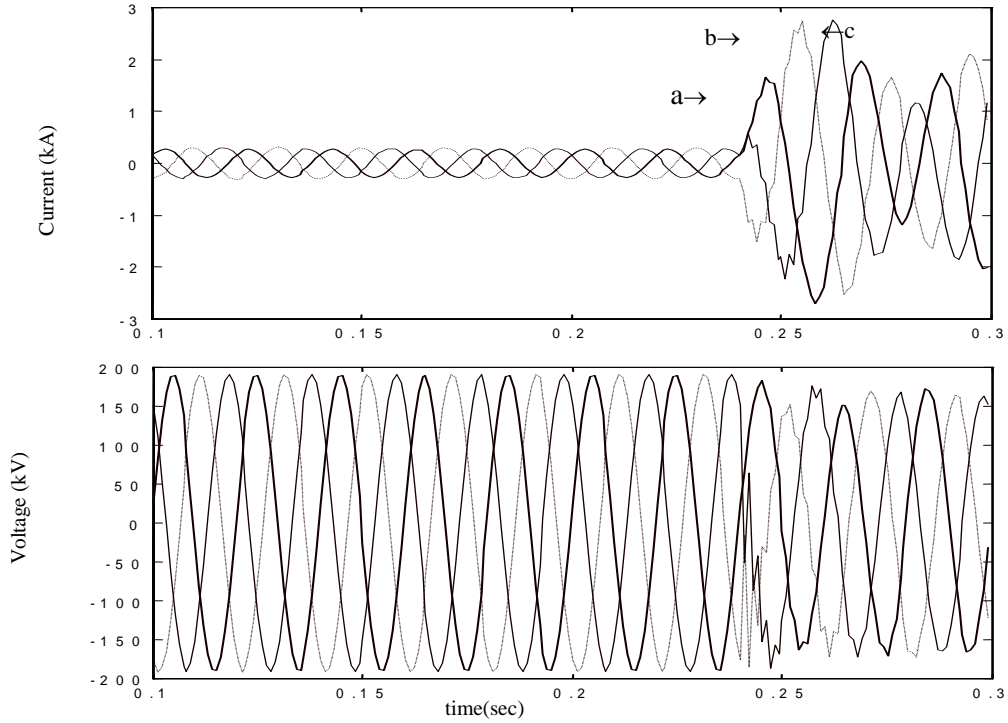
Fig. 5.6 Currents and Voltages during 3-phase fault

5.2.2 Wavelet Transform

Given a function *f(t)*, its continuous Wavelet Transform (CWT) can be calculated as follows:

$$\text{CWT}(f, x, y) = \frac{1}{\sqrt{a}} \int_{-\infty}^{\infty} f(t)\psi * \left(\frac{t - y}{x}\right) dt \tag{5.1}$$

Where *x* and *y* are scaling (dilation) and translation (time shift) constants, respectively, and ψ is the wavelet function. Wavelet Transform of sampled waveforms can be obtained by implementing the discrete Wavelet Transform, which is given by

$$\text{DWT}(f, x, y) = \frac{1}{\sqrt{x_0^m}} \sum_{k} f(k)\psi * \left(\frac{n - kx_0^m}{x_0^m}\right) \tag{5.2}$$

Where the parameters x and y in (5.1) are replaced by x_0^m and kx_0^m, k and m being integer variables. In a standard DWT, the coefficients are sampled from the CWT on a dyadic grid.

Associated with the wavelet is a scaling function $\varphi(t)$. The scaling function along with the wavelet function creates a multi-resolution analysis (MRA) of the signal. The scaling function of one level can be represented as a sum of a scaling function of the next finer level.

$$\varphi(t) = \sum_{n=-\infty}^{\infty} h(n)\sqrt{2}\varphi(2t-n) \tag{5.3}$$

The wavelet function is also related to the scaling function by

$$\psi(t) = \sum_{n=-\infty}^{\infty} h_1(n)\sqrt{2}\varphi(2t-n) \tag{5.4}$$

Where $h(k)$ and $h_1(k)$ represent the scaling and wavelet functions, respectively, and are related as

$$h_1(k) = (-1)^k h(1-k) \tag{5.5}$$

We can make use of the scaling function to represent the signal as

$$y(t) = \sum_{k=-\infty}^{\infty} c_{jo}(k)2^{jo/2}\varphi(2^{jo}t-k) + \sum_{k=-\infty}^{\infty}\sum_{j=jo}^{\infty} d_j(k)2^{j/2}\psi(2^j t-k) \tag{5.6}$$

Where jo represents the coarsest scale spanned by the scaling function.

The scaling and wavelet coefficients of the signal $y(t)$ can be evaluated by using a filter bank of quadrature mirror filters (QMF).

$$c_j(k) = \sum_{m=-\infty}^{\infty} c_{j+1}(m)h(m-2k) \tag{5.7}$$

$$d_j(k) = \sum_{m=-\infty}^{\infty} c_{j+1}(m)h_1(m-2k) \tag{5.8}$$

Equations (5.7) and (5.8) show that the coefficients at a coarser level can be attained by passing the coefficients at the finer level to their respective filters followed by a decimation of two. This will result in the number of samples in the coarser level to be approximately half of the number of samples at the finer level. For a signal that is

sampled at a frequency higher than the Nyquist frequency, the samples are used as $c_{j+1}(m)$. The filter bandwidth and center frequency for a dyadic wavelet filter at scale k is given as

$$B_k = \frac{f_s}{2^{k+1}} \tag{5.9}$$

$$f_k = \frac{3f_s}{2^{k+2}} \tag{5.10}$$

The three level wavelet decomposition structure is given in Fig. 5.7.
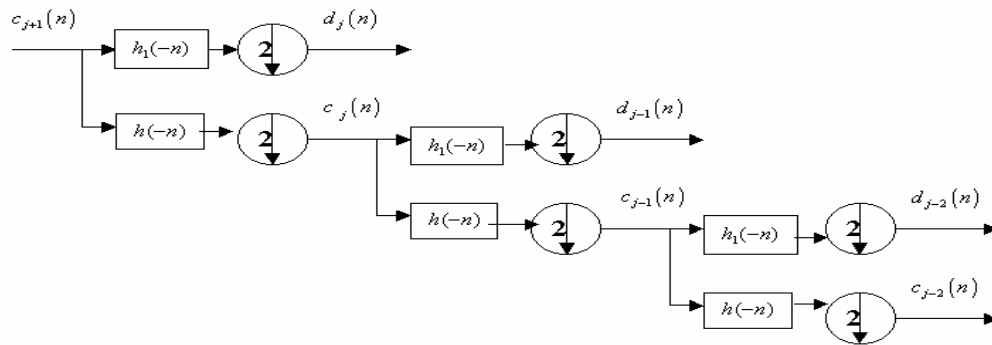

Fig. 5.7 Three level wavelet decomposition

Actual implementation of DWT involves successive pairs of high pass and low pass filters at each scaling stage of Wavelet Transform. This can be thought of as successive approximations of the same function, each approximation providing the incremental information related to a particular scale (frequency range), the first scale covering a broad frequency range at the high frequency end of the frequency spectrum, however, with progressively shorter bandwidths. Conversely, the first scale will have the highest time resolution, higher scales will cover increasingly longer time intervals. While in principle any admissible wavelet can be used in the Wavelet analysis, Daubechies Wavelet (DB4) is used in this work for both the purposes of fault section identification and phase selection for a transmission line.

If the used scaling function and the Wavelet function form an orthogonal basis, then Parseval's theorem relates the energy of the distorted signal to the energy in each expansion coefficients and their Wavelet coefficients. This means that the norm of energy of the signal can be partitioned in terms of expansion coefficients [62].This feature is

utilized here to differentiate different faults. The energy of the distorted signal will be partitioned at different resolution levels in different ways depending on the signals to be analyzed. The Energy of the signal is given by

$$E_{signal} = \int |y(t)|^2 \, dt = \sum_{k=-\infty}^{\infty} |c(k)|^2 + \sum_{j=jo}^{\infty} \sum_{k=-\infty}^{\infty} |d_j(k)|^2 \qquad (5.11)$$

Standard deviation can be considered as a measure of the energy for a distorted signal with zero mean and is utilized in this work as a feature to identify the faulty phase and the faulty section (i.e. before TCSC or beyond it) of the transmission system.

5.2.3 Simulation Results

(a) Phase selection

Accurate faulty phase selection is essential for digital distance relaying and single pole autoreclosure scheme. Traditional methods are based on the current and voltage phasors and thus are affected by remote end infeed, fault resistance and source impedances. Further in a digital relaying system to extract the phase(s) from the noisy signals available during the fault is again a complex task. In the proposed study therefore, we have proposed Wavelet based phase selection scheme, which uses the current signals of the three phases. Daubechies Wavelets (DB4) are applied to the signals during fault conditions for one cycle window with a sampling rate of 10 kHz and the corresponding coefficients at different scales were studied. Fig. 5.8 shows the standard deviations of different scales of different phases for line-to-line fault (ab type) at 80% of the line from the relaying point. It is clear from the figure that the curves of the faulty phase(s) (phase-a and phase-b) are well above the sound phase (phase-c). Further it is observed from Fig. 5.8 that the faulty phases possess high values of standard deviation under scale-5 to scale-10. This is in agreement with the fact that the energy of the signal is partitioned into different levels by DWT. As an index to distinguish the faulty phase from sound phase, we introduce the standard deviation based index (*EM*).

$$EM = \sum_{i=5}^{10} (\, Std_i \,)$$ (5.12)

where *Std* represents the standard deviation of the detailed output signal.

   i = the decomposition level.

   From Fig. 5.8 it is seen that the standard deviation becomes maximum at the 8th level of decomposition and is a measure of the energy of the signal (as it is computed from the squares of the variations of the detailed wavelet coefficients). Although a summation from level 5 to 10 is used here, the standard deviation at the 8th level could have yielded similar results.
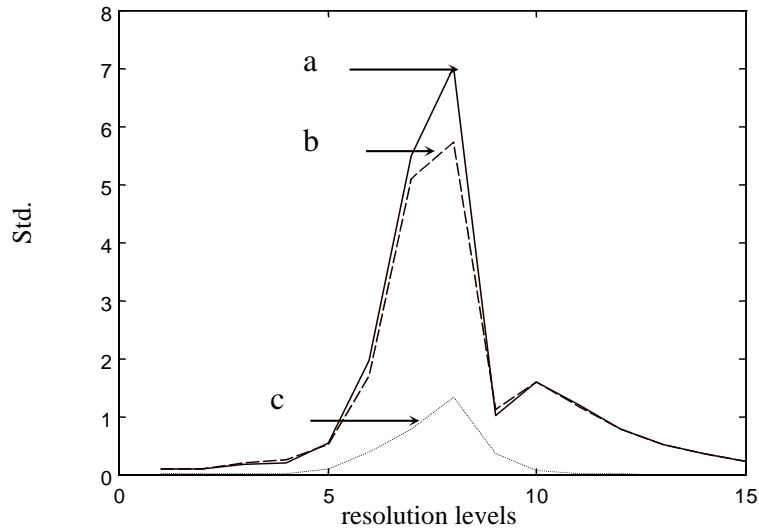

Fig. 5.8 Standard deviation of wavelet   coefficients at different levels

   The *EM* index for different types of faults and at different locations along the line is shown in Table-5.1. For example, the case of a-phase to ground fault at 10% of the line from the relay point provides *EM* values of 18.00, 1.96 and 1.83 for phase-a, phase-b and phase-c current signals, respectively. This clearly demonstrates that the faulty phase index value is quite high as compared to that of sound phase. Similar observation is noticed for a-phase to ground fault for 30% of the line and at a different initial power

flow condition. In the event of line-to-line fault at 40% of the line (ab type) the *EM* indices for phase-a and phase-b are significantly high as compared to the corresponding value of phase-c. The results depicted above are for fault cases within the TCSC. For faults beyond the TCSC, at 60% of the line for ab-g type fault the EM indices are 25.87, 24.94 and 3.87 for phases a, b and c, respectively. At 70% of the line for phase-a to ground fault the *EM* index of phase-a current signal is 11.80 as compared to 4.29 and 3.75 for phase-a and phase-c current signals, respectively. Toward the line end at 80% of the line for line-to-line fault (ab type) and at a different firing angle of TCSC the corresponding values of *EM* of phase-a and phase-b current signals are 17.66 and 15.86, respectively as compared to 3.08 for phase-c.

Further to test the validity of the approach for high impedance fault, at 70% of the line for phase-a to ground fault case with fault resistor of $100\,\Omega$ is initiated and the corresponding current signals are decomposed by the DWT. The *EM* values for phase-a are found to be high as compared to the corresponding values of phase-b and phase-c. Further to see the performance of the approach for different fault inception angles, phase-a to ground fault at 70% of the line is initiated at 90^0 instead of 0^0 as in earlier cases (considering phase-a voltage as reference) and it is found that *EM* index still provides the required distinction in selecting the faulty phase. For other types of faults like the phase-to-phase, phase-to-phase-to- ground, three-phase-to – ground the EM index yields similar results. The involved phases exhibit higher EM values in comparison to the unfaulted phases. Further if the fault also involves the ground, the EM index for the unfaulted phase is higher than the case when no ground is involved. However, change of energy from no fault to fault cases will be a better indicator for identifying the presence of ground. For example the change in energy in the c-phase for ab (phase a-to-phase-b) and ab-g (phase-a-to-phase-b-to-ground) is .0002, and 1.218, respectively. The above results in selecting the phases involved in the fault demonstrate the performance of the approach for different fault types, power system initial conditions, fault resistances and inception angles.

Table-5.1 Faulty phase selection

Faults	Values of index *EM*		
	Phase-a	Phase-b	Phase-c
'ag'-type fault at 10 % of the line	18.00	1.97	1.83
'ag'-type fault at 30 % of the line	19.87	2.31	1.84
'bg'-type fault at 30 % of the line	2.42	18.97	1.96
'cg'-type fault at 30 % of the line	1.85	2.36	19.03
'ab'-type fault at 40 % of the line	23.98	22.02	1.98
'bc'-type fault at 40 % of the line	1.96	23.67	22.96
'ca'-type fault at 40 % of the line	23.32	1.95	22.09
'abg'-type fault at 60 % of the line	25.87	24.94	3.87
'bcg'-type fault at 60 % of the line	3.56	25.21	24.69
'cag'-type fault at 60 % of the line	26.03	3.23	25.41
'ag'-type fault at 70 % of the line	11.80	4.30	3.76
'ab'-type fault at 80 % of the line	17.67	15.87	3.08
'abcg'-type fault at 70 % of the line	12.03	11.65	12.98
'bcg'-type fault at 70 % of the line	2.36	14.21	12.89
'cag'-type fault at 70 % of the line	12.65	3.21	13.67
'ag'-type fault at 70 % of the line with fault resistance $100\,\Omega$,at inception angle $0°$	8.16	3.66	3.15
'ag'-type fault at 70 % of the line with fault resistance $100\,\Omega$,at inception angle $90°$	8.16	3.66	3.15
'abg'-type fault at 70 % of the line with fault resistance $100\,\Omega$,at inception angle $90°$	9.63	8.72	3.26
'abcg'-type fault at 70 % of the line with fault resistance $100\,\Omega$,at inception angle $90°$	8.25	8.69	9.02

(b) Fault section identification

From stability point of view fault section identification is an important task for a transmission or distribution systems. To estimate the fault distance in the presence of a TCSC at the midpoint of a line a distance relay essentially requires a fault section identifier to discrimination the faults encountering the TCSC and not encountering it [3]. In this study the transmission system as shown in Fig. 5.1 is considered where the Wavelet based identifier should be able to distinguish faults within the TCSC and beyond it; whether on line-1 or line-2. Fig. 5.9 shows the typical fault current signals for faults at

30% and 70% of the line, respectively (phase-a to ground fault). It is a difficult task to distinguish these two signals as regard to the fault section identification. The wavelet scale-1 coefficients (for one cycle) of the corresponding faulty signals with a sampling rate of 10 kHz are presented in Fig. 5.10 and it is observed that the coefficients are significant for 70% case compared to 30% case. These two plots clearly distinguish the faults one excluding the TCSC and one including the TCSC in the fault loops. As to the expectation, high frequency transient components, which are more prominent when TCSC is present in the fault loop, are captured at scale-1 in Fig. 5.10 (70% case). However, from protection viewpoint a standard deviation-based index is proposed in this study to distinguish the above two figures. For this purpose, the standard deviation with zero mean of scale-1 coefficients is considered as a measure for identifying the faulted section.

Table-5.2 provides standard deviation values for few typical situations covering various types of faults involving phase-to-ground, phase-to-phase-to-ground, phase-to-phase, three-phase-to-ground, etc. The standard deviations of the two plots (30% and 70% cases) are 0.0006 and 0.0411 respectively and which clearly provide the necessary information to distinguish the two sections involved in the fault.
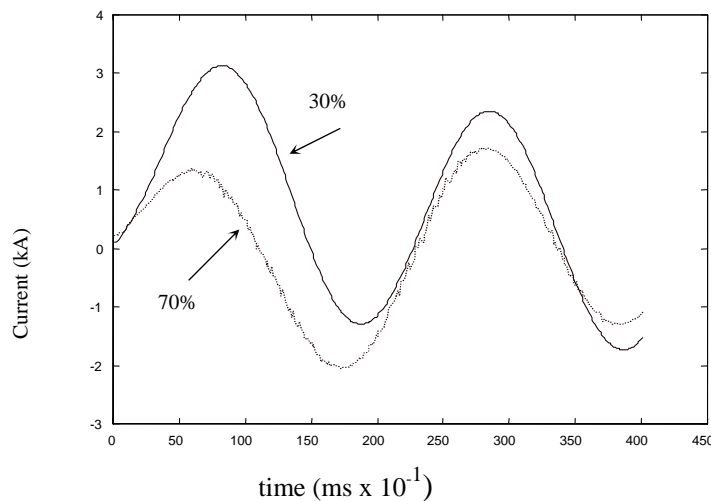

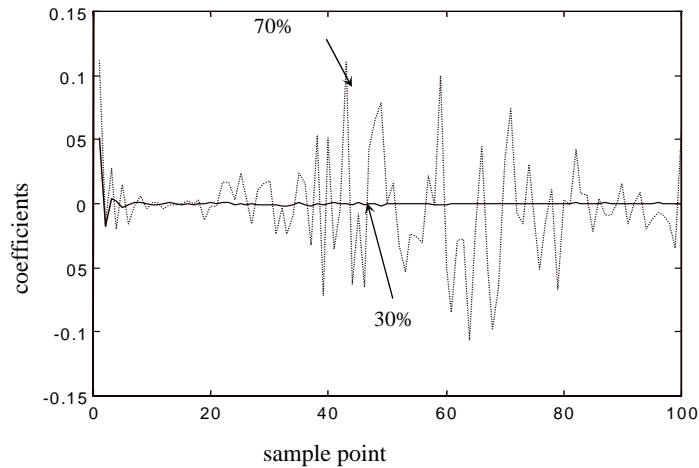**Fig. 5.9 Currents for faults at 30% and 70% of the line**

Fig. 5.10 Scale-1 DWT coefficients of fault currents at 30% and 70% of the line

Fig. 5.11 shows another case for line-to-line fault (ab-type), where scale-1 Wavelet coefficient plots are shown for faults at 40% and 80% of the line. Again it is observed that the plot for latter case which includes the TCSC in the fault loop (80%) differs significantly to that of the former case (40%). In Fig. 5.11 only phase-a signals are considered and similar observation is noticed for phase-b signals also for the above line-to-line fault case. The standard deviation of scale-1 wavelet coefficients of a-phase current for the two cases is 0.0022 and 0.0739, respectively. These index values for fault closure to the TCSC (48% and 52% positions) are also provided in the table. All the above results depict that the scale-1 standard deviation index is quite high for faults beyond TCSC than those for faults within TCSC.
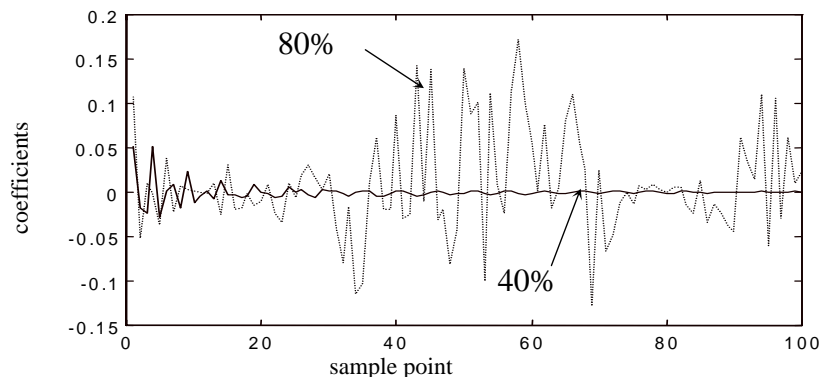

Fig. 5.11 Scale-1 DWT coefficients of fault current at 40% and 80% of the line

Table-5.2 Fault section identification

Faults	Standard deviation at scale-1 for faulty phase current signal
'ag'-type fault at 10 % of the line	0.0009(phase-a)
'ag'-type fault at 30 % of the line	0.0006(phase-a)
'bg'-type fault at 30 % of the line	0.0005(phase-b)
'cg'-type fault at 30 % of the line	0.0007(phase-c)
'ab'-type fault at 40 % of the line	0.0022(phase-a)
	0.0021(phase-b)
'bc'-type fault at 40 % of the line	0.0018(phase-b)
	0.0022(phase-c)
'ca'-type fault at 40 % of the line	0.0015(phase-c)
	0.0019(phase-a)
'ag'-type fault at 48 % of the line	0.0028(phase-a)
'ag'-type fault at 52 % of the line	0.0617(phase-a)
'abg'-type fault at 60 % of the line	0.0812(phase-a)
	0.0765(phase-b)
'bcg'-type fault at 60 % of the line	0.0789(phase-b)
	0.0863(phase-c)
'ag'-type fault at 70 % of the line	0.0411(phase-a)
'ab'-type fault at 80 % of the line	0.0739(phase-a)
	0.0663(phase-b)
'abcg'-type fault at 90 % of the line	0.0532(phase-a)
	0.0423(phase-b)
	0.0589(phase-c)
'ag'-type fault at 70 % of the line with fault resistance $100\,\Omega$,at inception angle 0º	0.0325(phase-a)
'ag'-type fault at 70 % of the line with fault resistance $100\,\Omega$,at inception angle 90º	0.0334(phase-a)
'abg'-type fault at 70 % of the line with fault resistance $100\,\Omega$,at inception angle 90º	0.0532(phase-a)
	0.0483(phase-b)
'abcg'-type fault at 90 % of the line with fault resistance $100\,\Omega$,at inception angle 90º	0.0326(phase-a)
	0.0239(phase-b)
	0.0395(phase-c)

5.3 Fault analysis of advanced series compensated line using S-Transform and pattern recognition approach

The S-Transform [27], is an extension of Wavelets; uses an analysis window whose width is decreasing with frequency providing a frequency dependent resolution. This recent transform may be seen as a continuous Wavelet Transform with a phase correction. It produces a constant relative bandwidth analysis like Wavelets while it maintains a direct link with the Fourier spectrum. In this paper the S-Transform is utilized for on-line fault analysis of a transmission system employing an ASC at the mid point. The normalized frequency spectrum clearly identifies the faulty phase from the current signals at the relay point. Using the faulty phase current signal only the new approach identifies the zone of the fault further, by distinguishing the frequency spectrums as obtained from S-Transform.

On-line fault analysis is essential for transmission line protection, autorecloser, system stability enhancement etc. Faulty phase identification is required for fault classification and estimating fault location (for line protection) and single pole autorecloser decision. Similarly, fault section identification is essential for system stability improvement or line protection. In the application of S-Transform, phase selection and fault section identification are efficiently accomplished for a transmission line employing an ASC at the mid point.

Traditional methods for faulty phase selection are based on the current and voltage phasors and are, therefore, affected by remote end infeed, fault resistance and source impedance. Further, the performance of the designed estimator to extract the phasors from the faulty signals, in the digital systems, will be affected by the presence of ASC and its accessories.   A new approach based on S-Transform is, therefore, proposed here to select the faulty phase accurately. A sampling rate of 1 kHz and window length of one cycle are considered in all cases. The system studied as given in Fig. 5.1

5.3.1 Simulation study and results

(a) Faulty phase selection

The normalized frequency contours are plotted in Fig. 5.12 for single phase fault involving ground (a-g). It is obvious that before the fault, the normalized frequency

contours for the three phases constitute a straight line, where as the post fault coefficients of phase-a provides number of lines unlike phase-b and phase-c coefficients. This is obvious as faulty phase current possesses number of non-fundamental frequency components. Further, at 40% of the line with an inception angle of 90^0 instead of 0^0 (phase-a voltage as reference) double- line-to-ground fault was initiated. Similar to the earlier observation, the faulty phases (phase-a and phase-b) are clearly distinguished from sound phase-c by normalized frequency contours as shown in Fig. 5.13.To demonstrate the effectiveness of the approach for faults beyond the ASC, a phase-to-phase (a-b) type fault involving ground was simulated at 80% of the line. Different currents of the three phases are used to compute their corresponding transformed coefficient plots which are shown in Fig. 5.14. Similar to the earlier classifications, the phase-a and phase-b coefficients show number of lines unlike a single line for phase-c after the fault inception. In above cases the S-Transform is found out without considering the prefault data samples. The window width considered for faulty phase selection is 1.0.
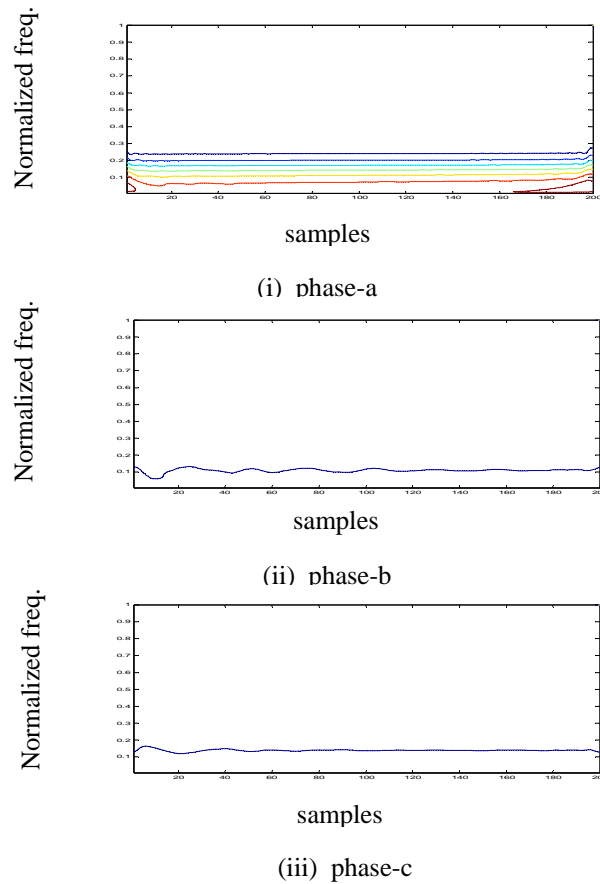
(i) phase-a

(ii) phase-b

(iii) phase-c

Fig. 5.12 Normalized frequency contours of L-G
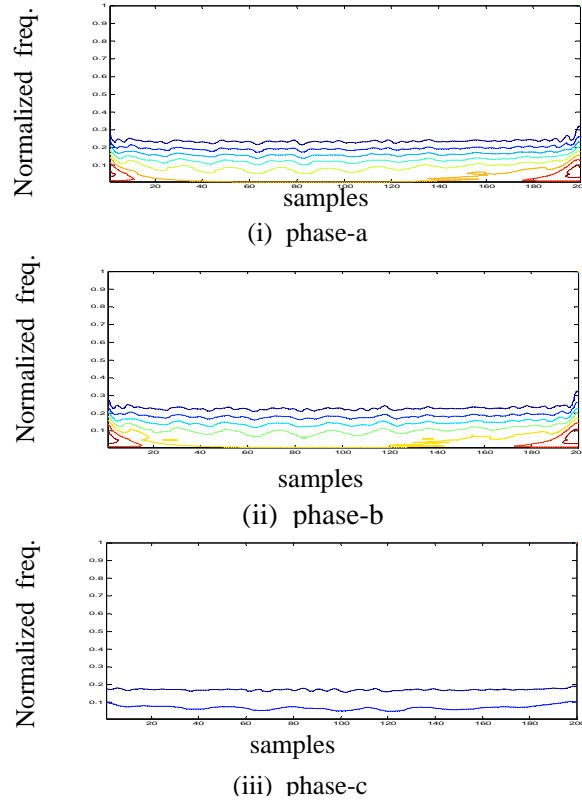**fault at 10% of the line**

(i) phase-a

(ii) phase-b

(iii) phase-c

**Fig. 5.13 Normalized frequency contours of LL-G
fault at 40% of the line**

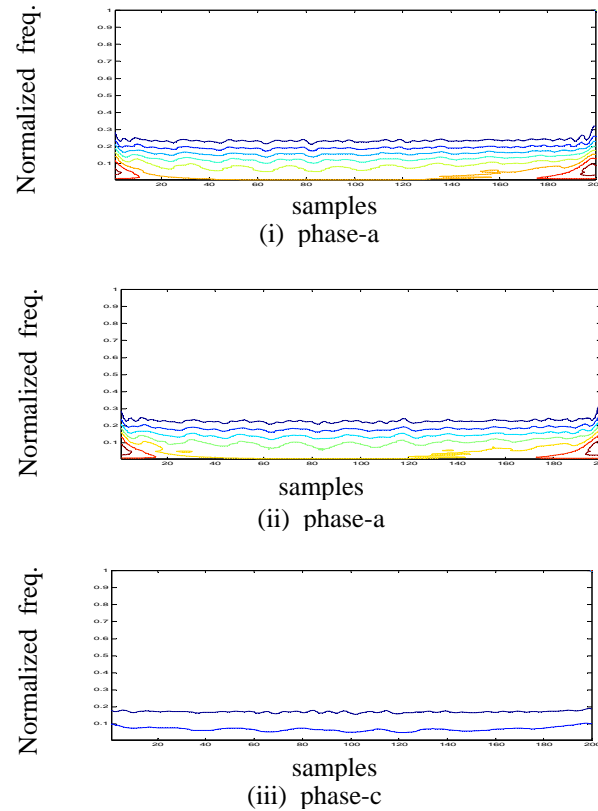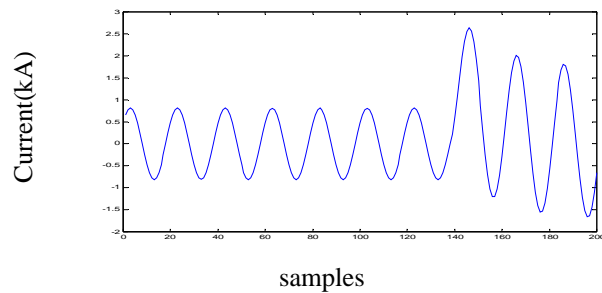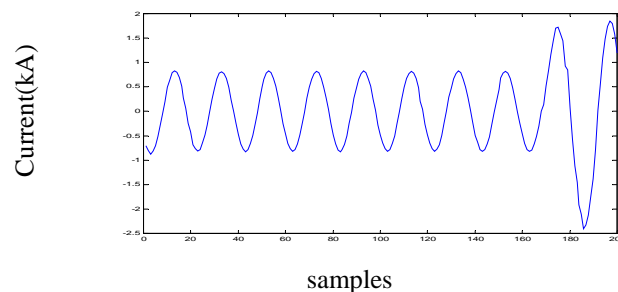
(i) phase-a

(ii) phase-a

(iii) phase-c

**Fig. 5.14 Normalized frequency contours of L-L
fault at 80% of the line**

(b) Fault Section Identification

Significant difference exists between fault signals, due to the presence of MOVs and ASC combination, for fault encountering the ASC and not encountering it. When the fault loop does not include the ASC the current signal contains decaying DC and high frequency components besides the fundamental components. In the other cases of fault loop enclosing the ASC, the signal consists of non fundamental decaying frequency components, odd harmonics, high frequency components and the fundamental. Fault section identification is essential for protection and stability points of view. Based on phasor measurements it may not be always possible to identify whether the fault encounters the ASC or not. S-Transform is applied to identify the fault section accurately at different fault situation.
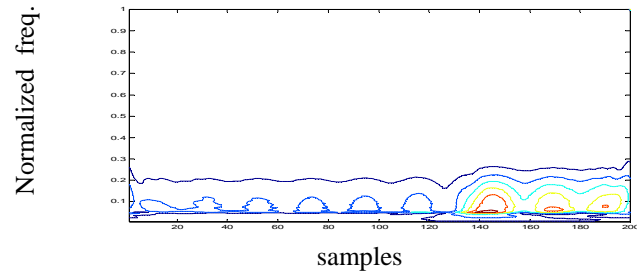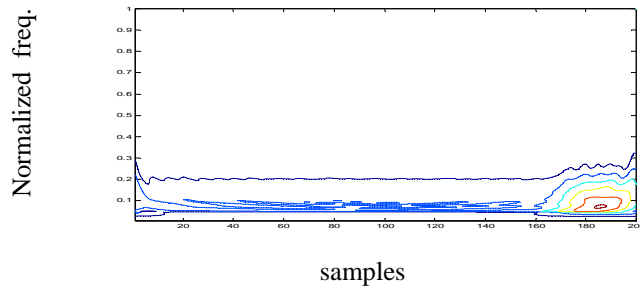

(i) phase-a 40%）

(ii) phase-a (60%）

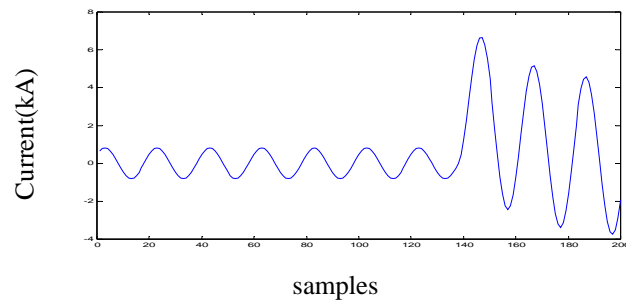**Fig. 5.15 Fault current of L-G fault at 40% and 60% of the line**
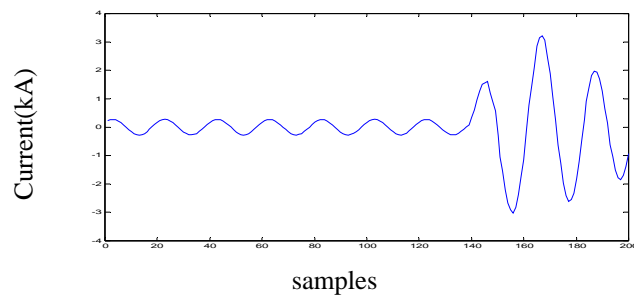
(i) phase-a (40%)

(ii) phase-a (60%)

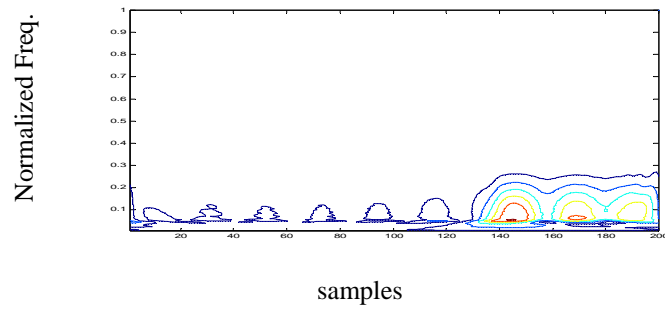**Fig. 5.16 Normalized frequency contours of L-G fault at 40% and 60% of the line**
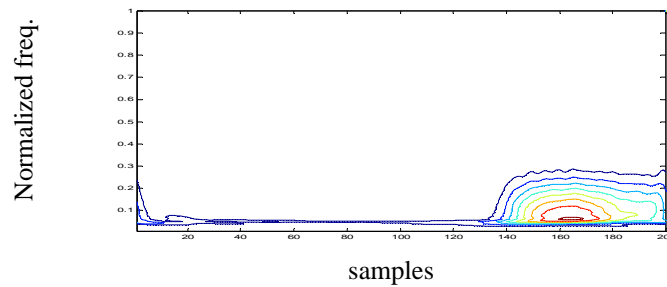

(i) phase-a(10%)

(ii) phase-a (90%)

Fig. 5.17 Fault currents of LL-G fault at 10% and 90% of the line

(i) phase-a (10%)

(ii) phase-a (90%)

Fig. 5.18 Fault currents of LL-G fault at 10% and 90% of the line

For detailed analysis phase-a-to-ground fault at 40% and 60% of the line faults are initiated. The current signals of the faulty phases (which are identified as in section a) are again analyzed by the S-Transform but with the consideration of prefault data samples. Such coefficients are plotted in Fig. 5.15 and Fig. 5.16, which indicate that in case of the fault at 40% location the contours posses number of centers whereas the 60% case contours are concentric. This clearly distinguishes the faults encountering the ASC and not encountering it. In the case of a double line-to-ground fault at fault locations of 10% and 90%   (ab-g type), phase-a current is analyzed and the normalized frequency contours are also plotted in Fig. 5.17 and Fig. 5.18. The window width for fault section identification is 0.1, and thus picks up higher harmonic components.

5.4   Conclusions

For power system monitoring and relaying purposes, fault section identification and phase selection are two difficult tasks. This is further complicated with the introduction of power electronics devices such as a TCSC in a power network. A transmission system possessing a TCSC and a fixed capacitor at the midpoint is simulated using the EMTDC package. Daubechies Wavelets are employed for both fault section identification and phase selection for all types of faults and different operating conditions of the power system. Two different indices based on energy measure are evaluated for phase and section identification tasks. It is found that the new Wavelet tool provides a very efficient method for fault analysis of Flexible AC Transmission Systems (FACTS). As Wavelet Transform gets affected in presence of noise and is not very suitable for phasor computation, another pattern recognition approach using S-transform is also presented and attempt is made to find improved results. The S-transform technique is employed for both fault section identification and phase selection of the transmission system. Different computed spectrums clearly demonstrate the potential of the approach for fault analysis for online propose even in the presence of high fault resistance, different initial conditions and fault inception angles.

Chapter-6

Power Transformer Protection using
Time-frequency analysis and pattern recognition

6.1   Introduction

Power transformers play a vital role in any electric power system network. So it is very important to avoid any mal-operation and false tripping by providing required relaying system. Protection of large power transformers is a very challenging job in power system relaying. The phenomenon of inrush current in the power transformers has been well known for many years and is an important aspect of harmonic restraint differential relay. The inrush current contains a large second harmonic component in comparison to an internal fault. The existing method based on differential protection using 2nd harmonic restraint works successfully when the 2nd harmonic is highly pronounced compared to fault. But in some cases the 2nd harmonic component remains same for inrush current as well as for fault current. In such cases the existing 2nd harmonic restraint fails. Thus a new pattern recognition approach using S-Transform with Complex window is presented to distinguish between inrush and fault currents. As S-Transform is obtained by multiplying the real window with Fourier sinusoid and Fourier sinusoid has time-invariant frequency, S-Transform is unsuitable for resolving waveforms whose frequency changes with time. This problem can be overcome by using complex gaussian window with a user designed complex phase function. The phase function modulates the frequency of the Fourier sinusoid to give better time-frequency localization of the time series. That means if the time series contains a specific asinusoidal waveform that is expected at all scales, then the complex gaussian window can give better time-frequency resolution of event signatures than the un-modulated, real valued gaussian window of the original signal.

6.2 Power Transformer Protection using S-Transform with Complex Window and Pattern Recognition Approach

This proposed research presents a new approach for power transformer protection using S-Transform with complex window to distinguish between inrush current and internal fault. The S-Transform with complex window is used to extract patterns of transient current samples during inrush and faults. S-Transform is a very powerful tool for nonstationary signal analysis giving the information of transient currents both in time and frequency domain. The spectral energy is calculated for inrush and internal faults and an *energy index* is found out to distinguish between inrush magnetizing current and internal faults. The simulation results and the results obtained using real-time data from a transformer in the laboratory environment indicate the robustness of the proposed technique.

6.2.1 Background

Most important issue in power transformer protection is to distinguish inrush current from internal faults. The inrush current contains a large second harmonic component in comparison to an internal fault. Sometimes also, the second harmonic may be generated in case of internal faults in power transformer. This may be due to CT saturation and distributive capacitance in long transmission line to which the power transformer is connected. Apart from these, the inrush current magnitude is relatively small in modern power transformers due to design improvements. This means the inrush current in modern transformer may be equal to the fault current by design which may cause difficulty in distinguishing the inrush current from fault current. Therefore, the traditionally provided protection system with harmonic restraint will not be capable of discriminating between inrush current and internal fault.

As both inrush current and internal faults are non-stationary signals, the most important requirement is to extract features from the signal. For feature extraction or pattern recognition from non-stationary signal STFT (Short Time Fourier Transform), DWT (Discrete Wavelet Transform) have been used extensively. In case of DWT [25, 67, 68], the variations of the detailed coefficients are obtained to distinguish between

magnetizing inrush and fault. The Wavelet transform specifically decomposes a signal from high frequency to low frequency bands through an iterative procedure and this procedure performs very well for high frequency transients but not so well for low frequency components including second, third and fifth harmonic components of current present in the magnetizing inrush or faults. Consequently the Wavelet decomposition coefficients in a frequency band reflect the overall effect of all signal components in the frequency band, rather than the specific fundamental and harmonic ones. Also the frequency properties of the decomposition filter bands are not ideal and suffer leakage effects where the signal frequency is closer to the edge of a frequency band. Therefore, a more suitable signal processing technique is considered in this study for recognizing the current signal patterns in a transformer.

The S-Transform is an invertible time-frequency spectral localization technique [27-30] that combines elements of Wavelet Transform and Short-Time Fourier Transform. The S-Transform uses an analysis window whose width is decreasing with frequency providing a frequency dependent resolution. S-Transform is continuous Wavelet transform with a phase correction. It produces a constant relative bandwidth analysis like wavelets while it maintains a direct link with Fourier spectrum. The S-Transform has an advantage in that it provides multiresolution analysis while retaining the absolute phase of each frequency. This has led to its application for detection and interpretation of non-stationary signals. Further, the S-Transform provides frequency contours which clearly localizes the signals at a higher noise level [35]. In this study, a new pattern recognition approach using S-Transform with Complex window [31] is presented to distinguish between inrush and fault currents. As S-Transform is obtained by multiplying the real window with Fourier sinusoid and Fourier sinusoid has time-invariant frequency, S-Transform is unsuitable for resolving waveforms whose frequency changes with time. This problem can be overcome by using complex gaussian window with a user designed complex phase function. The phase function modulates the frequency of the Fourier sinusoid to give better time-frequency localization of the time series. That means if the time series contains a specific asinusoidal waveform that is expected at all scales, then the complex gaussian window can give better time-frequency

resolution of event signatures than the un-modulated, real valued gaussian window of the original signal.

When a fault occurs on the secondary side of a transformer, the transient current is captured by the respective CTs at primary and secondary side of the transformer. Also inrush current is captured in the same way. After the signal is retrieved, S-Transform is used to process the signal samples to provide the relevant features for detection and recognition. The spectral energy of inrush current and fault current at different contour levels are computed from the S-Transform output matrix. From the spectral energy, an *energy index* is calculated which discriminate between inrush and fault current and the relay restrains or operates accordingly. Also time frequency contours in both fault and inrush are presented   to distinguish both the events.

6.2.2 A variant of S-Transform: S-Transform with complex window

The generalized S-Transform is defined as

$$S(\tau, f, p) = \int_{-\infty}^{\infty} h(t)\{w(\tau - t, f, p) \times exp(-2\pi i f\ t)\}dt, \tag{6.1}$$

where w is the window function of the S-Transform and *p* denotes the set of parameters that determines the shape and property of the window function, w.

The alternative expression of (6.1) using Fourier transform can be given as:

$$S(\tau, f, p) = \int_{-\infty}^{\infty} H(\alpha + f)W(\alpha, f, p)\,exp(+2\pi i\alpha\tau)\,d\tau \tag{6.2}$$

where

$$H(f) = \int_{-\infty}^{\infty} h(t)\,exp(-2\pi ift)\,dt \tag{6.3}$$

$$W(\alpha, f, p) = \int_{-\infty}^{\infty} w(t, f, p)\,exp(-2\pi i\alpha t)\,dt \tag{6.4}$$

The variables α and f in the above expression have the same units.

For S-Transform to converge to Fourier transform *H(f)*

$$\int_{-\infty}^{\infty} S(\tau, f, p)\, d\tau = H(f) \tag{6.5}$$

For w to be the window of S-Transform, the following condition must be satisfied:

$$w(\tau - t, f, p)\exp(-2\pi i f t) = A(\tau - t, f, p)\exp\{-2\pi i \phi(\tau - t, f, p)\} \tag{6.6}$$

where A and ϕ are the amplitude and phase of w. If both sides are multiplied by Fourier sinusoids, w becomes:

$$w(\tau - t, f, p)\exp(-2\pi f t) = A(\tau - t, f, p)\exp\{-2\pi i [ft + \phi(\tau - t, f, p)]\} \tag{6.7}$$

As the amplitude A and phase angle ϕ of the S-Transform output are known, the instantaneous frequency F can be defined as the time derivative of the total phase:

$$F = f + \frac{\partial}{\partial t}\varphi(\tau - t, f, p) \tag{6.8}$$

The S-Transform gives the best localized spectrum when the analyzing function matches with the shape of the time series of the signal. The analyzing function is defined by the multiplication of the Fourier sinusoid with the Gaussian window with phase modulation through an appropriate complex factor and normalization. This gives to complex Gaussian window w_{cg} as

$$w_{cg}(\tau - t, f, \sigma) = \begin{cases} P\exp\left[-\dfrac{f^{2(\tau - t)^2}}{2}\right]\exp(-2\pi\pi i f(\tau - t) \\ + 2\pi\pi i\ \mathrm{sgn}(f)\ \sigma\ log\left[\sigma + |f|(\tau - t)\right], \\ \qquad\qquad t \le \tau + \sigma/|f|, \quad 0, \quad t \ge \tau + \sigma/|f|. \end{cases} \tag{6.9}$$

The pre-factor p is defined as

$$P^{-1} = \int_{-\sigma/|f|}^{\infty} \exp\left\{\frac{f^{2\tau^2}}{2} - 2\pi i f\tau + 2\pi i\ sign(f) \times \sigma\ log\left[\sigma + |f|\tau\right]\right\} d\tau, \tag{6.10}$$

where the positive parameter σ controls the degree of phase modulation. When $w_{cg} \neq 0,$ the instantaneous frequency becomes equal to

$$F = \frac{\sigma f}{\sigma + |f|(\tau - t)} \tag{6.11}$$

The discrete S-Transform is obtained by sampling (6.2) in the frequency domain and given by:

$$S_{cg} = \left[jT, \frac{n}{MT}, p \right] = \sum_{m=-M/2}^{M/2-1} H\left[\frac{n+m}{MT} \right] \times W_{cg} \left[\frac{m}{MT}, \frac{n}{MT}, p \right] \times exp\left[\frac{+2\pi imj}{M} \right], \tag{6.12}$$

where T is the sampling interval, M is the numbers of sample points and j is the discrete time index. m and n are discrete frequency indices.

The discrete window function is obtained by:

$$W_{cg}\left[\frac{m}{MT}, \frac{n}{NT}, \sigma \right] = p \sum_{k=max(-\sigma M/|n|,-M/2}^{M/2-1} exp\left[\frac{-n^2}{2M^2} - \frac{2\pi ink}{M} \right] \times exp\left\{ -2\pi i\left[\frac{nk}{M} - \sigma\, sign(n) \times log(\sigma + \frac{|n|k}{M} \right] \right\} \tag{6.13}$$

where P is defined as:

$$p^{-1} = p \sum_{k=max(-\sigma M/|n|,-M/2}^{M/2-1} exp\left[\frac{-n^2 k^2}{2M^2} \right] \times exp\left\{ -2\pi i\left[\frac{nk}{M} - \sigma\, sign(n) \times log(\sigma + \frac{|n|k}{M} \right] \right\} \tag{6.14}$$

and k is the discrete time index.

6.2.3 System Studied

The simulation study has been done on the system comprising a 2000MVA generator and 1000 MVA with 500kV/220kV transformer shown in Fig. 6.1. The generator X/R ratio is 10. The primary winding voltage , R(pu) and L(pu) are 500kV, 0.003 0.09 respectively and secondary winding voltage, R(pu) and L(pu) are 220kV , 0.003, 0.09 respectively. Also simulation tests are done on 100 MVA capacity transformer with other parameters remaining same. The winding configuration such as Y-Y, Y-D, D-Y, and D-D are taken into consideration for extensive study. The study has been made for both for inrush current and different internal faults with and without load.

Faults are created for winding to ground, winding to winding with and without load. The sampling rate is chosen 1.0 kHz at 50 Hz frequency. A cycle contains 20 samples. One cycle data of inrush and fault have been processed through S-Transform to give the spectral energy at different contour levels. The simulation model is developed using Matlab-Simulink software modules. For studying the performance of proposed approach under noisy conditions, random noise with   SNR up to 20 dB has been added to the differential current signal. The load taken here is 100 MW and 80 MVAR.

Also real time tests (experimental) have been conducted for a single-phase transformer of 5 kVA capacity with 400 V/ 230 V in the laboratory. The winding configuration is Y-Y for the experimental set up. The inrush current and internal faults like winding-to-winding and winding to ground for different turn positions are measured by using a power scope.
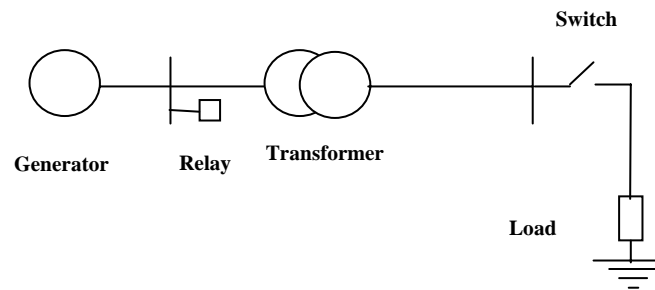

Fig. 6.1 System Model

6.2.4 Simulation Results and Discussion

(a) Differential Protection based on 2ⁿᵈ harmonic restraint

The differential protection based on 2nd harmonic restraint using Adaptive Linear Combiner (ADALINE) [69] is tested. The results of differential protection based on 2nd harmonic restraint are given in Fig. 6(a) and Fig. 6(b). A factor of 6 is multiplied to the actual amplitude of the second harmonic component present in the current waveform to produce the restraint signal. The operating signal is the magnitude of the fundamental component. As seen from the Fig. 6.2 (a), the tripping signal for inrush and fault based on

2nd harmonic restraint using ADALINE are well separated and a threshold can be set for the tripping signal above which relay restrains (inrush) and below which relay operates (fault). This is possible when the 2nd harmonic magnitude compared to fundamental exceeds 20% and the fault current has a lower 2nd harmonic component compared to the fundamental component. But when the 2nd harmonic component is nearly 10% in both the cases, the tripping signal for inrush and inrush current overlap each other and no threshold can be set for the tripping signal as shown in Fig. 6.2 (b). Thus the 2nd harmonic restraint fails in such cases having low second harmonic component compared to the fundamental.
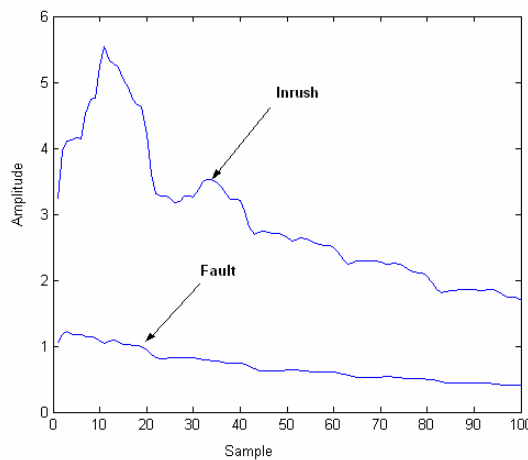
Fig. 6.2 (a) Tripping signals obtained form ADALINE when the 2nd harmonic component is 60% and 10% in inrush current and fault respectively
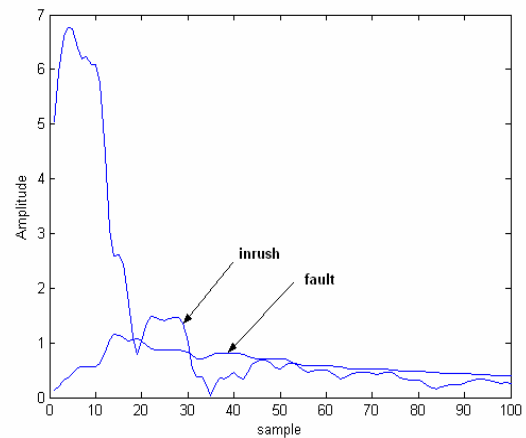
Fig.6.2 (b) Tripping signals obtained form ADALINE when the 2nd harmonic component is 10% in both inrush current and fault respectively.

The above problem is solved by the proposed method, which discriminates the inrush current and internal fault even if the 2nd harmonic component is same in both inrush and internal fault with the existing operating conditions and configurations. In this case the proposed *energy index* is 2.57 for inrush current and 3.89 for internal faults, which are well separated with the set threshold. The generated S-contours for inrush and internal faults are given in Fig. 6.2(c) and Fig. 6.2 (d), respectively. The S-contours with

contour level-1 for inrush and internal fault are given in Fig. 6.2(e) and Fig. 6.2(f), respectively. The above study is made on synthesizing the inrush and fault current and processing the respective signals through ADALINE and S-Transform. After confirming the results on synthesized data, the corresponding signals for simulation models and experimental set up are tested and results are given in the following sections.
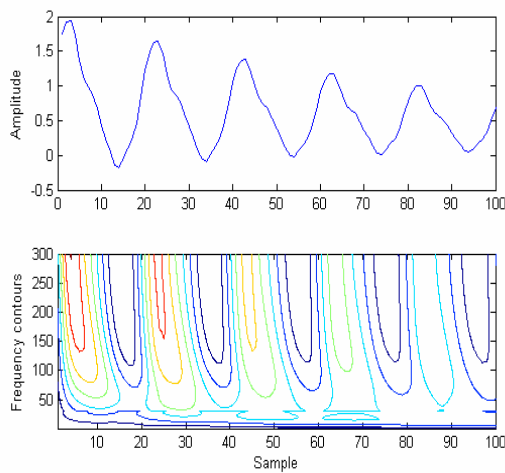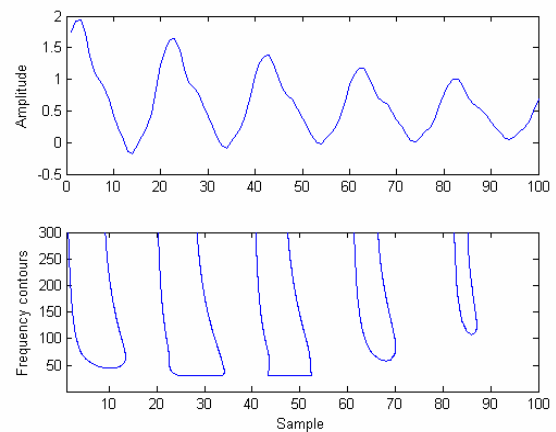

Fig. 6.2(c) S-contours for inrush current

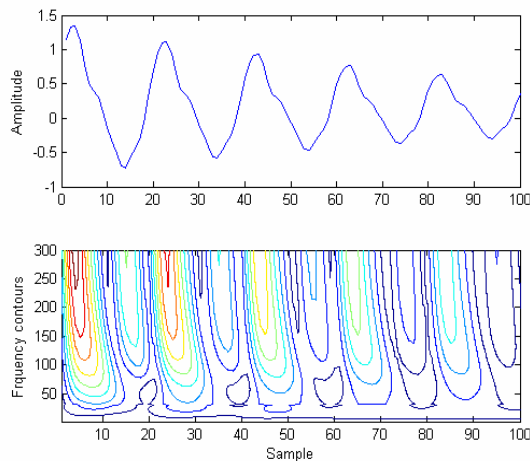**Fig. 6.2(e) S-contours for inrush current at contour level-1**

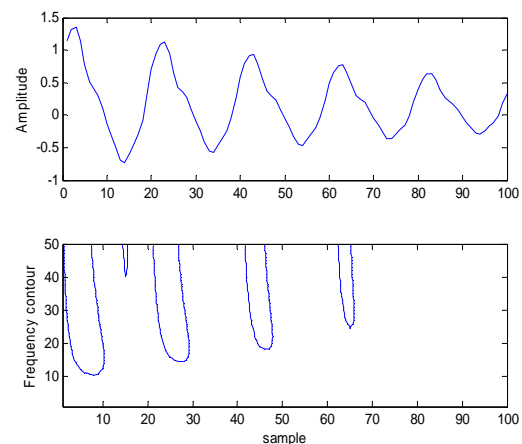**Fig. 6.2(d) S-contours for internal fault**

Fig.6.2 (f) S-contours for internal fault at contour level-1

(b) Feature extraction using S-Transform

Data for inrush current and internal faults are generated from the simulation model given in Fig. 6.1. The S-Transform of the corresponding data is computed. The frequency contours (S-contours), and the spectral energy (energy) of S-Transform of inrush current and fault signals are calculated for one-cycle data from the inception of inrush and fault conditions. The frequency contours (levels 1 to 9) are shown in Fig. 6. 3(a) through Fig. 6.3 (l) with frequency. But the frequency contours for counter level-1 is obtained as shown in Fig. 6.4(a) through Fig. 6.4 (k) for simulation data. It is clear from the frequency contour (S-contour) with contour level-1 to level-9 that in case of inrush current, the contours are present only during positive peaks of the current waveform compared to various fault conditions. For faults occurring on the transformer, the frequency contours are found with positive and negative sections of the fault current waveform. However, S-Transform output contour level-1 for inrush current shows that the frequency contour is concentric around second harmonic frequency and in case of faults, the frequency contours are around fundamental frequency. Similarly the data retrieved from real time transformer tests in the laboratory, are processed through S-Transform to yield the frequency contours for both inrush current and internal faults. The frequency contours for real time generated data are as shown in Fig. 6.5(a) through Fig. 6.5 (e) with contour level-1 to contour level-9. Fig. 6.6(a) through Fig. 6.6 (e) depict frequency contours at contour level-1 only for real time data. From the figures it is clearly seen that the inrush current having different frequency contours exhibits interrupted patterns in comparison to internal fault current showing regular patterns.

Table-6.1 and Table-6.3 depict the spectral energy content of inrush current and internal faults for various conditions. It is clearly seen that the spectral energy content of inrush currents are much less compared to the spectral energy content of internal faults for S-contours with contour level-1 through contour level-9. But the spectral energy content of inrush current is more than the spectral energy content of internal faults for S-contours with contour level-1only. The energy calculations lead to the *energy index* which discriminates inrush current from internal faults.
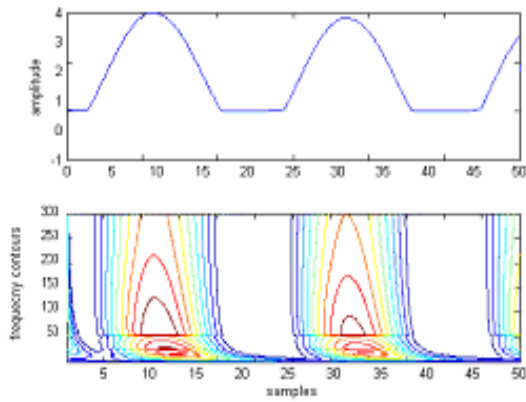
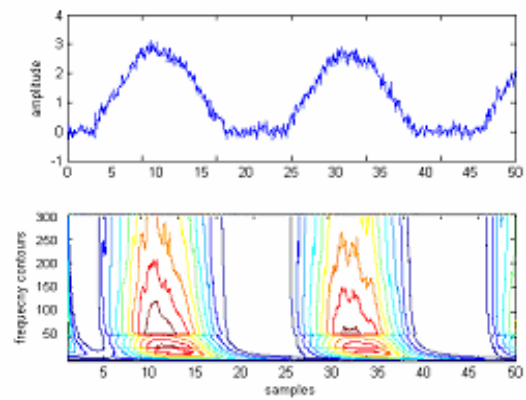**Fig. 6.3(a) S-contours for inrush current of a-phase**

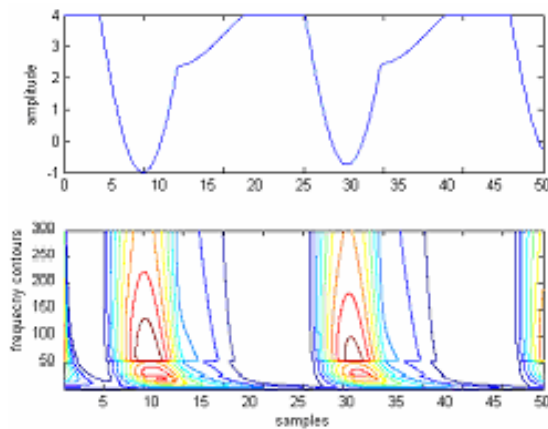**Fig. 6.3(d) S-contours for inrush current of a-phase with SNR 20 db**

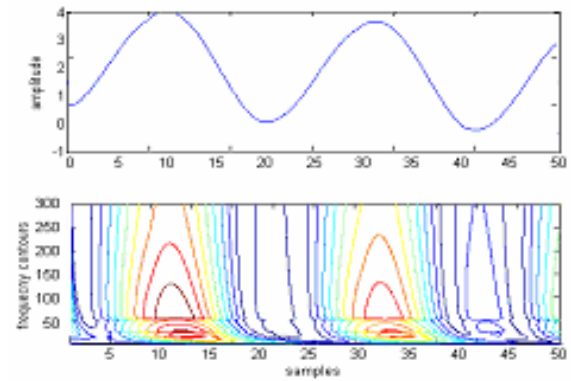**Fig. 6.3(b) S-contours for inrush current of b-phase**

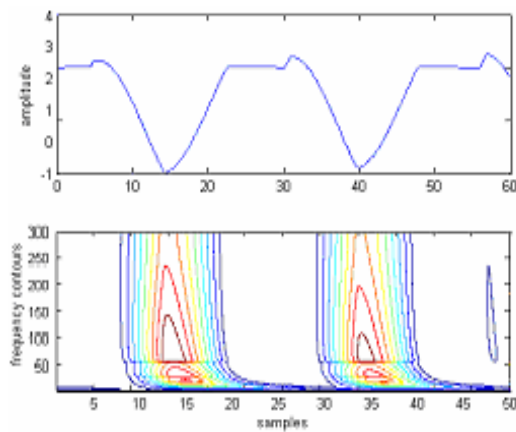**Fig. 6.3(e) S-contours for winding to ground fault of a-phase**

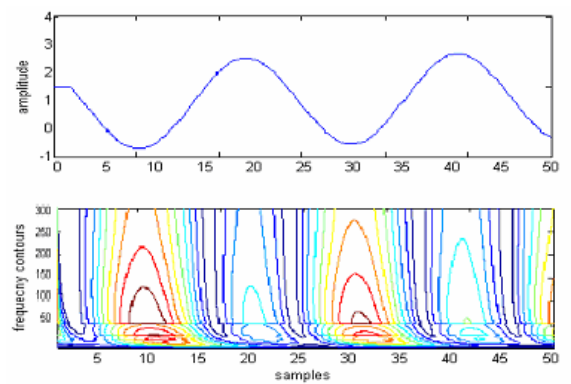**Fig. 6.3(c) S-contours for inrush current of c-phase**

Fig. 6.3(f) S-contours for winding to ground fault of b-phase
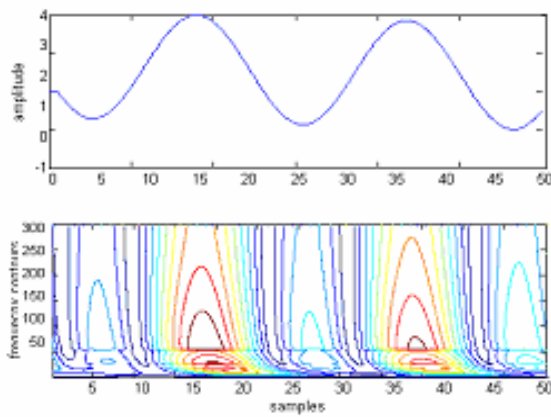
Fig. 6.3(g) S-contours for winding to ground fault of c phase

Fig. 6.3(j) S-contours for winding to winding fault of a-c with load (a-phase)

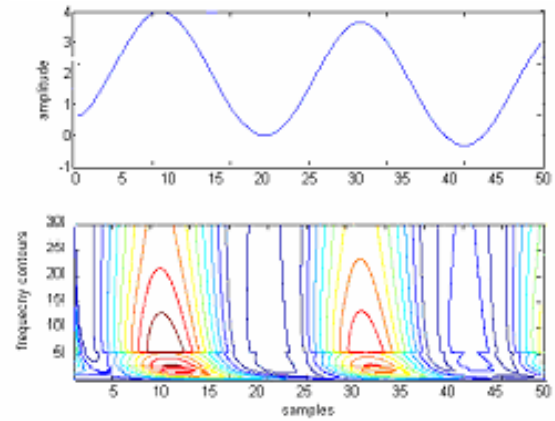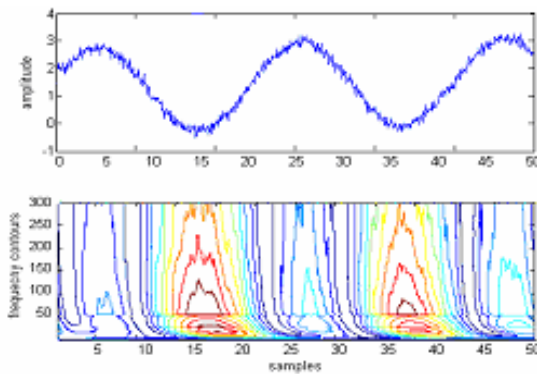**Fig. 6.3(h) S-contours for winding to ground fault of c-phase with SNR 20 db**
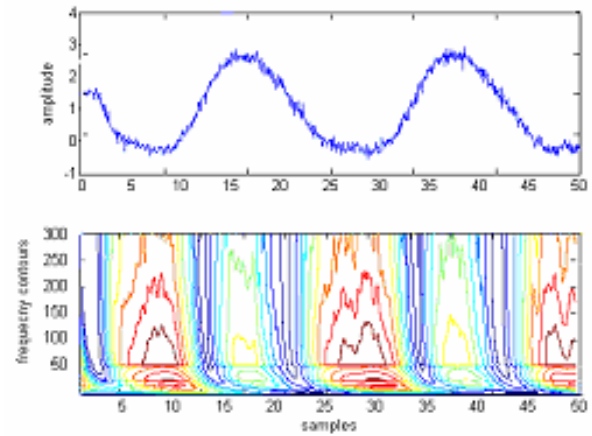
Fig. 6.3(k) S-contours for b-phase winding to winding fault (b-c fault) with SNR 20 dB
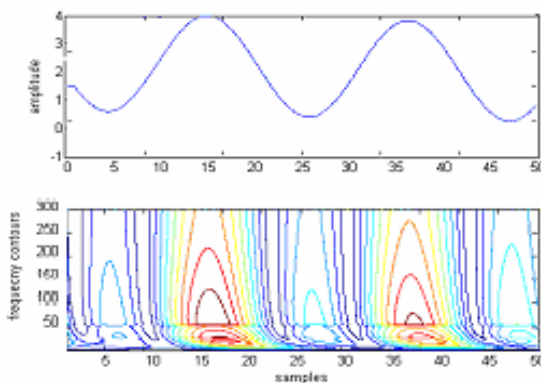
Fig. 6.3(i) S-contours for winding to ground fault of b-phase with load
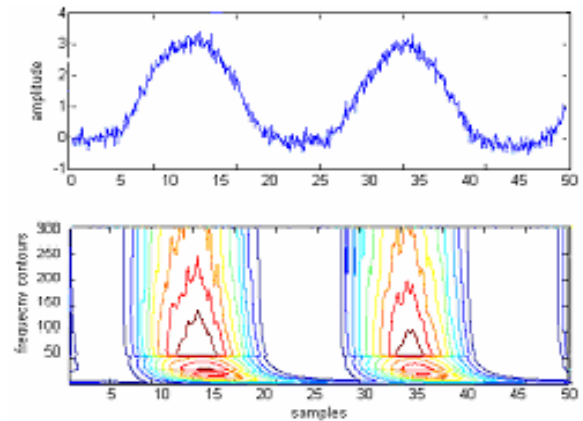
Fig. 6.3(l) S-contours for inrush current (loaded) for a-Phase with SNR 20 dB
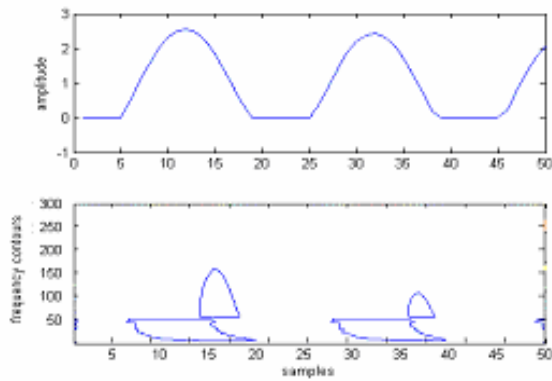
Fig. 6.4(a) S-contours for inrush current of a-phase at contour level-1
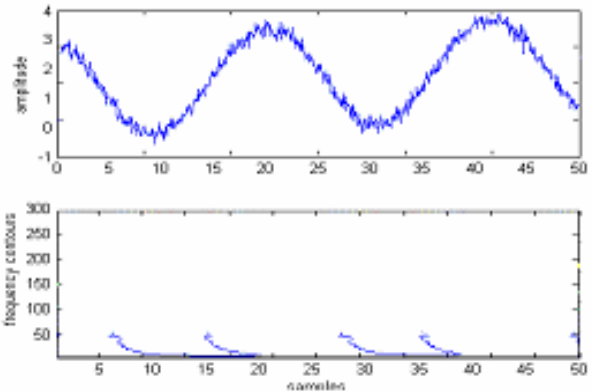
Fig. 6.4(d) S-contours for b-phase winding-winding-ground fault (bc-g fault) at contour level-1with SNR 20 dB
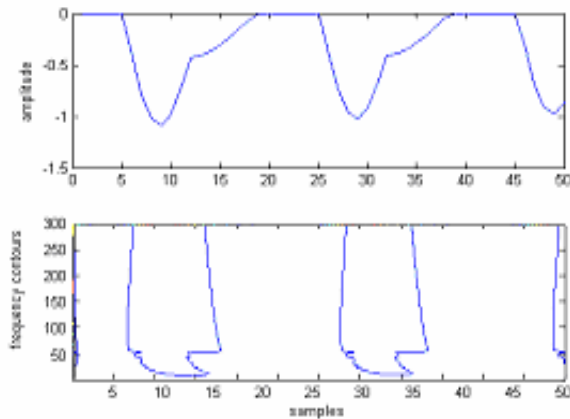
Fig. 6.4(b) S-contours for inrush current of b-phase at contour level-1
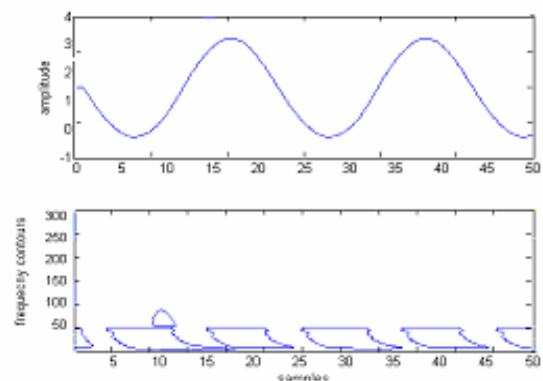
Fig. 6.4(e) S-contours for b-phase winding-winding fault (b-c fault) at contour level-1
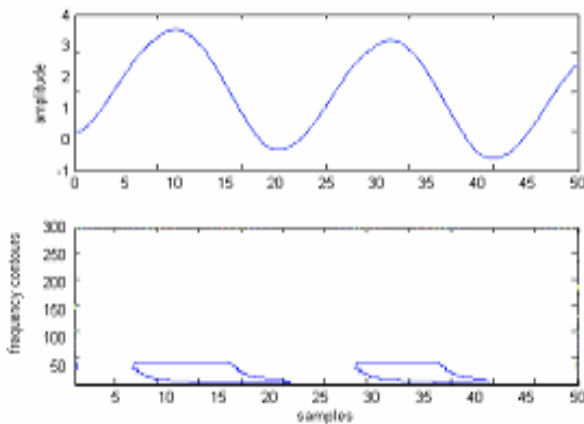
Fig. 6.4(c) S-contours for a-phase winding-winding fault (a-b fault) at contour level-1
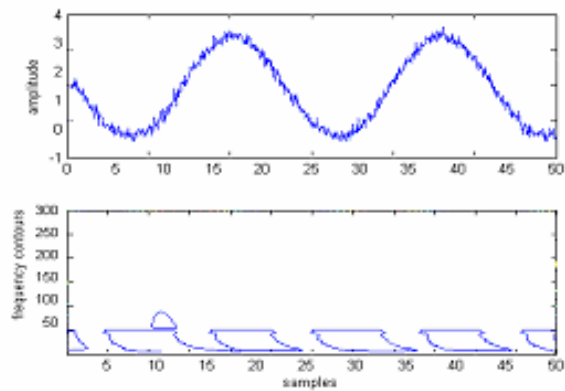
Fig. 6.4(f) S-contours for inrush current of b-phase (b-c fault) at contour level-1 with SNR 20 dB
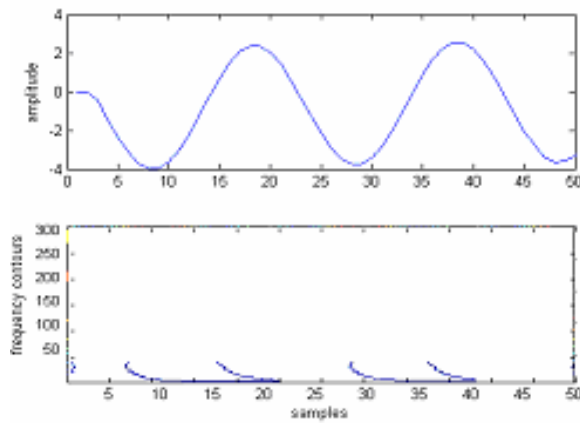
Fig. 6.4(g) S-contours for inrush current of c-phase (ac fault) at contour level-1
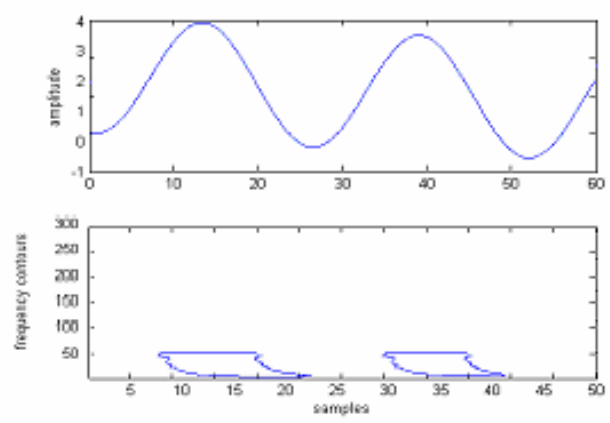
Fig. 6.4(j) S-contours for inrush current of a-phase (a-g fault) at contour level-1
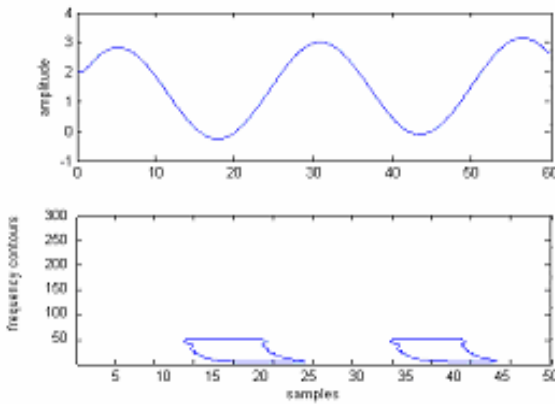
Fig. 6.4(h) S-contours for inrush current of c-phase (bc-g fault) at contour level-1
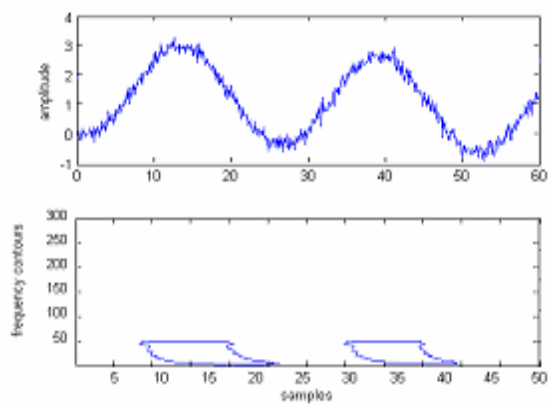
Fig. 6.4(k) S-contours for inrush current of a-phase (a-g fault) at contour level-1 with SNR 20 dB
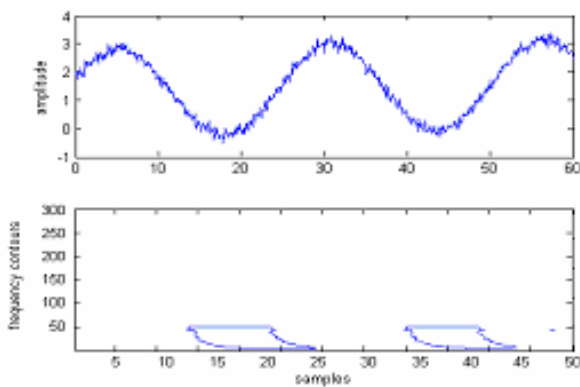
Fig. 6.4(i) S-contours for inrush current of c-phase (bc-g fault) at contour level-1 with SNR 20 dB
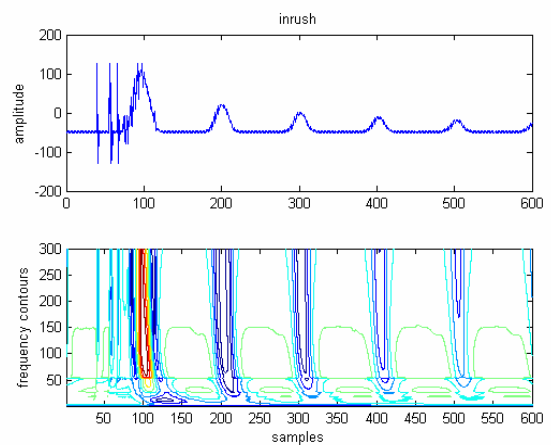
Fig. 6.5(a) S-contours for inrush current (experimental data)

143
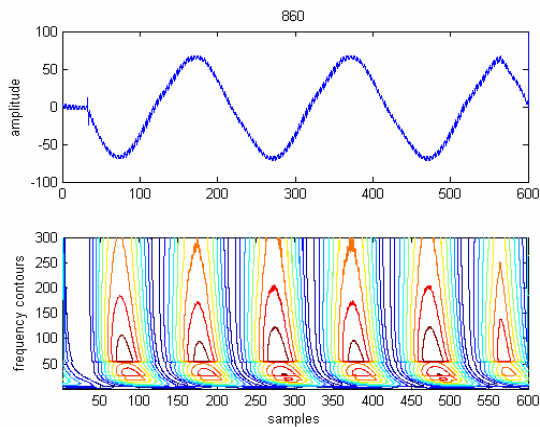
Fig. 6.5(b) S-contours for 86%-0% turn to turn fault (experimental data)
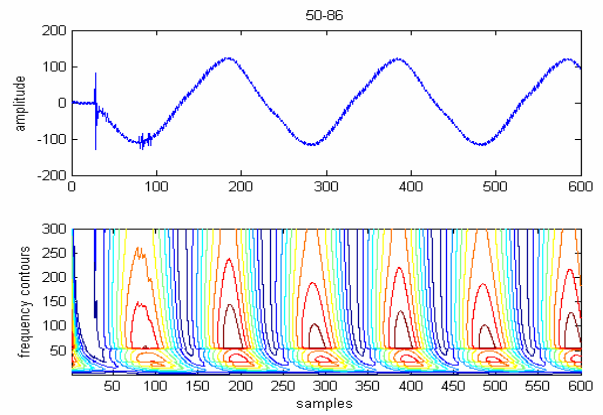
Fig. 6.5(e) S-contours for 50%-86% turn to turn fault (experimental data)
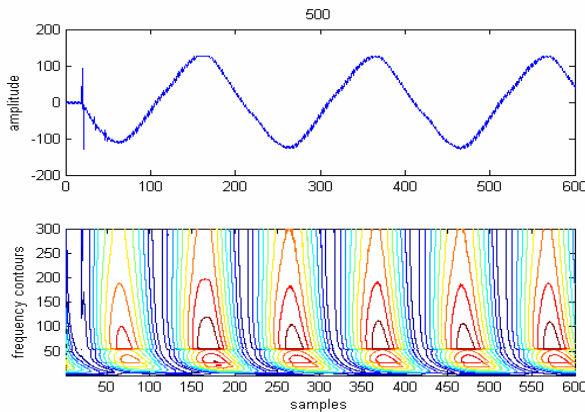
Fig. 6.5(c) S-contours for 50%-0% turn to turn faults (experimental data)
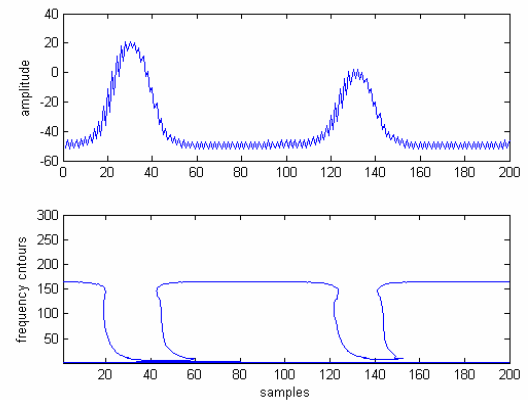
Fig. 6.6(a) S-contours for inrush current at contour level-1 (experimental data)
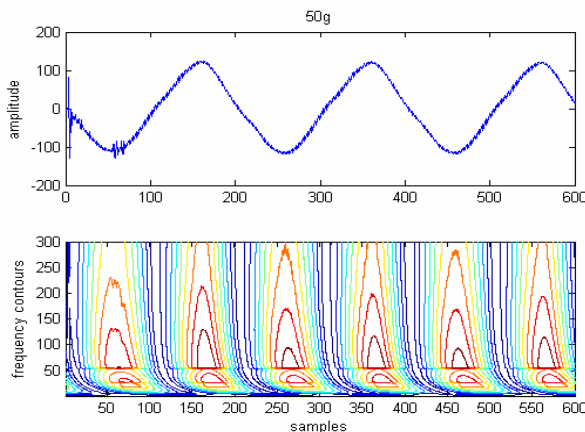
Fig. 6.5(d) S-contours 50% turn to ground fault (experimental data)
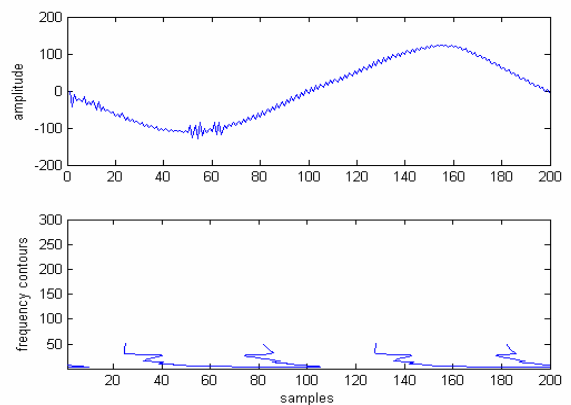
Fig. 6.6(b) S-contours for inrush current at contour level-1 for 50-0 fault (experimental data)
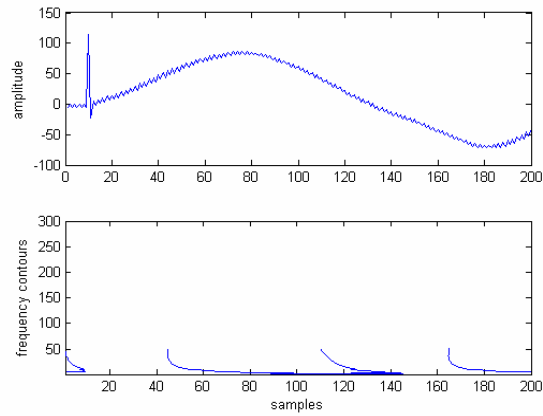
Fig. 6.6(c) S-contours for inrush current at contour level-1 for 50-86 fault (experimental data)
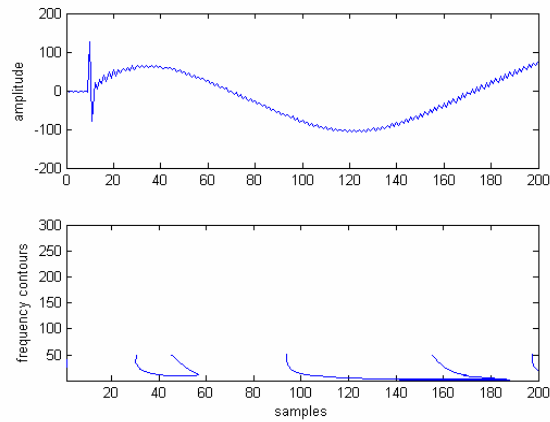
Fig. 6.6(d) S-contours for inrush current at contour level-1at 86-100 fault (experimental data)
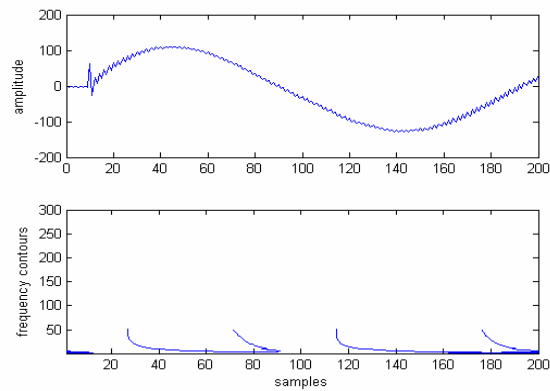
Fig. 6.6(e) S-contours for inrush current at contour level-1at 86-g fault (experimental data)

(c) Energy Index to distinguish inrush current from faults

From above results, *Energy Index* is found out to distinguish inrush current from internal faults. The Energy Index is given as:

$$\text{Energy Index} = \frac{\text{Energy of S-contours with contours level-1 to contour level-9}}{\text{Energy of S-contours with contours level-1}} \quad (6.15)$$

The devised index has been derived from the ratio of energy of S-contours from level 1 to 9 to Energy of S-contours at level-1, which clearly indicates the ratio of energy content of all harmonic components to the energy of the fundamental or second harmonic depends on the kind of events under analysis, inrush or fault. The *energy index* is 1.09(minimum) and 1.22(maximum) for inrush current and 4.01(minimum) and 5.48(maximum) for internal faults for signals without noise. Also the energy index for signals with noise gives the similar result which clearly distinguishes inrush from faults. Table-6.2 depicts *energy index* for simulation test with 1000 MVA capacity and Table-6.4 provides the *energy index* for simulation test with 100 MVA capacity transformer. The *energy index* for experimental set up is given in Table-6.6. For experimental data the *energy index* is above 1.65 for inrush current and 9.66(maximum) and 6.07(minimum) for internal faults, which clearly distinguishes faults from inrush condition.

To distinguish the inrush from internal faults, a suitable threshold value of 3.0 is set for *energy index,* below which it is inrush current and above which internal fault. The threshold value is chosen after testing the model under different operating conditions and capacities of the transformer. The tests have been done for 100 MVA and 1000 MVA transformers with different configuration such as Y-Y, Y-D, D-Y, and D-D. It is found that the *energy index* is below 1.03 for inrush current and above 3.51 for internal faults taking both results into consideration for simulation study when the 2nd harmonic magnitude compared to fundamental exceeds 20% and the fault current has a lower 2nd harmonic component compared to the fundamental component.

As seen in Table-6.2, the proposed technique also works successfully in case of the 2nd harmonic component is same (10-15%) in both inrush and internal faults. The *energy index* for 1000 MVA transformer is below 2.45 and above 3.24 for inrush and internal fault respectively. Similarly the *energy index* for inrush and internal fault are 2.52 and 3.24 respectively with SNR 20 dB. Also the similar observations are made in

Table-6.4 for 100 MVA transformers, where the *energy index* is below 2.24 and above 3.29 for inrush and internal fault respectively. Similarly the *energy index* is below 2.12 and above 3.24 for inrush and internal fault respectively with SNR 20 dB. The results for above cases are depicted in Table-6.2 and Table-6.4 in bold and italics. The *energy index* is 1.65 for inrush and 6.07 for internal fault for experimental test as given in Table-6.6. Thus form above results it is seen that the proposed technique works successfully where 2nd harmonic restraint fails. The flow chart to distinguish inrush current from fault is given in Fig. 6.7. In the proposed method, the energy content of S-Transform of one cycle current signal is taken for calculation. The one cycle data takes 20 ms and time taken for S-Transform and the algorithm is nearly 10 ms. Thus the total time taken by the proposed protection scheme is 30 ms approximately from the inception of fault.

Table-6.1 Energy for inrush and fault conditions for simulation data
(1000 MVA transformer)

Events (Simulation data)	Energy (at contour level-1)	Energy (for contours level-1 to level-9)	Energy (at contour level-1) (SNR 20 dB)	Energy (for contours level-1 to level-9 with SNR 20 dB)
Inrush-a(Y-Y)	38.02	45.02	41.06	56.35
Inrush-b(Y-D)	32.64	35.64	39.64	45.23
Inrush-c(Y-Y)	36.78	40.12	34.65	42.65
Inrush-a (loaded)(D-D)	35.62	43.65	39.82	47.69
Inrush-b (loaded)(Y-Y)	29.64	33.54	35.48	39.48
Inrush-c (loaded)(Y-D)	32.87	36.98	32.98	37.45
a-g fault(Y-Y)	24.35	119.63	24.46	120.53
b-g fault(Y-D)	25.24	110.02	26.41	113.05
c-g fault(Y-Y)	24.15	114.32	24.58	104.03
a-b fault(a phase)(D-Y)	21.97	120.53	22.23	153.06
a-b fault(b-phase)(D-D)	22.35	112.56	23.34	113.62
ca-g fault(a phase)(D-Y)	24.52	115.64	24.76	110.25
ca-g fault(c phase)(Y-Y)	21.26	120.65	21.34	114.68
bc-g fault(b phase)(D-Y)	25.64	102.83	24.68	108.03
bc-g fault(c phase)(D-D)	26.35	112.46	26.58	93.52
Inrush and Fault both contain 10-15% 2nd harmonic				
Inrush-a(Y-Y)	*29.36*	*62.34*	*31.25*	*67.85*
Inrush-b(Y-D)	*31.26*	*60.57*	*32.65*	*61.58*
Inrush-c(Y-Y)	*29.64*	*72.68*	*30.68*	*77.59*
a-b fault(a phase)(D-Y)	*25.63*	*88.96*	*26.31*	*94.85*
a-b fault(b-phase)(D-D)	*23.87*	*98.678*	*24.68*	*100.26*
ca-g fault(a phase)(D-Y)	*22.68*	*73.68*	*23.68*	*76.84*
ca-g fault(c phase)(Y-Y)	*21.48*	*82.68*	*22.64*	*86.35*

**Table-6.2 Energy Index for inrush and fault conditions
for simulation data (1000 MVA transformer)**

Events(Simulation data)	Energy Index	Energy Index(SNR 20dB)
Inrush-a(Y-Y)	1.18	1.37
Inrush-b(Y-D)	1.09	1.14
Inrush-c(Y-Y)	1.09	1.23
Inrush-a (loaded)(D-D)	1.22	1.19
Inrush-b (loaded)(Y-Y)	1.13	1.11
Inrush-c (loaded)(Y-D)	1.12	1.13
a-g fault(Y-Y)	4.91	4.92
b-g fault(Y-D)	4.35	4.28
c-g fault(Y-Y)	4.73	4.23
a-b fault(a phase)(D-Y)	5.48	6.88
a-b fault(b-phase)(D-D)	5.03	4.86
ca-g fault(a phase)(D-Y)	4.71	4.45
ca-g fault(c phase)(Y-Y)	5.67	5.37
bc-g fault(b phase)(D-Y)	4.01	4.37
bc-g fault(c phase)(D-D)	4.26	3.51
Inrush and Fault both contain 10-15% 2nd harmonic		
Inrush-a(Y-Y)	*2.12*	*2.17*
Inrush-b(Y-D)	*1.93*	*1.88*
Inrush-c(Y-Y)	*2.45*	*2.52*
a-b fault(a phase)(D-Y)	*3.47*	*3.60*
a-b fault(b-phase)(D-D)	*4.13*	*4.06*
ca-g fault(a phase)(D-Y)	*3.24*	*3.24*
ca-g fault(c phase)(Y-Y)	*3.84*	*3.81*

**Table-6.3 Energy for inrush and fault conditions for simulation data
(100 MVA transformer)**

Events (Simulation data)	Energy (at contour level-1)	Energy (for contours level-1 to level-9)	Energy (at contour level-1) (SNR 20 dB)	Energy (for contours level-1 to level-9 with SNR 20 dB)
Inrush-a(Y-Y)	36.25	41.65	38.91	55.12
Inrush-b(Y-D)	30.26	32.65	36.54	40.65
Inrush-c(Y-Y)	34.65	39.48	31.56	39.84
Inrush-a (loaded)(D-D)	32.65	40.21	36.58	42.78
Inrush-b (loaded)(Y-Y)	30.65	31.65	35.48	37.68
Inrush-c (loaded)(Y-D)	29.87	35.14	29.47	33.45
a-g fault(Y-Y)	22.65	111.65	22.64	112.65
b-g fault(Y-D)	21.65	120.65	23.54	111.62
c-g fault(Y-Y)	22.87	124.36	21.87	100.87
a-b fault(a phase)(D-Y)	19.68	125.64	19.38	146.87
a-b fault(b-phase)(D-D)	20.46	109.64	21.56	109.84
ca-g fault(a phase)(D-Y)	23.64	114.65	22.35	104.68
ca-g fault(c phase)(Y-Y)	20.75	119.78	20.84	99.64
bc-g fault(b phase)(D-Y)	22.65	120.65	23.48	102.47
bc-g fault(c phase)(D-D)	23.48	118.65	25.57	101.58

Inrush and Fault both contain 10-15% 2nd harmonic				
Inrush-a(Y-Y)	*29.68*	*66.54*	*31.25*	*66.54*
Inrush-b(Y-D)	*28.69*	*55.98*	*29.68*	*62.65*
Inrush-c(Y-Y)	*26.87*	*58.95*	*28.65*	*59.68*
a-b fault(a phase)(D-Y)	*22.35*	*94.65*	*21.65*	*82.57*
a-b fault(b-phase)(D-D)	*24.68*	*88.21*	*25.14*	*81.69*
ca-g fault(a phase)(D-Y)	*25.44*	*94.65*	*26.54*	*95.87*
ca-g fault(c phase)(Y-Y)	*24.99*	*82.45*	*26.54*	*100.23*

Table-6.4 Energy Index for inrush and fault conditions
for simulation data (100 MVA transformer)

Events (Simulation data)	Energy Index	Energy Index(SNR 20 dB)
Inrush-a(Y-Y)	1.14	1.41
Inrush-b(Y-D)	1.07	1.11
Inrush-c(Y-Y)	1.13	1.26
Inrush-a (loaded)(D-D)	1.23	1.16
Inrush-b (loaded)(Y-Y)	1.03	1.06
Inrush-c (loaded)(Y-D)	1.17	1.13
a-g fault(Y-Y)	4.92	4.97
b-g fault(Y-D)	5.57	4.74
c-g fault(Y-Y)	5.43	4.61
a-b fault(a phase)(D-Y)	6.38	7.57
a-b fault(b-phase)(D-D)	5.35	5.09
ca-g fault(a phase)(D-Y)	4.84	4.68
ca-g fault(c phase)(Y-Y)	5.77	4.78
bc-g fault(b phase)(D-Y)	5.32	4.36
bc-g fault(c phase)(D-D)	5.05	3.97
Inrush and Fault both contain 10-15% 2nd harmonic		
Inrush-a(Y-Y)	*2.24*	*2.12*
Inrush-b(Y-D)	*1.95*	*2.11*
Inrush-c(Y-Y)	*2.19*	*2.08*
a-b fault(a phase)(D-Y)	*4.23*	*3.81*
a-b fault(b-phase)(D-D)	*3.57*	*3.24*
ca-g fault(a phase)(D-Y)	*3.72*	*3.61*
ca-g fault(c phase)(Y-Y)	*3.29*	*3.77*

.

**Table-6.5 Energy for inrush and fault conditions
for experimental data.**

Events (Experimental data))	Energy (at contour level-1)	Energy (for contours level-1 to level-9)
Inrush(Y-Y)	91.56	142.65
Inrush (loaded)(Y-Y)	80.67	133.65
50-0 fault(Y-Y)	42.32	256.98
50-g fault(Y-Y)	33.68	325.64
86-0 fault(Y-Y)	46.87	314.85
86-g fault(Y-Y)	34.56	241.85
50-86 fault(Y-Y)	44.12	310.65
86-100 fault(Y-Y)	55.98	371.89
50-100 fault(Y-Y)	52.41	342.98

**Table-6.6 Energy Index for inrush and fault conditions
for experimental data**

Events (Experimental data)	Energy Index
Inrush(Y-Y)	1.55
Inrush (loaded)(Y-Y)	1.65
50-0 fault(Y-Y)	6.07
50-g fault(Y-Y)	9.66
86-0 fault(Y-Y)	6.71
86-g fault(Y-Y)	6.99
50-86 fault(Y-Y)	7.04
86-100 fault(Y-Y)	6.64
50-100 fault(Y-Y)	6.54

START

CURRENT SIGNAL

S-TRANSFORM

S-CONTOURS FOR CONTOUR LEVEL-1

S-CONTOURS FOR CONTOUR LEVEL-1 TO LEVEL-9

E1=ENERGY FOR LEVEL-1

E2=ENERGY FOR LEVEL- TO LEVEL-9

ENERGY   INDEX
=
E2/E1

ENERGY INDEX>=3

NO

YES

INTERNAL FAULT
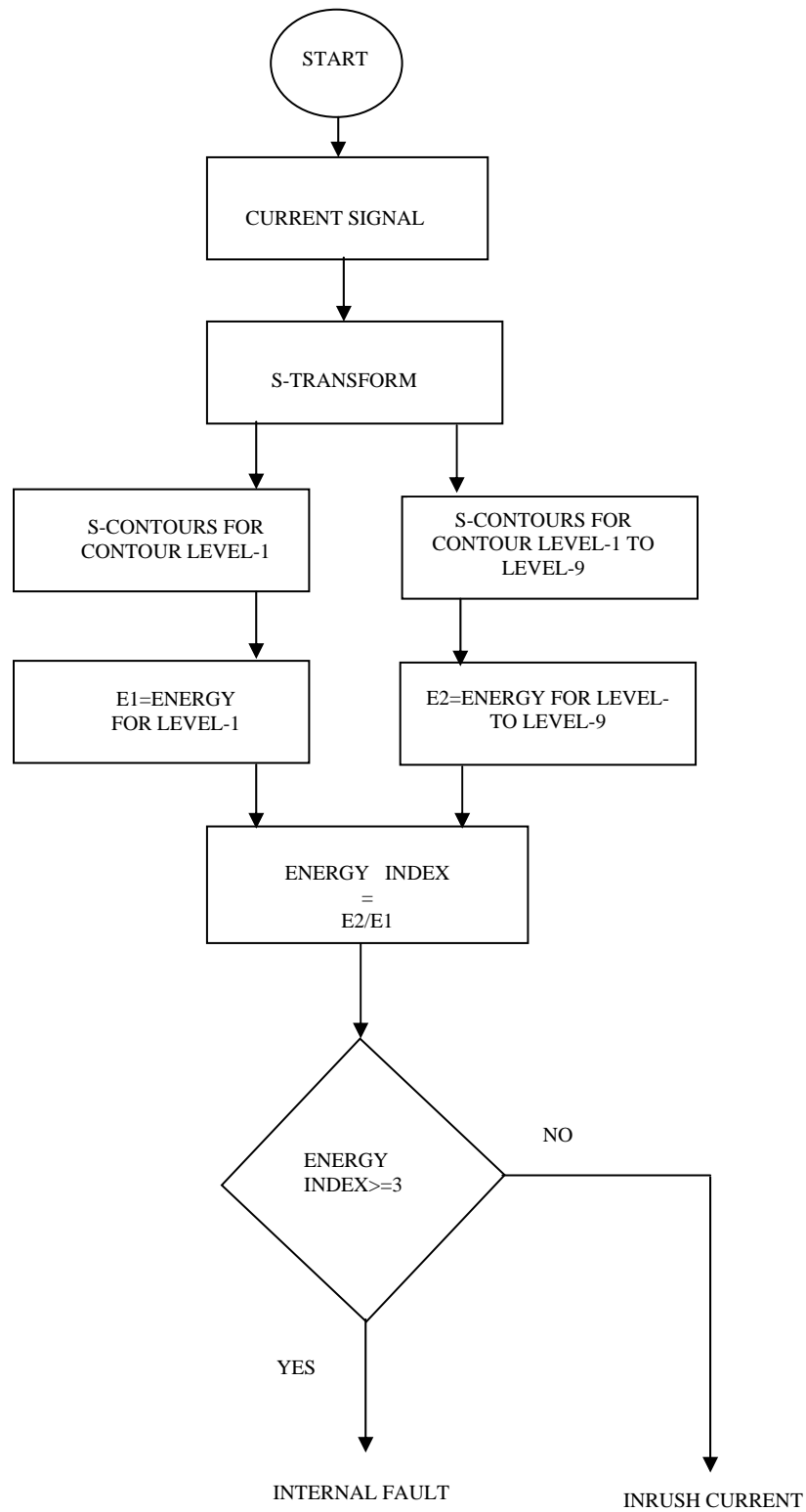
INRUSH CURRENT

Fig. 6.7 Flow chart to distinguish inrush current from internal faults

6.3   Conclusions

The proposed research presents a new approach for discrimination between inrush current and internal faults in power transformer by pattern recognition technique using S-Transform. S-Transform is found to be very powerful tool for non-stationary signal analysis, gives the frequency contours for inrush current and internal faults very distinctly as shown in the figures where second harmonic is pronounced in case of inrush current compared to faults. The spectral energy is computed for inrush current and internal faults at different contour levels. The *energy Index* is calculated to distinguish inrush current and internal faults. Also the results under noisy conditions provide significant distinctions between faults and inrush current. The proposed technique is compared with the existing differential protection based on 2nd harmonic restraint and found successful compared to the later. Also the proposed one is very robust as S-Transform is very less prone to noise compared to Wavelet Transform and so the application can be extended for protection schemes for large power transformers.

Chapter-7

Summary and Conclusions

7.1   Summary

The modern power utility and deregulated market conditions will require safe and secured operation of the power system with respect to generation, transmission and distribution. The performance of a power network is frequently affected by the transmission line faults, which give rise to disruption in power flow. Therefore, transmission of electric power and necessary protective measures are the vital issues, which needs to be addressed properly. Distance and differential protection are used to protect the transmission line and power transformer against faults by measuring the line voltages and currents using digital fault recorders.

The major problem involved in the transmission line protection is to detect, classify, locate the fault accurately, and clear as fast as possible. Various operating parameters like fault resistance in the fault path, inception angle, source impedance, type and location of faults affect largely the performance of the fault classifier and locator. Similarly, existing 2nd harmonic restraint differential protection of power transformer in distinguishing inrush current and faults, faces problems when 2nd harmonic component is approximately of the same magnitude in both the signals.

The proposed approach presents a novel technique for distance and differential protection, using time-frequency analysis and pattern recognition approach. Chapter-1 discusses the problems and brief review of earlier techniques to the distance and differential protection algorithms. Also it outlines the objectives of the proposed thesis. In Chapter-2, the time-frequency transform such as S-Transform based distance relaying schemes are discussed for single circuit and double-circuit lines. The fault detection and classification takes place within 18 samples of fault inception based on a sampling rate of 20 per cycle. The fault location determined using polynomial curve fitting is below 3%. Thus the algorithm detects the fault and identifies the line within one cycle of inception of fault and provides accurate results even in the presence of white noise of low SNR values.

Another variant of S-Transform, known as HS-Transform is used fault classification and location determination of transmission line. HS-Transform based time-frequency analysis is used for feature extraction by computing the standard deviation and change in energy at varying window and fed to the RBFNN for fault classification and fault location determination respectively. RBFNN locator gives the distance of the fault from the relaying point and the error calculated for all kinds of faults is below 2%, which is an improvement over S-Transform based protection.

Chapter-3 presents machine intelligence techniques such as Support Vector Machine (SVM) for distance relaying of transmission line including Thyristor Controlled Series Compensator (TCSC). Half cycle post fault current samples and firing angles are used as input to the SVMs and the output is the corresponding classification. SVM-1 is used for fault classification, SVM-2 is used for ground detection and SVM-3 is used for section identification for the TCSC on the line, respectively. The error found is less that 5% taking all SVMs to consideration. Also SVM based protection scheme is designed for single circuit transmission line for fault classification and ground detection. Here $1/4^{th}$ cycle post fault current and voltage samples are collected at the relaying point and fed to the SVMs as inputs and provides information about the faulty phase involved. The zero-sequence current is used to train and test the SVM for ground detection. The SVMs provide fault classification and ground detection with error less than 3% for single circuit transmission line without FACTS.

In Chapter-4, the performance of a differential equation based fault locator for transmission line including Unified Power Flow Controller (UPFC) is investigated with different operating conditions of the UPFC and transmission line. The proposed numerical protection scheme calculates line inductance to the fault point which directly reflects the fault location from the relaying point. It provides error less than 12% for extreme operating conditions of the UPFC.

Chapter-5 presents protection of compensated transmission line using time-frequency analysis and pattern recognition approach. Both Wavelet Transform and S-Transform are applied for faulty phase and faulty section identification. Different frequency components of current signals are considered to select the phase(s) involved

with a fault. To identify the fault-section the new approach utilizes the difference in high frequency components of the current signals. For both phase selection and section identification tasks, new energy and standard deviation based indices are also calculated for the transmission system. Another pattern recognition approach using S-Transform is also presented and attempt is made to find improved results Different computed frequency spectrums using S-Transform clearly demonstrate the potential benefit of the approach for fault analysis, even in the presence of high fault resistance, different initial conditions and fault inception angles.

In Chapter-6, a differential protection scheme for power transformer using time-frequency analysis and pattern recognition approach is designed. S-Transform is found to be very powerful tool for non-stationary signal analysis, gives the frequency contours for inrush current and internal faults very distinctly. The spectral energy is computed for inrush current and internal faults at different contour levels. The *energy Index* is calculated to distinguish inrush current and internal faults. Also the results under noisy conditions provide significant distinctions between faults and inrush. Laboratory results confirm the validity of the proposed pattern recognition approach.

7.2   General Conclusions

The research studies conducted yields the following conclusions:

1. The protection schemes designed for single circuit and double circuit using time-frequency transform such as S-Transform, provide accurate, fast and robust fault classifier for fault detection and classification. The tripping signal is generated within one cycle of fault inception. The fault classification and impedance calculation to the fault point is accurate avoiding over reaching and under reaching phenomena. The polynomial curve fitting based fault locator provides fault location with error limited to 3%.

2. Another distance relaying scheme using a variant of S-Transform, known as HS – Transform, is designed. The combined HS-Transform and RBFNN based protection scheme provides faulty phase selection and fault location determination respectively. The fault locator gives the distance of the fault from the relaying

point with error below 2% with wide variations in operating conditions. This overcomes the error due to the inaccuracies in the input phasor data where raw voltage and current are used to train the neural network for classification and location task. The HS-Transform seems to be better than S-Transform in providing more accurate fault location.

3. An intelligent technique based distance relaying scheme using Support Vector Machine (SVM) is designed which provides fault classification with ground detection. The proposed technique provides accurate classification results for line including FACTS with ½ cycle of faulted current and voltage signal form fault inception, which shows the accuracy and fastness of the proposed technique. Similar observations are made for single circuit transmission line, where ¼ cycle post fault current and voltage signal provides fault classification and ground detection with error less than 3%.

4. An attempt is made to investigate the performance of differential equation based fault locator for transmission line including Unified Power Flow Controller (UPFC). The designed fault locator provides fault location with error less than 12% with extreme operating conditions of the UPFC. Thus the proposed method provides a new approach for fault location in presence of UPFC with wide variation in operating conditions.

5. Compensated transmission line protection scheme using time-frequency analysis and pattern recognition approach, investigates the performance of Wavelet Transform and S-Transform for faulty phase selection and fault section identification. Different frequency components of current signals at specific Wavelet decomposition level are considered to select the faulty phase and section involved with a fault. But frequency spectrums computed form S-Transform clearly demonstrate the potential of the approach for fault analysis for online purpose even in the presence of high fault resistance, different initial conditions and fault inception angles.

6. A differential protection scheme for power transformer using time frequency analysis and pattern recognition approach is designed. The proposed method

extracts time-frequency contours of the signals and derives an energy index, which clearly distinguishes the inrush current from the fault. The proposed technique works successfully when the 2nd harmonic content is approximately same for both fault and inrush current where as the existing 2nd harmonic restraint fails substantially.

7.3   Future Scope

The proposed research can be extended for applying the similar techniques to the transmission line having other FACTS devices which are not included in the proposed study. The impact of the FACTS devices such as STATCOM, UPFC, and GUPFC on the performance of distance relaying is to be studied and a through investigation to be made with different pre-fault parameters setting of the FACTS devices and wide variations in operating conditions. The fault location in presence of FACTS devices is considerably affected and still a critical task to be studied further. The protection and relay coordination with remote sensing may be considered as a potential area for future study.

References

[1]   A. G. Phadke, J. S. Thorp, "Computer Relaying for Power Systems, *New Yerk: Wiley,* 1988.

[2]   M. S. Sachdev *et al.*, "Advancements in microprocessor-based protection and communication", in *IEEE Tutorial course*, 1997.

[3]   A. Girgis, A. A. Sallam, and A. K. El-Din, "An adaptive protection scheme for advanced series compensated (ASC) transmission lines", *IEEE Trans. on Power Delivery*, Vol. 13, No.1, pp.414-420, 1998.

[4]   A. M. Ranjbar and B. J. Cory, "" An improved method for the digital protection of high voltage transmission lines", IEEE Trans. On Power Apparatus and Systems, vol.94, no.2, pp.544-550, 1975.

[5]   M. Akke and J. T. Thorp, "Some improvements in the three phase differential equation for fast transmission line protection*", IEEE Trans. On Power Delivery*, vol.13, no.1, pp.66-72, 1998.

[6]   T. Dalstein, and B. Kluicke, " Neural Network approach to fault classification for high speed protection relaying", *IEEE transaction, P & D*, vol-10, No 2, pp.1002-1011, 1995.

[7]   H. Wang, and W.W. Keeerthipala, "Fuzzy Neuro Approach to fault classification for transmission line protection", *IEEE transaction on Power Delivery*, vol-13, No 4, pp.1093-1102, , 1998.

[8]   O.A.S Yaussef, "New Algorithms for phase selection based on wavelet transforms", *IEEE transactions on Power Delivery*, vol-17, pp.908-914, , 2002.

[9]   F. Martin, and J.A. Aguado, "Wavelet based ANN approach for Transmission line protection*", IEEE transaction on Power Delivery*, vol-18, No.4, pp.1572-1574, , 2003.

[10]   Feng Liang, and B. Jeyasurya, "Transmission line Distance Protection using Wavelet transform algorithm", *IEEE transaction on Power Delivery*, vol.19, No.2, pp.545-553, 2004.

[11]   A.M.Gouda, S.H.Kanown, M.M.A. Salam, and A.Y. Chikhani, "Wavelet based Signal Processing for disturbance classification and measurement", *IEE Proc., Gen. Trans. Distrib.*, vol-149, No.3, pp.3109-3118.

[12]   L.Y, Elangovan S., "Fault noise based approach to phase selection using wavelets based feature extraction", *Electric Mach Power System*-1999, 27: 389-398.

[13]   K. Yu, and Y. H. Song ,"Wavelet Transform and Neural Network Approach to Developing Adaptive Single Pole Auto Reclosing Schemes For EHV Transmission Systems", *IEEE Power Engineering Review*, pp. 67-69, December, 1998.

[14]   S. J. Huang, and C. T. Hsieh, " High-Impedance Fault Detection Utilizing Morlet Wavelet Transform Approach", *IEEE Transactions on Power Delivery*, Vol. 14, No. 4, pp. 1401-1410, 1999.

[15]   O.A.S Yaussef, "Online applications of wavelet transform to power system relaying", *IEEE transactions on Power Delivery*, vol-18, No.4, pp. 1158-1165, 2003.

[16]   O.A.S Yaussef, "Combined Fuzzy-Logic wavelet based fault classification for power system relaying", *IEEE transaction on Power Delivery*, vol-19, No.2, 2004, pp.582-589.

[17]   A.H.Osman, and O.P.Malik, "Transmission line protection based on wavelet transform", *IEEE transaction on Power Delivery*, vol-19, No.2, pp.515-523, , 2004.

[18]   D.Chanda, N.K Kishore, A.K Sinha, "A wavelet multi-resolution analysis for location of faults on transmission lines", *Electric Power and Energy systems*, vol-25, PP.59-69, 2003.

[19]   Wei Chen, O.P Malik, X. Yin, D. Chen, and Z. Zhang, " Study of wavelet based ultra high speed directional transmission line protection", *IEEE Trans. On Power Delivery,* vol. 18, no. 4, pp.1134-1139, 2003.

[20]   Whei-Min Lin, Chin-Der Yang, Jia-Hong Linn, and Ming-Tong Tsay, " A fault classification method by RBF neural network with OLS learning procedure", *IEEE Trans. On Power Delivery*, vol. 16, no.4, pp. 473-477, 2001.

[21] P.K.Dash, A.K. Pradhan, and G. Panda, "A novel Fuzzy Neural Network based distance relaying scheme", *IEEE transaction on Power Delivery*, vol-15, No 3, pp. 902-907, 2000.

[22] C. E. De Mori Pereira and L. C. Zanetta, Jr, "Fault location in transmission lines using one-terminal post fault voltage data", *IEEE Trans. On Power Delivery*, vol.19, No.2, 2004

[23] S. Brahma, "New fault location method for a single multi-terminal transmission line using synchronized phasor measurements", *IEEE Trans. On Power Delivery*, vol.21, No.3, pp. 1148-1153, 2006

[24] G. Song, J. Suonan, Q. Xu, P. Chen, and Y. Ge, " Parallel transmission line lines fault location algorithm based on differential component net", *IEEE Trans. On Power Delivery*, vol. 20, N0.4, 2005.

[25] Omar A.S. Youssef, "Discrimination between faults and magnetizing inrush currents in transformers based on wavelet transforms", *Electric Power System Research,* Elsevier Science, pp.1-8, 2002.

[26] P L. Mao and R.K. Aggarwal, "A novel approach to the classification of the transient phenomena in power transformers using combined wavelet transform and neural network", *IEEE Transn. On power delivery*, vol.16, no.4, pp.654-660, October 2001.

[27] Stockwell, R.G., Mansinha, L. and Lowe, R.P., 'Localization of complex Spectrum: The S-transform', *Jour. Assoc. Expl. Geophysics*, vol-XVII, No-3, pp. 99-114, , July-1996.

[28] Mansinha, L., Stockwell. R. G. and Lowe, R.P., "Pattern analysis with two dimensional spectral localization: Application of two dimensional S-transforms', *Physica A*, 239, pp.286-295, 1997.

[29] R. G. Stockwell, L. Mansinha, and R. P. Lowe, Localization of the complex Spectrum : The S Transform ", *IEEE Transaction on Signal Processing*, vol. 44, No. 4 , pp. 998-2001, 1996.

[30] Pinnegar, C.R and Mansinha, Lalu, 'The S-transform with windows of arbitrary and varying window", *Geophysics*, vol-68, pp.381-385, 2003.

[31]   C.R.Pinnegar, L.Mansinha, "Time local Fourier analysis with a scalable, phase modulated analyzing function: the S-transform with a complex window", *Signal Processing, Elsevier science*, vol.84, pp.1167-1176, 2004.

[32]   C.J.C. Burges, "A tutorial on support vector machines for pattern recognition", *Data Mining Knowledge Discovery*, 2 (2), pp. l21–167, 1998.

[33]   C.J.C. Burges, "Geometry and invariance in kernel based methods", in: B. Schoelkopf, C.J.C. Burges, A.J.Smola (Eds.), Advances in Kernel Methods— Support Vector Learning, *The MIT Press, Cam-Cambridge*, MA, pp. 89–116, 1999.

[34]   O. Chapelle, V.N. Vapnik, "Model selection for support vector machines", in: S. Solla, T.K. Leen, K.-R.Muller (Eds.), Advances in Neural Information Processing Systems, Vol. 12, *The MIT Press, Cambridge, A*, pp. 230–236, 2000.

[35]   Dash, P.K., Panigrahi, B.K. and Panda, G., 'Power quality analysis using S-transform', *IEEE Power Delivery*, vol. 18, pp.406-411, 2003.

[36]   M.H.J.Boolen, "Traveling wave based protection of double circuit lines", *Proceeding Inst.Elect. Engg. C*, vol.140, no.1, pp.37-47, Jan, 1993.

[37]   M.M.Issa and M. Masoud, "A novel digital distance relaying technique for transmission line protection", *IEEE Trans. On Power Delivery*, vol.16, pp380-384, July, 2001.

[38]   M.I.Gilany, O.P.Malik, and G. S. Hope, "A digital technique for parallel transmission lines using a single relay at each end", *IEEE Trans. on Power Delivery*, vbol.7, pp.118-123, Jan, 1992.

[39]   A.G.Jongepier and L. van der sluis, "Adaptive distance protection of a double circuit line", *IEEE Trans. On Power Delivery*, vol.9, pp.1289-1295, Jyly, 1994

[40]   B.J.Mann and I.F.Morrison," Relaying a three phase transmission line with a digital computer", *IEEE Trans. On Power Apparatus and Systems*, vol. PAS 90, NO-2, PP.742-750, Mar. /April, 1971.

[41]   T. McConaghy, H. Lung, E. Bosse, V. Vardan, "Classification of audio radar signals using Radial Basis Function Neural Network", *IEEE Trans. on Inst. And Measurement*, pp. 1771-1779, vol.52, No.6, December 2003.

[42] O. Chapelle, V.N. Vapnik, O. Bousquet, S. Mukherjee, "Choosing multiple parameters for support vector machines", *Mach. Learn*. 46 (1–3) (2002) 131–159.

[43] R. Collobert, S. Bangio, "SVM Torch: a support vector machine for large-scale regression and classification problems", *J. Mach. Learn. Res. 1*, pp.143–160,2001.

[44] N. Cristianini, J. Shawe-Taylor, "An Introduction to Support Vector Machines and Other Kernel-Based Learning Methods", *Cambridge University Press*, Cambridge, 2000.

[45] Y. Yajima, H. Ohi, M. Mori, "Extracting feature subspace for kernel based support vector machines", *tech. rep., Technical Report 2001–5, Department of Industrial Engineering and Management, Tokyo Institute of Technology*, 2001.

[46] Helbing S G, Karady, G. G, "Investigations of an advanced Form of Series Compensation", *IEEE Trans. on Power Delivery*, Vol. 9, No. 2,April 1994, pp. 939-946.

[47] Larsen E V, Clark K, Miske S A, Urbanek J, "Characteristics and Rating Considerations of Thyristor Controlled Series Compensation", *IEEE Transactions on Power Delivery*, Vol. 9, No. 2, April 1994, pp. 992- 1000.

[48] M. Noroozian, L. Angquist, M. Ghandhari, and G. Anderson, "Improving Power System Dynamics by series connected FACTS devices", *IEEE Trans. on Power Delivery,* Vol.12, No.4, 1997, pp.1635-1641.

[49] P.K Dash, A. K. Pradhan, Ganapati Panda, and A.C. Liew, "Adaptive relay setting for flexible AC Transmission Systems(FACTS)", *IEEE Trans. On Power delivery*, vol.15, no.1, pp.38-43, Jan-2000.

[50] Y. H. Song, A. T. Johns, and Q. Y. Xuan, "Artificial Neural Network Based Protection Scheme for Controllable series-compensated EHV transmission lines", *IEE Proc. Gen. Trans. Dist.*, Vol. 143, No.6, pp.535-540, , 1996.

[51] Y.H. Song, Q.Y. Xuan, and A.T. Johns, "Protection Scheme for EHV Transmission Systems with Thyristor Controlled Series Compensation using Radial Basis Function Neural Networks", *Electric Machines and Power Systems*, pp.553-565, 1997.

[52]   Gavin C. Cawley, Nicola L.C. Talbot, "Fast exact leave-one-out cross-validation of sparse least-squares support vector machines", *Neural Networks, Elsevier*, vol.17, pp.1467-1475, 2004.

[53]   T.Joachims. "Estimating the generalization performance of a SVM efficiently", *in proc. 17th international conf. Machine learning, San Francisco, CA: Morgan Kaufman*, 2000.

[54]   M.Kearns and D. Ron, "Algorithmic stability and sanity-check bounds for leave-one-out cross validation", *in proc. 10th conf. comput. Learning theory, New York: ACM*, pp.152-162, 1997.

[55]   P.K.Dash, S. R. Samantaray, "Phase selection and fault section identification in thyristor controlled series compensated line using discrete wavelet transform", *International journal of Electrical Power and Energy Systems, Elsevier Science,* vol.26,pp.725-732, November 2004.

[56]   Hong-Tzer Yang, Chiung-Chou Liao, 'A de-noising scheme for enhancing Wavelet-based power quality monitoring system', *IEEE. Transaction on Power Delivery*, Vol.16, No.3, pp.353-360, July 2001.

[57]   L. Gyugyi, "Unified Power flow concept for flexible ac Transmission systems", *IEE Proc.-C,* Vol. 139, No. 4, 1992, pp.323-332.

[58]   E. V. Larsen, K. Clark, S. A. Miske, and J. Urbanek, "'Characteristics and Rating consideration of Thyristor Controlled Series Compensation", *IEEE Trans. on Power Delivery,* Vol. 9, No.2, 1994, pp.992-999.

[59]   S. Santoso, E. J. Powers, and P. Hofmann, "Power Quality Assessment via Wavelet Transform Analysis", *IEEE Transactions on Power Delivery*, Vol. 11, No. 2, April 96, pp. 924—930.

[60]   S. Santoso, E. J. Powers, and W. M. Grady, "Power Quality Disturbance Data Compression Using Wavelet Transform Methods", *IEEE Transactions on Power Delivery*, Vol. 12, No. 3, July 1997, pp. 1250-1257.

[61]   P. Pillay and A. Bhattacharjee, "Application of Wavelets to Model short-term Power System Disturbances", *IEEE Transactions on Power systems*. Vol. 11, No. 4, pp. 2031-2037, November 1996.

[62]   M. Gouda, M. M. A. Salama, M. R. Sultan, and A. Y. Chikhani, "Power Quality Detection and Classification using Wavelet-Multiresolution Signal Decomposition", *IEEE Transactions on Power Delivery*, Vol. 14, No. 4, October, pp. 1469-1476,1999.

[63]   Y. Liao and S. Elangovan, "Fault Noise Based Approach to Phase Selection using Wavelets Based Feature Extraction", *Electric Machines and Power System*, Vol.-27, pp. 389-398, 1999.

[64]   K. Yu, and Y. H. Song ,"Wavelet Transform and Neural Network Approach to Developing Adaptive Single Pole Auto Reclosing Schemes For EHV Transmission Systems", *IEEE Power Engineering Review*, pp. 67-69, December, 1998.

[65]   S. J. Huang, and C. T. Hsieh, " High-Impedance Fault Detection Utilizing Morlet Wavelet Transform Approach", IEEE *Transactions on Power Delivery*, Vol. 14, No. 4, pp. 1401-1410, October, 1999.

[66]   Manitoba HVDC Research Center, "EMTDC – Electromagnetic Transients Simulation Program', 1988.

[67]   S.N. Hon, W. Qin," A wavelet based method to Discriminate between inrush and internal faults", pp.927-931, *IEEE Trans. On Power Delivery*, 2000.

[68]   F. Jiang, ZQ. Bo, P.S.M Chin, M.A.Redfern, Z. Chen, "Power transformer protection based on transient detection using discrete wavelet transform (DWT)", *IEEE Trans. On Power Delivery*, 2000.

[69]   P.K.Dash, D.P.Swain, A.C.Liew, S.Rahman, "An adaptive Linear Combiner for on-line tracking of Power System Harmonics", *IEEE Trans. On Power System*, vol. 11, No.4, pp.1730-1735, 1996.

Subhransu Ranjan Samantaray

Date of Birth: 30th May 1976

Education: B. E. (Electrical Engineering)- 1999

University College of Engineering, Burla, Orissa, India

Joined the PhD programme at Electronics and Communication

Engineering Department, NIT, Rourkela (January'2005)

.
Permanent Address:

C/o Gaura Chandra Samantaray

AT /P.O: Khandasahi, Salepur
Cuttack, Orissa, India

E-mail: sbh_samant@yahoo.co.in

Publications

Journals:

1.   S.R.Samantaray, B.K.Panigrahi, P.K.Dash, G.P.anda, "Power transformer protection using S-transform with complex window and pattern recognition approach", *IEE Proceeding on Generation, Transmission and Distribution.* (Accepted-September 2006).

2.   P.K.Dash, S.R.Samantaray, G.Panda, B.K.Panigrahi, "Time-frequency transform approach for the protection of parallel transmission lines", *IEE Proceeding on Generation, Transmission and Distribution.* (Accepted- Mar 2006).

3.   P. K. Dash, S. R. Samantaray, G. Panda," Fault classification and section identification of an advanced series compensated transmission line using Support Vector Machine", *IEEE Transactions on Power Delivery*, vol.22, issue-1, pp.67-73, January 2007.

4.	P.K.Dash, S.R.Samantaray, "A novel distance protection scheme using time-frequency analysis and pattern recognition approach", *International Journal of Electrical Power and Energy Systems, Elsevier Science, vol.29, issue-2, pp.129-137, February 2007.*

5.	S.R.Samantaray, P.K.Dash, G.Panda, "Power System events classification using pattern recognition approach", *International Journal of Emerging Electric Power System,*vol.6, issue-1,May-2006

6.	S.R.Samantaray, P.K.Dash, G.Panda, "Fault classification and location using HS-Transform and radial basis function neural network", *Electric Power System Research*, Elsevier Science, vol.76, pp. 897-905, June 2006.

7.	S.R.Samantaray, P.K.Dash, G. Panda and B.K.Panigrahi, "Distance protection of compensated transmission line using Computational Intelligence", *Lecture Notes in Computer Science, Springer Verlag*, pp. 163-169, Vol. 3801/2005.

8.	P.K.Dash and S.R.Samantaray, "An accurate fault classification algorithm using a minimal radial basis function neural network", *International journal of Engineering intelligent systems,* vol.12, No.4, pp.205-210, December 2004.

9.	P.K.Dash and S.R.Samantaray, "Phase selection and fault section identification in thyristor controlled series compensated line using wavelet transform", *International journal of Electrical Power and Energy system, Elsevier science,* Vol 26, pp.725-732,November 2004.

Journal (Under Review)

10.	S. R. Samantaray, P. K. Dash, G. Panda, "Distance relaying for transmission line using support vector machine and radial basis function neural network", *International journal of electrical power and energy systems, Elsevier science.*(Revised- November-2006)

11.	B.K.Panigrahi, S.R.Samantaray, P.K.Dash, "High impedance fault detection in power distribution networks using time-frequency and time-time transform", *IEEE Transactions on Power Delivery.* (September 2006)

12.	B.K.Panigrahi, P.K.Dash, S.R.Samantaray, "Detection, Quantification and Classification of Power Quality Disturbances Using Advanced Signal Processing Technique and Support Vector Machine", *IEE Proceeding on Generation, Transmission and Distribution.(October-2006)*

Conferences

1. P.K.Dash, S.R. Samantaray, G. Panda*," Fault analysis of advanced series compensated line using S-transform and pattern recognition approach", *International Power Engineering Conference-IPEC-2005* (IEEE Power Engg Society), Singapore, 28 Nov.-02 Dec, 2005.

2. S.R.Samantaray, P.K.Dash, G. Panda and B.K.Panigrahi, "Distance protection of compensated transmission line using Computational Intelligence"**,** *International Conference on Computational Intelligence and security,CIS-2005*,(IEEE Computational Intelligence Society),15-19th December,2005, Hong Kong, China.

3. S.R.Samantaray, P.K.Dash, G.Panda, "Distance Relaying of Thyristor Controlled Series Compensated line using AI", National Power Electronics Conference, *NPEC-2005*, IIT, Kharagpur, 21-22nd December, 2005.

4. S.R.Samantaray, P.K.Dash, G.Panda, "Transmission Line Fault Detection Using Time-Frequency Analysis", *IEEE INDICON-2005*, IIT, Chennai, 11-12th December, 2005.

5. S.R.Samantaray, "Signal processing application in power system relaying", *National conference on recent advances in power, signal processing and control, APSC-2004***,** NIT, Rourkela,16-17th November 2004.

6. P.KDash, S.R.Samantaray, G.Panda, P.K.Rout, S.Routray, N.Nayak, " A novel phase selection technique in digital relaying using RBFNN, *NCSC-2006*, Bhubaneswar, India, 24-26 March, 2006.

7. S.R.Samantaray, B.K.Panigrahi, P.K.Dash and G. Panda, "Discrimination between inrush current and internal faults using time frequency analysis", *IEEE international conference PEDES-2006*, IIT Delhi, Delhi 12-15, 2006,